DOE/BC/14664-12
Distribution Category UC-122

POLYSACHARIDES AND BACTERIAL PLUGGING

FINAL REPORT
1992-1993

By
H. Scott Fogler

February 1995

Work Performed Under Contract No. DE-AC22-90BC14664

Prepared for
U.S. Department of Energy
Assistant Secretary for Fossil Energy

Chandra Nautiyal, Project Manager
Bartlesville Project Office
P.O. Box 1398
Bartlesville, OK 74005

Prepared by
The University of Michigan
Ann Arbor, MI 48109-2136

DISCLAIMER

DISCLAIMER

Portions of this document may be illegible in electronic image products. Images are produced from the best available original document.

Abstract

In situ core plugging experiments and transport experiments, using the model bacteria *Leuconostoc m.*, have been conducted. Results demonstrated that cellular polysaccharide production increases cell distribution in porous media and causes an overall decrease in media permeability. Further, a parallel core plugging experiment was conducted and showed the feasibility of this system to divert injection fluid from high permeability zones into low permeability zones within porous media as is needed for profile modification. To implement this type of application, however, controlled placement of cells and rates of polymer production are needed. Therefore, kinetic studies were performed.

A kinetic model , i.e. the modeling of the production of cells and polysaccharides, was subsequently developed for *Leuconostoc m.* bacteria. This model is based on data generated from batch growth experiments and allows for the prediction of saccharide utilization, cell generation, and dextran production. These predictions can be used to develop injection strategies for field implementation.

Transport and *in situ* growth micromodel experiments have shown how dextran allow cells to remain as clusters after cell division which enhanced cell capture and retention in porous media. *In situ* growth in porous media results in three injection pressure regimes: 1) initially no measurable change in injection pressure, 2) dramatic increase in injection pressure, and 3) injection pressure oscillations. These regimes coincide with the development of the internal biofilm that initially does not restrict flow until its thickness becomes significant. At a critical point, the biofilm undergoes sloughing which produces cell and dextran aggregates that are transported and recaptures. Pressure oscillations are observed during this phase.

Additional Damkohler experiments have been performed to determine the effects of the nutrient injection rate and nutrient concentration on the rate of porous media plugging. As shown experimentally and as predicted by a model for *in situ* growth, an increase in nutrient concentration and/or injection rate will result in a faster rate of porous media plugging. Through continuum model simulations, it has been shown that the initial cell profiles play a key role on the core plugging rate. Controlling the location of the inoculating cells is thus another key factor in using bacteria for profile modification.

TABLE OF CONTENTS

LIST OF FIGURES

LIST OF TABLES

LIST OF PLATES

Executive Summary

Bacterial products such as bio-gasses, surfactants, and polysaccharides are all metabolic products that can enhance oil recovery during flooding. Exploiting the ability of the cells to produce these products requires an understanding of how the bacteria are transported through the reservoir. A basic understanding of cell transport has already been well documented if one considers bacteria as a colloidal particle. However bacteria differ from particle transport due to their ability to produce polysaccharides which are shown to influence permeability reduction in porous media.

In situ core plugging experiments, using the model bacteria *Leuconostoc mesenteroides*, have demonstrated the importance of understanding the influences of polysaccharides (dextran) on cell transport and retention in porous media in addition to their effect on the permeability of the porous media. High permeability core (14 Darcies) plugging experiments have exhibited dramatic damage on the order of 1000 times decrease in permeability which is due to bacterial polysaccharide production alone. Low permeability core (98 mD) plugging experiments have demonstrated, however, permeability reduction due to both cell growth and polymer production, the latter being more profound. In addition, the transport experiments in micromodels support the observation of the staining of the plugged cores that the polysaccharide influence the distribution of cells within porous media.

Noting that *in situ* cellular production of polysaccharides will dramatically reduce the permeability of porous media, an experiment to determine the feasibility of using bacteria for profile modification was conducted. This feasibility study was accomplished by conducting a parallel core plugging experiment where a high permeability core (13.4 D) and a low permeability core (66 mD) were connected in parallel, inoculated with cells, and injected with bacterial feed solution at constant volumetric flow rate. The results of the

parallel core plugging experiments have shown that fluid flow can be diverted to the extent that there is flow normalized, but there is a degeneration of the system with further feed injection. Thus, to be able to exploit the ability of the cells to plug the porous media for profile modification requires an understanding of the growth kinetics of the bacteria.

Batch growth experiments were conducted to acquire data for modeling cell growth under various feed conditions. From these batch experiments, it was found that cell utilization of fructose and glucose is simultaneous and thus there is no preferential growth on either monosaccharide. However, cell growth on a combination of sucrose and glucose has demonstrated the cells ability to catabolize sucrose at a faster rate than the monosaccharide. For this reason it is believed that cell catabolism of sucrose involves the secretion of an exo-enzyme that converts the sucrose into dextran (polysaccharide), glucose, and fructose; subsequently monosaccharides are transported into the cell for growth. From initial batch growth experiments, it was found that the rate of cell growth can be correlated to the concentration of sucrose and yeast extract in the growth media, while the production of dextran is only dependent upon the sucrose concentrations. In addition, cell growth experiments in the presence and absence of montmorillonite clay have shown that the presence of surfaces does not influence the cell growth rate.

From the batch growth data, the specific growth rate for these cells, the rate of substrate utilization, and dextran production was modeled. These models are now available for the prediction of *in situ* cell growth.

Transport experiments, in which cell grown in monosaccharides (un-coated) or sucrose (dextran coated) were injected into a micromodel, have shown that cells grown in sucrose form clusters that aided in cell capture and retention. This phenomenon was observed qualitatively with the use of image recording. Inlet pressure data were also obtained.

In situ grow experiments, also conducted in micromodels, have shown that sucrose in the feed solution aids in the development of a thick biofilm that results in mechanical plugging of the porous media. These experiments started with the injection of un-coated cells (cells with no dextran) into the micromodel followed by the injection of a feed solution. In one experiment the feed consisted of monosaccharides (no -polymer production induced) which resulted in the development of a thin biofilm on the micromodel walls. During this feeding period there was no observable change in the injection pressure. Subsequent switching of the feed from monosaccharides to sucrose allowed the biofilm to thicken , resulting in a dramatic increase in injection pressure. As growth continued the pressure increased to the point where the injection fluid began to shear aggregate biofilm in the pore bodies into smaller aggregates. The capture of these smaller aggregates further down in the micromodel resulted in oscillation of the injection pressure. Similar findings were observed for the micromodel experiment that was feed sucrose sequentially after inoculation, hence excluding the initial biofilm development on monosaccharide. For quantitative purposes an *in situ* growth experiment was repeated for consolidated ceramic cores in which the inlet and axial pressures were sampled periodically along with sucrose and cell effluent concentrations. The results were used to develop an *in situ* growth model that predicts permeability reduction.

Damkohler experiments were conducted and have shown how the porous media's plugging rate is affected by the growth rate of the cells. Both injection rate and nutrient concentration were varied from experiment to experiment (and are thus called the Damkohler experiments). Increasing the flow rate had shorten the length in time when damage was measurable. Similarly, an increase in the nutrient concentration had decreased the time before measurable damage occurs. These results are expected based on the growth kinetics, because the cell's growth rate is dependent on the availability of nutrient provided. The *in situ* growth model (continuum) is able to predict the plugging rate of the porous media under these various nutrient injection conditions. This model in conjunction with

experimental *in situ* growth plugging data has shown that mass transfer and cell growth lag time are important in the predicting of the cell's *in situ* growth rate and resulting porous media plugging. This model has also demonstrated the importance of the initial cell profile on the rate of core plugging. Simulations under three profile conditions: exponentially decreasing, constant, and exponential increasing profile (relative to face conditions but equal cell numbers) has been shown to increase the rate of core plugging, respectively.

1.0 Introduction

Bacterial products such as bio-gasses, surfactants, and organic acids are all metabolic products that can enhance oil recovery during flooding [Grula and Russell,1985, Bryant and Burchfield, 1989]. Exploiting the ability of the cells to produce these products is typically called Microbial Enhanced Oil Recovery or MEOR. Accompanying cellular generation of these beneficial metabolites is biomass which includes both cell and polysaccharide production. The biomass can reduce the permeability of the reservoir. This permeability reduction can be detrimental if it occurs at the well face, but can be beneficial if it occurs in the high permeable, water-swept zones. Under these latter conditions, the biomass acts as a water diverting agent during flooding.

To achieve diversion requires an understanding of bacterial transport and retention within a reservoir. Therefore, the objective of this research is to determine the conditions under which proper placement of the cells into the reservoir and adequate biomass production (i.e., cell growth and polymer production) occurs.

In the following sections, results from experimental work demonstrate the importance of polysaccharides in controlling cell transport. It is shown that cellular production of polysaccharides rather than just cell growth reduces the permeability of porous media. In addition, transport of polymer-free versus polymer-producing cells are compared under conditions of varying ionic strength of transport solutions (Task II). The kinetics for cell growth, substrate utilization, and polymer production are determined experimentally to support development of models to describe the production of biomass (Task I). Finally core plugging experiments show the influence of nutrient injection rates and nutrient concentrations on the rate of plugging (Task III). An in situ growth model has been developed to predict the influence of injection stategy on porous media plugging.

1.1 References

Bryant, R.S. and Burchfield, T.E.: "Review of Microbial Technology for Improving Oil Recovery", SPE Reservoir Eng., (May 1989), 151-154

Grula, Mary M. and H.H. Russell, *Isolation and Screening of Anaerobic Clostridia for Characteristics Useful in Enhanced Oil Recovery*, DOE/BC/10811-1, (Oct. 1985)

2.0 Background

Transport and retention mechanisms have been documented for particle transport through porous media and are also expected to control bacterial transport. Table 2.1 lists the dominating mechanisms which influence particle capture, retention and decolmatage. However, bacterial transport through, and retention by porous media may differ from particle transport, because cells are capable of producing polysaccharides which affects their ability to adhere to surfaces [Sutherland, 1980, Fletcher *et al.* 1980, Fowler and McKay, 1980, Allison and Sutherland, 1986].

To determine the importance of polysaccharides as a retentive mechanism for bacteria in porous media, core plugging experiments and cell transport experiments have been conducted. Numerous bacteria species exist in the substrata and experimental study of every species would be difficult, too costly, and time consuming. Therefore, a model bacteria, *Leuconostoc mesenteroides* has been selected for these experiments. It has the unique ability to produce dextran, a polysaccharide, when fed sucrose and when it is limited to a glucose and/or fructose feed, no dextran is produced [Monsan *et al.*, 1987]. Hence, cellular polysaccharide production can be controlled which allows for the formulation of comparative experiments that can demonstrate the effects of polysaccharides on cell transport and retention in porous media.

Table 2.1. Deep bed filtration retention, capture and decolmatage mechanisms [Herzig, Leclerc, and Le Goff, 1970].

Filtration type	Particle size	Retention sites	Retention forces	Capture mechanism	Spontaneous decolmatage	Provoked decolmatage
Mechanical	> 30 μm	Constrictions, cervices, caverns	Friction, fluid pressure	Sedimentation, direct interception	Improbable	Flow direction reversal
Physico-chemical	~ 1 μm (<3 μm)	Surface sites	Van der Waals, electrokinetic forces	Direct interception	Possible	Increase in flowrate
Colloidal	< 0.1 μm	Surface sites	Van der Waals, electrokinetic, chemical bonding	Direct interception	Possible	Increase in flowrate

2.1 Core Plugging Experiments

The purpose of these experiments is to show that cellular polysaccharide production is a dominating factor affecting the loss of reservoir permeability. This phenomena was demonstrated by conducting *in situ* bacterial growth experiments using the model bacteria under polymer production (sucrose) and polymer suppression (glucose and/or fructose) feed conditions. Figures 2.1 and 2.2 illustrate the results of plugging experiments for high and low permeability ceramic cores, 14.7 D and 98 mD respectively. For both plugging experiments, the selected media had a median pore size that was either the same magnitude but larger in size relative to the bacteria, or an order of magnitude greater. Appendix 2.A gives the complete pore size distribution data for the two ceramic cores as determined by mercury porosimetry and it also gives details of the apparatus used to conduct the core plugging experiments.

The plugging of the ceramic cores resulted from inoculating the cores with cells grown in a glucose-fructose media, followed by the injection of a glucose-fructose or sucrose feed at a constant rate of 0.1 mL/min. (1.18 cm/hr). The pressure drop across the

cores was monitored to determine the overall permeability reduction, i.e. plugging, of the cores. The differences in the plugging of the cores as a function of time might be attributed to differences in the cell growth rate due to the use of different nutrient sugars, or to the ability of the cells to produce polysaccharide. However, batch growth experiments, which are detailed in Section 4.1.2, have demonstrated that the cell's replication rate is roughly equivalent for the two different feeds; hence the plugging of the core during sucrose injection was attributed to the production of polysaccharides. In addition, when the respective cores are sterilized by gamma radiation, cut axially and stained with crystal violet, the resulting stain pattern demonstrates a hindrance of cell transport due to the cells' ability to secrete polysaccharides.

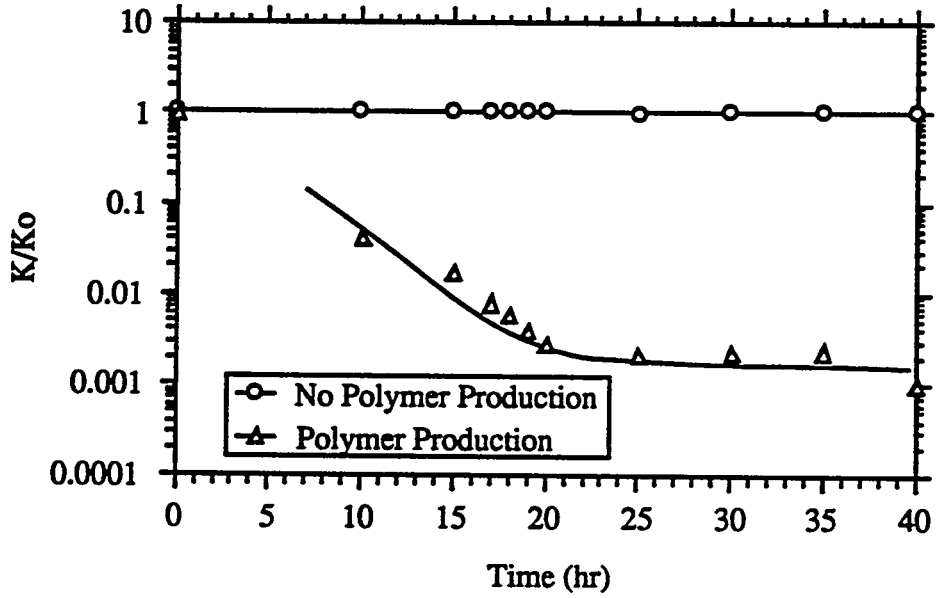

Figure 2.1. Permeability reduction due to dextran synthesis in high permeability core (14.7 Darcies with median pore throat size of 33 μm)

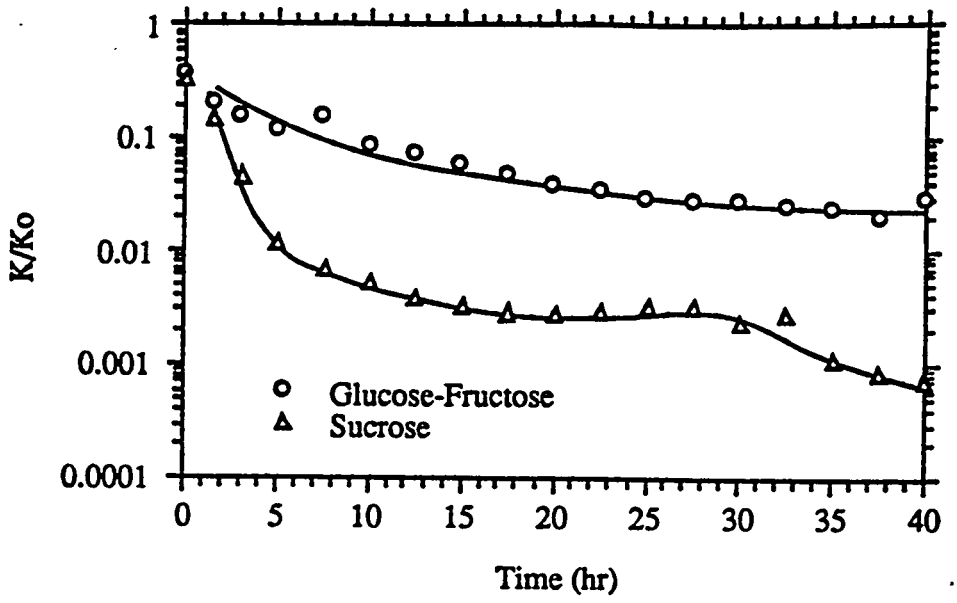

Figure 2.2. Permeability reduction due to dextran synthesis in low permeability core (98 milliDarcies)

2.2 Parallel Core Plugging Experiments

The results obtained for the core plugging experiments, which demonstrate the controllability of bacterial plugs in porous media by the type of nutrient injected, confers towards the application of profile modification. Such a technique would commence with the injection of cells (cells without any associated polysaccharide) into the reservoir, followed by the injection of a sucrose growth media to promote cell growth and bacterial polysaccharide production. It would be expected that the permeability ratio of the two different zones would limit cell entry to the low permeability zones. The injection of the sucrose growth media would then provide the cells with the needed nutrients for growth and polysaccharide production. The results of such a strategy would be a reduction of the permeability in the high permeability zone, thus diverting fluid flow into the unswept zones.

To emulate this scenario, a parallel core experiment (Par-3) was conducted. Table 3 gives the relevant procedural conditions, such as the cores' initial permeability, the inoculum conditions and the resulting flow diversion and depth of plug penetration. The experiment started with the growing of an inoculum and sterilization of the core apparatus as detailed in Appendix 2.A. The inoculum was prepared by growing the cells in a glucose-fructose media for approximately 1 day, followed by their removal from the growth media by centrifugation and resuspension in new media. The cores were saturated with the respective media as presented in Table 2.2, placed into the parallel core apparatus, and then inoculated with cells. A sucrose media was then injected at a constant volumetric rate into the parallel core apparatus and the resulting pressure drops and effluent flow rates were monitored.

This experiment exhibited the dominance of flow through the high permeability core initially as illustrated by Figure 6. The large differences in the permeability of the cores dictated that the high permeability core would support over 99% of the fluid flow initially (the high permeability core emulating a water swept zone within a reservoir). Constant inlet pressure to the parallel core system during inoculation indicates that the injection of cells did not cause any measurable damage to the cores. For the first few hours after the commencement of nutrient injection, no plugging was realized. However, as feeding progressed, the fluid was diverted from the high permeability core into the low permeability core as shown in Figure 2.3. This diversion was the result of biomass generation in the high permeability core. The flow of nutrient solution through the cores was equal after 20 hours. With additional nutrient injection, Par-3 exhibited a maximum flow diversion ratio of 1.3 at 30 hours, followed by a degeneration of the flow diversion. This degeneration is believed to be the result of cell growth in the low permeability core.

Table 2.2. Parallel core plugging experimental conditions and results.

	PAR-3
High Permeability Core	
- permeability	13.4 D
- length	6.25 cm
Low Permeability Core	
- permeability	66 mD
- length	6.30 cm
Permeability ratio (K_h/K_l)	203
Cores saturation media	15 g sucrose/L 10 g yeast extract/L
Inoculum	
- initial growth medium	7.9 g glucose/L 7.9 g fructose/L
- inoculum preparation	centrifuged at 4400 g 300 mL sol'n 15 g sucrose/L 10 g yeast extract/L
- injected rate into core	5 mL/min.
- inoculum concentration (cells/L)	~ 1×10^{11}
Feed	15.0 g sucrose/L 10 g yeast extract/L
Maximum flow diversion (Ql/Qh)	1.3
Depth of penetration of bacterial plug into high permeability core	4.4 cm

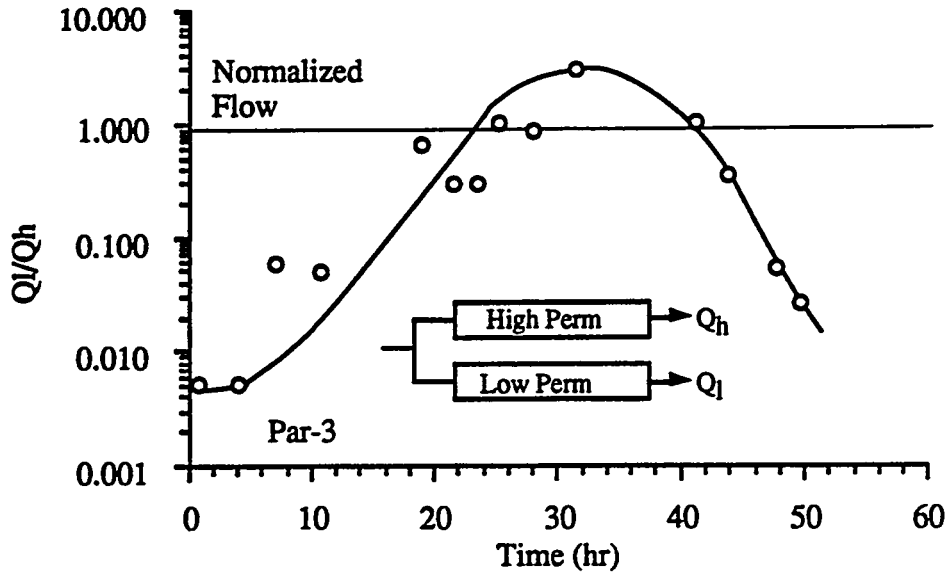

Figure 2.3. Low permeability to high permeability flow ratio for parallel core experiments Par-3 (Experimental conditions are presented in Table 2.2)

This experiment thus supports the idea that the use of micro-organisms for diversion is plausible. However the control of when and where damage occurs within the reservoir proves to be difficult because diversion was only temporary. Hence, there is a need for further investigation of the growth kinetics for *Leuconostoc m.* cells to enable the development of an injection strategy for the exploitation of this plugging phenomena. This investigation is ongoing; currently available results are provided in the next section.

2.3 References

Allison, D.G. and I.W. Sutherland, The Role of Exopolysaccharides in Adhesion of Freshwater Bacteria, *J. of Gen. Micro.*, **133**, 1319-1327, 1987

Fletcher, M., M.J. Lathan, J.M. Lynch, and P.R. Rutter, Chapter 3, *Microbial Adhesion to Surfaces*, edited by R.C.W. Berkeley, J.M. Lynch, J. Melling, P.R. Rutter, and B.Vincent, Ellis Horwood Limited, West Sussex, England, 1980

Fowler, H.W. and A.J. McKay, Chapter 7, *Microbial Adhesion to Surfaces*, edited by R.C.W. Berkeley, J.M. Lynch, J. Melling, P.R. Rutter, and B.Vincent, Ellis Horwood Limited, West Sussex, England, 1980

Herzig, J.P., D.M. Leclerc, and P. Le Goff, Flow of Suspensions Through Porous Media-Application to Deep Filtration, *Ind. and Eng. Chem.*, **62**, 8-35, 1970

Monsan, P., F. Paul, D. Auriol, and A. Lopez: "Dextran Synthesis Using Immobilized *Leuconostoc mesenteroides* Dextransucrase" Methods in Enzymology, Vol 136, 1987, 239-252

Sutherland, I.W., Chapter 18, *Microbial Adhesion to Surfaces*, edited by R.C.W. Berkeley, J.M. Lynch, J. Melling, P.R. Rutter, and B.Vincent, Ellis Horwood Limited, West Sussex, England, 1980

Appendix 2.A

Experimental Apparatus

The results from the mercury porosimetry experiments on the high and low permeability cores are provided in Figure 2.A.1. These curve have been generated by taking the mercury imbibition data versus pressure and fitting it to normal and log-normal distribution curves. Table 2.A.1 presents the resulting parameters from the fits. It can be seen from the data that both cores had pore distributions which are of the same order of magnitude or greater than the size of the bacteria illustrated by Figure 2.A.1

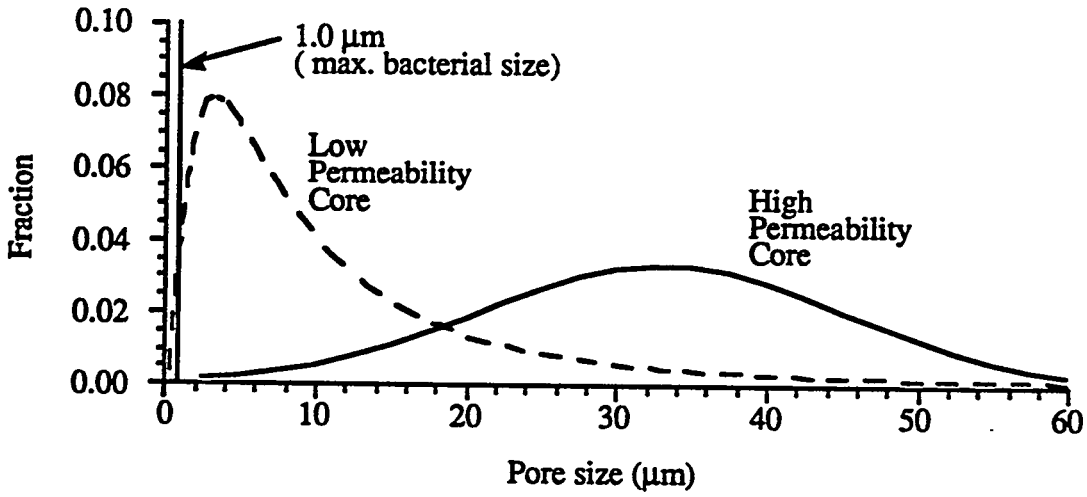

Figure 2.A.1. Pore size distribution for the high and low permeability cores.

Table 2.A.1. List of the physical characteristics of the ceramic core.

	High Perm.	Low Perm.
Porosity	0.555	0.536
Permeability (Darcies)	14.7	0.098
Means pore size (µm)	33.2†	3.27**
Standard Deviation	12.1	0.94

† - based on normal distribution
** - based on log-normal distribution

Figure 2.A.2 illustrates the apparatus used to conduct the core plugging experiments. This equipment consist of a Hassler cell with unique supporting equipment. This equipment includes the self-contained piston container, the nutrient accumulator and prefiltration unit and filter isolated pressure tap where digital pressure transducers have been connected. All filters serve to maintain system sterility. The filters were found to have minimal effect on the pressure readings.

Sterilization of the system was accomplished by ethanol soaking for the Hassler cell itself, and autoclaving for all other components. Cell transfer and equipment connection were conducted according to standard aseptic procedure.

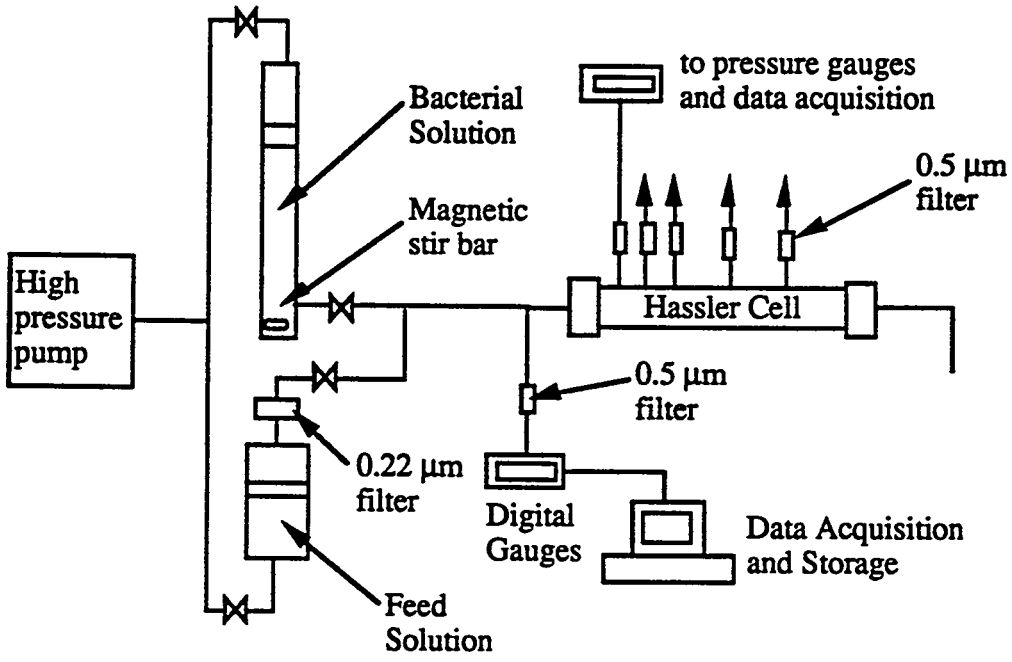

Figure 2.A.2. Hassler cell apparatus used for core plugging experiments

3.0 Task I - Cell Kinetics

Task Description:

To determine the exact growth kinetics of the Leuconostoc m. bacteria and how they are affected by 1) nutrient feed, and 2) surface effects.

Bacteria located within reservoirs are expected to experience the same four stages of growth as they would in a batch reactors, as depicted in Figure 3.1. These stages are the lag, exponential (or log) , stationary , and death phases. Of these four phases, the most significant with respect to core plugging was found to be the exponential growth phase. The exponential phase of growth becomes important when the reservoir are continuously fed polymer inducing nutrients. The cells are assumed to enter the exponential phase after acclimatization to the new nutrients. During this phase of growth, the cells are capable of constantly assimilating nutrients and replicating and is characterized by a straight line when the log of the cell concentration is plotted with respects to time , as illustrated by Figure 3.1.

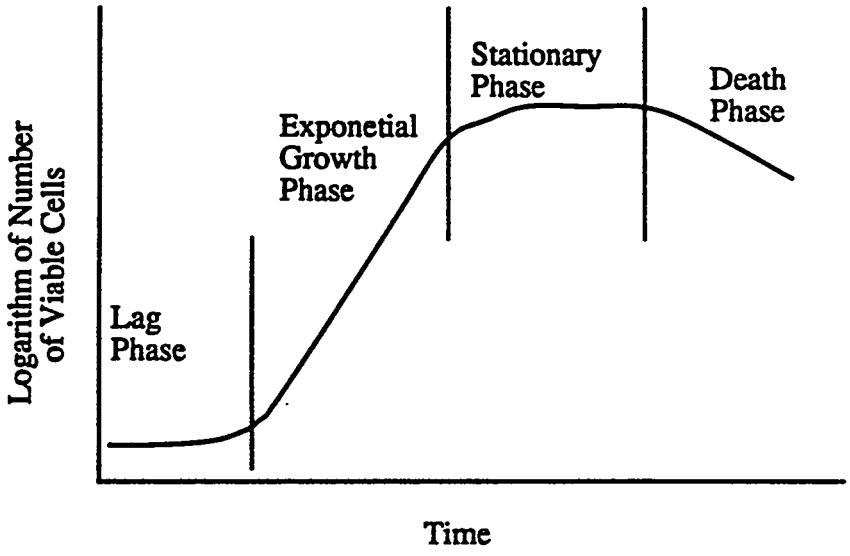

Figure 3.1. Typical batch growth curve of a microbial culture

Continuously stirred batch experiments have been conducted to determine the rates of cellular and polysaccharide (dextran) production and the nutrient consumption. These experiments in which the type and concentration of saccharide provided as a carbon source, and the concentration of yeast extract were varied. In addition, the effects of clay particles on the growth rate were performed. However these results showed no significant influence of the particles on the cell's growth rate and thus the results are presented in Appendix 3.A.

3.1 Materials and Methods

Continuously stirred batch experiments were conducted to determine the rates of cellular and polysaccharide (dextran) production and the nutrient consumption. These experiments consisted of mixing the desired media for cellular growth, sterilizing this media by autoclaving, and then inoculating the media with *Leuconostoc m.* cells. Typically reactor volumes varied from 0.5 to 0.8 L. Reactor temperatures were maintain at a constant 24 ± 1 C. The inoculum consisted of cells originating from a stock of ATCC 14935 cells (American Type Culture Collection). Inoculum used in the kinetic studies did not have more than 3 media transfers in order to prevent phenotypical alterations of the bacteria. Bacteria with less than 3 media transfers exhibited very short lag times. These lag times were typically found to be less than one hour during growth experiments lasting 10 to 12 hours. The media used for cell cultivation as inoculum was a combination of glucose-fructose and yeast extract, as presented in Appendix 3.B. The inoculation for the mechanism determination experiments consisted of culture cells grown for 18 to 24 hours on the glucose and fructose media (the stationary phase for growth). All other experiments used inoculum that was further processed by separating the cells by centrifuging from their original media before they were transferred into the batch reactors.

The cell concentrations were determined spectrophotometrically for substrate preference experiments, while for all other experiments the cell concentrations were determined by using a Coulter Counter. Sucrose, fructose and glucose were also monitored throughout the experiments. Glucose concentrations were determined by hexokinase-dehydrogenase technique [Chaplin *et al*, 1986] and the sum of fructose and glucose concentration was determined by the dinitrosalicylic acid technique. Fructose concentrations were calculated by subtracting the glucose concentrations from the respective total concentration values determined by the dinitrosalicylic technique. Sucrose concentrations were determined by adding invertase to the samples of the supernatant to hydrate the disaccharide, thus producing glucose and fructose that were then assayed using the dinitrosalicylic acid technique. The sucrose concentrations were calculated from the difference between the concentration of monosaccharide before and after invertase treatment (note that sucrose standards were always conducted during sample analysis to determine the invertase conversion efficiency). Both cell and saccharide concentrations were determined in triplicate. Amino acid concentrations were determined by high performance liquid chromatograph (HPLC).

The dextran concentrations were determined by sample purification, followed by reducing sugar analysis. This purification step begins by centrifuging the cell suspension at 14,000 *g* to separate cells and insoluble dextran from a known volume of batch reactor solution. The resulting pellets were repeatedly suspended in 0.1 M phosphate buffer solution (pH of 6.0), centrifuged, and separated from the supernatant to remove impurities such as soluble reducing sugars. Three washes were needed to remove the impurities. Next dextranase (EC 3.2.1.11 Sigma Grade III in 0.1 M phosphate buffer) was added to break down the insoluble dextran into soluble oligosaccharides. These samples were incubated for a 1 hour period at 37°C. The suspensions were then centrifuged to separate the cells from the soluble oligosaccharides. The concentration of oligosaccharides in the

supernatant was analyzed with the phenol-sulfuric acid assaying technique detailed by Chaplin *et al* [1986]. These dextran assays were determined in triplicate.

Measurements of the activity of sucrose reducing enzyme(s), measured as free or suspended enzymes, were carried out by taking cell suspension samples during cell growth, centrifuging the sample at 14,000 *g* for 10 minutes, and adding a buffered sucrose reagent solution (acetic acid buffer pH 5.2 - assay temperature 30 ± 1°C) to the resulting supernatant, as detailed by Lawford *et al* [1979]. Initial (t = 0.0 min.) and final (t = 50.0 min.) fructose and glucose concentrations were determined, in triplicate, using the procedure detailed earlier. From these data, the activity of the enzyme(s) was then calculated as the ability of the solution to convert sucrose into products (*i.e.*, 1 Unit equals the liberation of 1 µmole of monosaccharide/min. at 30°C and a pH of 5.2).

3.2 Theory

Knowledge of the cell growth kinetics and dextran production is important, if BPM is to be used successfully. A complex media is required for growth of *Leuconostoc m.* For this study the media consisted of yeast extract, mono or disaccharides, trace minerals, and a buffer (see Appendix 3.B). Yeast extract was provided as a carbon source, and as a source of growth factors such as amino acids. Saccharides were provided to the cells as both a carbon and energy source. The overall metabolic reactions for sucrose, glucose, and fructose are well documented [Stanier *et al*, 1986] and are as follows:

$$\text{Sucrose} + \text{Cells} \rightarrow \text{Polysaccharide (Dextran)} + \text{Ethanol} + \text{Acetate} + \text{Mannitol} + \text{Lactate} + CO_2 + \text{Glucose} + \text{Fructose} + \text{Cells} \qquad 3.1)$$

$$\text{Glucose} + \text{Cells} \rightarrow \text{Ethanol} + \text{Acetate} + \text{Lactate} + CO_2 + \text{Cells} \qquad 3.2)$$

$$\text{Fructose} + \text{Cells} \rightarrow \text{Mannitol} + \text{Cells} \qquad 3.3)$$

These overall reactions describe how the cell metabolizes the various saccharides to produce cell mass, dextran and final metabolic products. However, these equations do not provide information on the intermediate reactions that govern the growth kinetics of the bacterium.

Dextran production by *Leuconostoc m.* is catalyzed by the enzyme dextransucrase, represented as *E* in the following equations.

$$\text{Sucrose} \xrightarrow{E} \text{Dextran} + \text{Fructose} \qquad 3.4)$$

$$\text{Sucrose} \xrightarrow{E} \text{Glucose} + \text{Fructose} \qquad 3.5)$$

This enzyme converts sucrose to dextran (Equation 3.4). At the same time the enzyme dextransucrase is responsible for the liberation of glucose from sucrose as illustrated by Equation 3.5 [Ebert *et al*, 1968, Lawford *et al*, 1979].

3.2.1 Modeling

Several models exist that describe the dependency of specific growth rate on limiting nutrients. For mathematical simplicity, the Monod model for multiple limiting growth nutrients has been selected to describe the functionality of the growth rate constant. For multiple growth limiting nutrients, this model is expressed as:

$$\mu = \mu_{max} \prod_{i=1}^{n} \frac{C_i}{K_i + C_i}. \qquad 3.6)$$

where:

- μ - specific growth rate (h^{-1}),
- μ_{max} - maximum specific growth rate (h^{-1}),
- n - number of limiting components,
- C_i - concentration of limiting component i (g/L),
- K_i - Monod constant for component i (g/L).

Ebert *et al* [1968] and Lawford *et al* [1979] have developed a model that describes batch production of dextran, fructose, and glucose. This model follows the generalized form:

$$r_i = V_{max_i} \left(\frac{C_s}{K_d + C_s} \right) \qquad 3.7)$$

where:

r_i - rate of product i formation per unit volume (g/L·h)
V_{max_i} - maximum velocity for species i (g/L·h)
(dependent upon enzyme concentration- C_e),
K_d - Michaelis-Menton constant (g/L),
C_s - sucrose concentration (g/L).

This equation expresses the dependency of product i (dextran, glucose, and fructose) production rate on the sucrose and enzyme concentration. Sucrose is the reactant consumed while the enzyme, **E**, catalyzes the reaction and thus influences the maximum velocity, V_{max_i}.

Enzyme production is modeled by the general product formation equation presented by Leudeking and Piret [1959]. This equation assumes product formation is the result of both growth and non-growth associated contributions:

$$r_i = Y_{i/x}\, r_x + k_i\, C_x \qquad 3.8)$$

where:

$Y_{i/x}$ - growth attributed product i constant (g/cell)
k_i - non-growth attributed product i constants (h^{-1})
r_x - rate of cell production (g/L·h),
C_x - cell concentration (cells/L).

Equation 3.8 can also be used to describe the corresponding consumption of nutrients that accompanies cell growth. In this situation, $Y_{i/x}$ is the yield coefficient and k_i is the amount of substrate required for cell maintenance.

3.3 Results and Discussion

Four key experiments, using various combination of sucrose, fructose, and/or glucose and yeast extract as growth media, were conducted to formulate a reaction mechanism and a kinetic model for cell growth on sucrose. Additional sucrose growth batch experiments were then used to determine the functionality and parameter values of the specific growth rate, the dextran production rate, and the nutrient consumption rate laws.

3.3.1 Growth Experiments to Determine Substrate Utilization Mechanism

The effect of sucrose, or glucose and fructose, on cell growth rate was examined by conducting two batch reactor experiments. One batch experiment used a growth media containing yeast extract and sucrose, while in the other experiment the reactor media contained yeast extract, glucose, and fructose. Sucrose, being a disaccharide, is composed of glucose and fructose that are connected by a glycosidic bond. Therefore, to make the growth media equivalent in saccharide content, 7.9 g/L of each glucose and fructose were added to one reactor, while sucrose was added at a concentration of 15.0 g/L to the other. Appendix 3.B lists the recipes used for the kinetic experiments. Each reactor was inoculated with cells in their stationary phase of growth. Figure 3.2 shows the cell densities as a function of time for the two batch cultures. As seen in Figure 3.2, the cell's growth was virtually the same. This result, which have been duplicated, was expected because the two feeds used in the batch experiments were stoichiometrically equivalent.

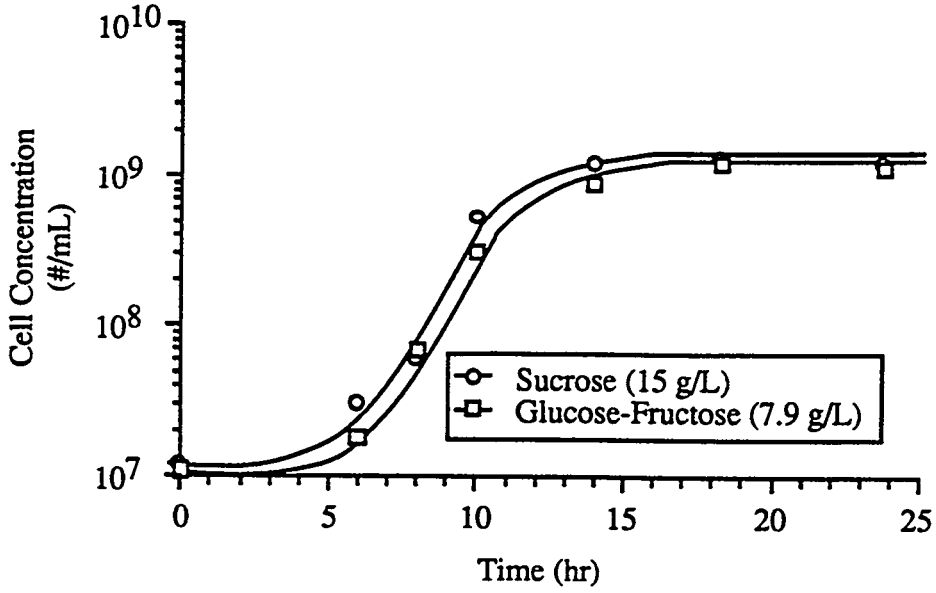

Figure 3.2. Dependency of the cell growth rate on a sucrose and glucose-fructose medium (15 g sucrose/L, 7.9 g glucose/L and 7.9 g fructose/L)

Figure 3.3 presents the results of cells grown in a media containing yeast extract, glucose, and fructose and shows the consumption of glucose and fructose occurs simultaneously. As shown by Figure 3.3, the concentration of fructose begins to decrease 6 hours after inoculation, while that of glucose begins to decrease at approximately 7.5 hours after inoculation. These results demonstrate the ability of the cells to consume both glucose and fructose simultaneously and *not* preferentially.

A batch experiment was carried out to determine whether sucrose or glucose is consumed preferentially. The growth medium used for this experiment initially contained the two saccharides and yeast extract. As illustrated in the Figure 3.4, the cells consume almost all the sucrose before they begin to consume glucose. In fact, the concentration of glucose increases with time as the cells consume sucrose. This increase in glucose concentration and the appearance of fructose in the bulk solution is the result of sucrose metabolism for growth and dextran production. In the past, it was believed that the sole

products of dextran synthesis from sucrose were dextran and fructose [Ebert *et al*, 1968]. However Lawford *et al.* have noted that the dextransucrase enzyme (the enzyme responsible for dextran production) from *Leuconostoc* B512 bacteria also liberated glucose during dextran synthesis [Lawford *et al*, 1979]. Our observations of glucose production during dextran and cell production for *Leuconostoc* B523 growth support Lawford's results.

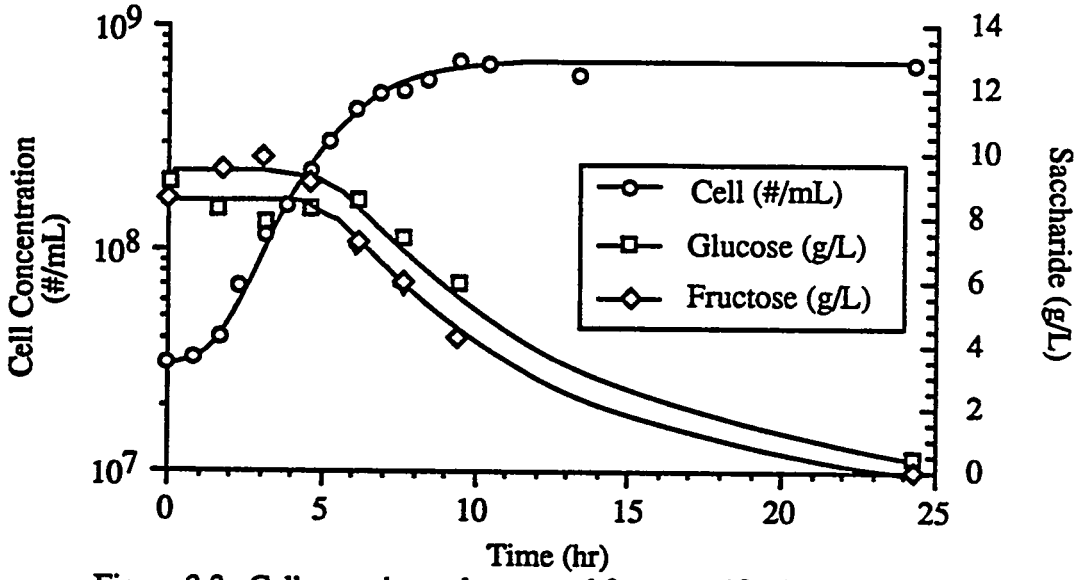

Figure 3.3. Cell growth on glucose and fructose, 10 g Yeast Extract/L.

As a result of the four experiments, a substrate utilization mechanism, presented in Figure 3.5, was developed. The mechanism predicts the external catabolism of sucrose to produce dextran, glucose, and fructose. The monosaccharides are then transported into the cell as nutrients for growth.

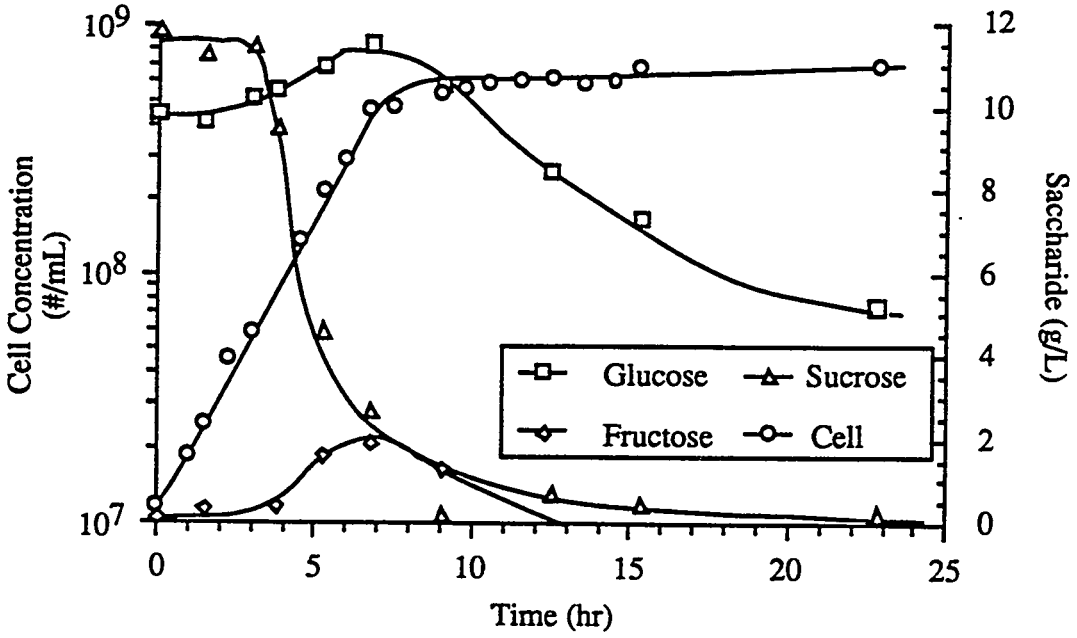

Figure 3.4. Cell growth on sucrose and glucose, 2 g yeast extract /L

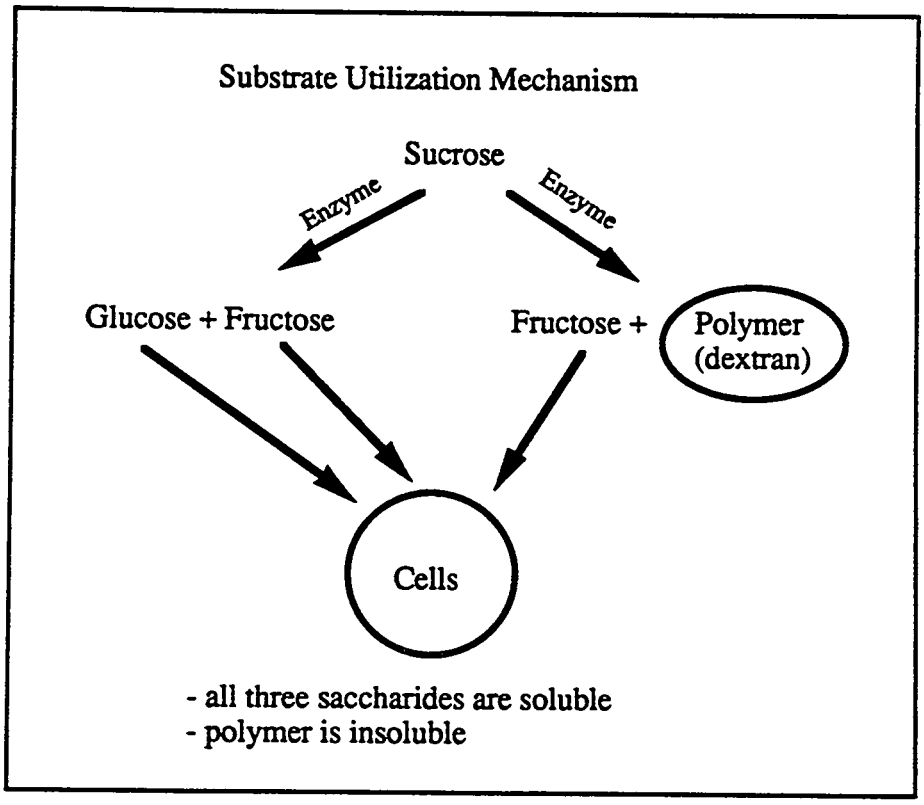

Figure 3.5. Substrate utilization mechanism

3.3.2 Specific Growth Rate Experimental Results

In this study the dependency of the specific growth rate, μ, on the concentration of the yeast extract and sucrose was determined. Figure 3.6 shows the initial specific growth rates as a function of the initial sucrose (and yeast extract) concentration for two series of batch growth experiments. Note that the initial specific growth rate was calculated using cell growth data under the conditions where the sucrose concentration of the media did not change appreciably. Both data sets show an initial growth on yeast extract nutrient media alone, with increases in the growth rates as sucrose concentrations are increased. The data also illustrate an optimal growth rate, indicating retardation of cell growth at high sucrose concentrations.

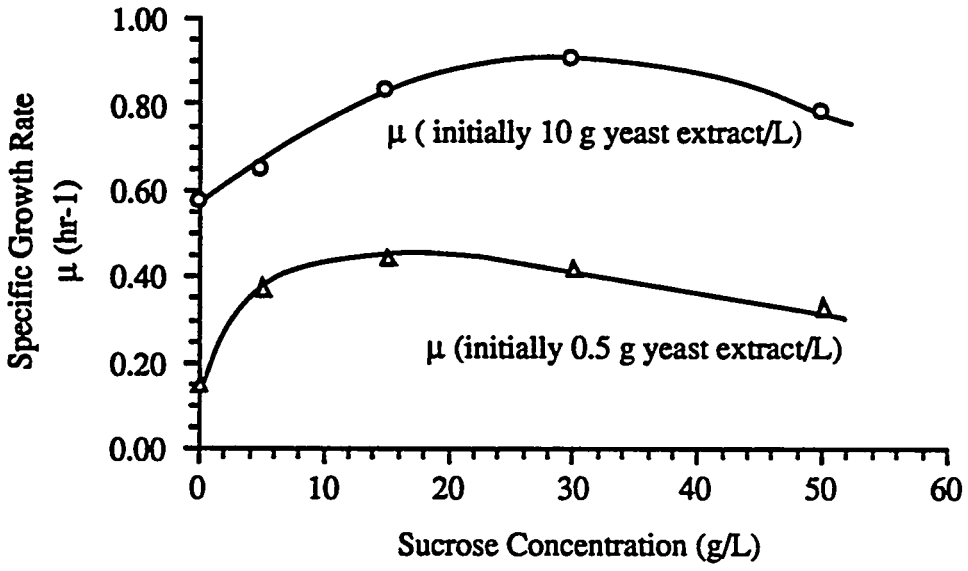

Figure 3.6. Specific growth rate as determined by batch culture experiments in media composed of varying sucrose concentrations and 10 or 0.5 g yeast extract/L.

Figure 3.7 presents the initial growth rate constants as a function of the initial yeast extract concentration without any sucrose present. These batch experiments contained a medium of trace mineral, as detailed in Appendix 3.B, and varying yeast extract

concentrations. As can be seen, the maximum growth rate of the cells on yeast extract alone is approached for yeast extract concentrations greater than 10 g yeast extract /L. Because yeast extract is itself a complex mixture containing amino acids, vitamins, purines and pyrimidines, it was expected that one or more components in the yeast extract were limiting cell growth. A comparison of the components needed by cells for growth [14] with the components found in yeast extract (Difco Laboratories, Detroit Michigan) gave an estimation of the chemical species that possibly limit cell growth yields. This comparison predicted that amino acids are the chemical species that would limit growth. Samples from three batch experiments were analyzed for free amino acid to determine which amino acids were being consumed to the greatest extent and thus limiting cell growth. Table III.1 summarizes the initial and end conditions for the three experiments. The results for cell growth on 5.0 g sucrose/L and 0.5 g yeast extract/L are representative of all three batch experiments and are presented in Figure 3.8. One observes up to 78 % utilization of the five amino acids that demonstrated the highest utilization during growth. Although not shown in the figure, all the sucrose in KE–25 D was consumed within 8 hours, the time at which dramatic decrease in amino acid concentration stopped. The maximum in the concentration of the free amino acids at approximately 3 hours is believed to be the result of the cell's ability to break the complex macromolecules (contained in the yeast extract) into free amino acids that are produced at a faster rate than they are consumed. However as growth continues, the rate of consumption surpasses production, resulting in the depletion of the free amino acids.

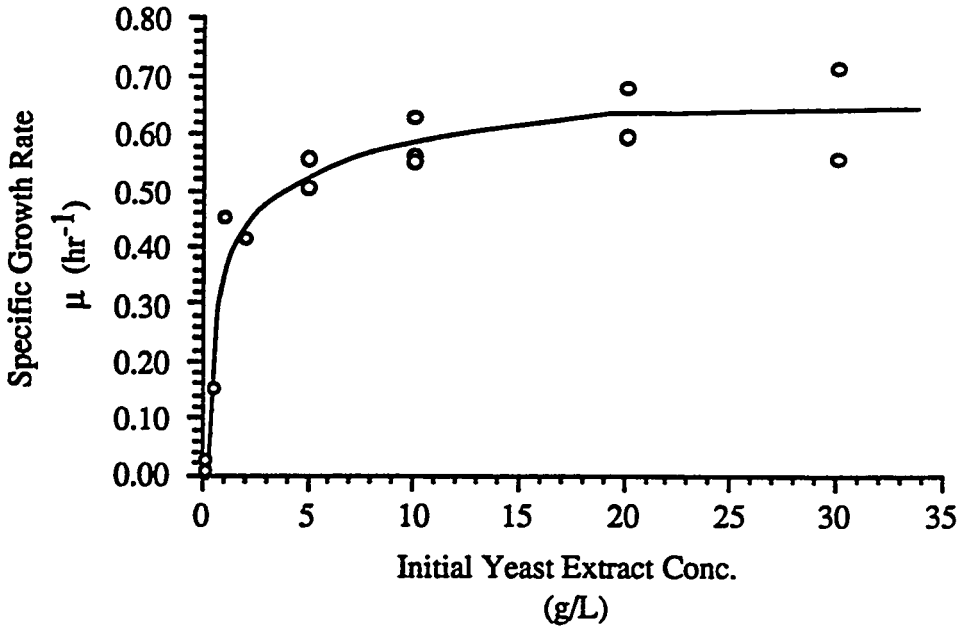

Figure 3.7. Specific growth rate constant as a function of yeast extract.

Table III.1. Summary of amino acid results.

Experiment	Nutrient Feed		Initial Specific Growth Rate μ (hr^{-1})	Sucrose Conversion	Amino Acids ** Conversion
	Sucrose g/L	Yeast Extract g/L			
KE-24D	5.0	10.0	0.649	100 %	0.0 †
KE-25D	5.0	0.5	0.377	100 %	up to 78 %
KE-28	0.0	1.1	0.166	none	up to 26 %

† - no statistical change in amino acid concentration

** - highest conversion (Valine, Tyrosine, Isoleucine, Leucine, Phenylalanine)

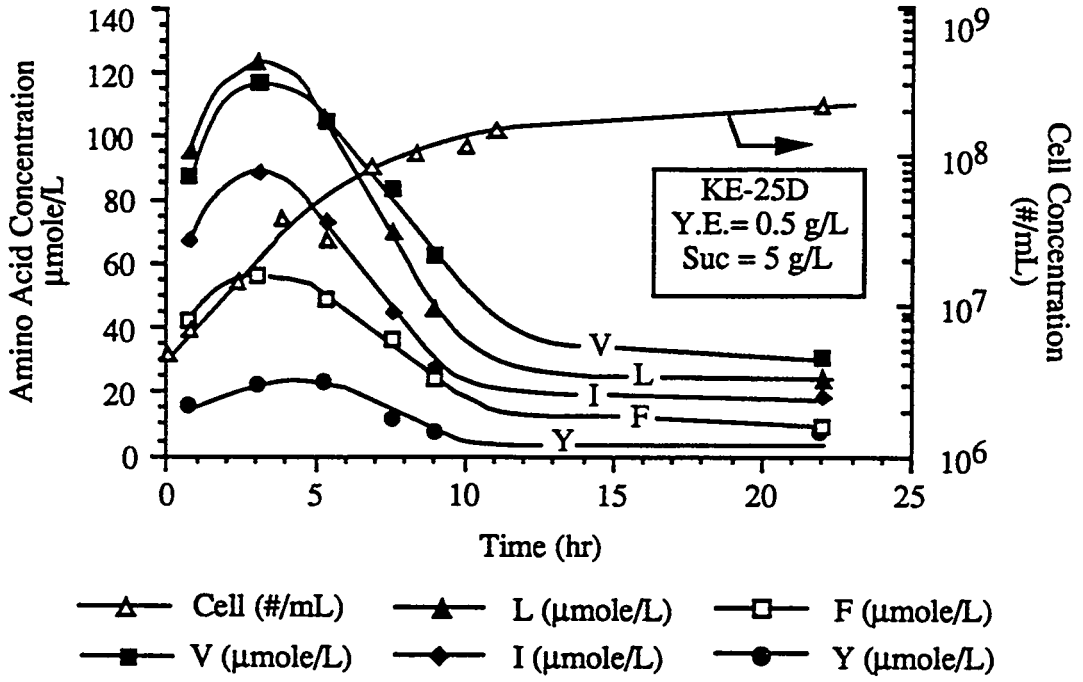

Figure 3.8. Amino acid consumption for batch growth of cells in 0.5 g yeast extract/L and 5.0 g sucrose/L

The results in Table III.1 indicates that the amino acids are primarily used by the cells as growth-factors during replication when a sufficient carbon source such as sucrose is present. Both experiments that used a growth medium containing sucrose, KE-24D (not shown) and KE-25D, demonstrated complete sucrose consumption with only partial consumption of the amino acids. When sucrose is provided as the sole carbon source (an absence of yeast extract), the cell exhibited no measurable growth. Yeast extract alone does not provide a sufficient carbon source to produce comparable yields when sucrose is present at equivalent concentrations. For low yeast extract concentration and no sucrose, relatively small changes in supernatant concentration of amino acids were observed.

Because these results indicate that multiple amino acids are consumed and that they may limit the cell growth rate, the development of a cell growth model is more complex

than that of a single-nutrient model. However, knowing that each of the growth-factors is always provided to the cells in yeast extract and that their concentrations will be approximately the same, a model can be developed assuming that the effect of all growth factors can be incorporated into a single parameter, the yeast extract concentration. This approach yields a specific growth rate model with only two parameters.

The results from the amino acid assays also allowed for determination of a minimal yeast extract to sucrose ratio of 0.14 g yeast extract/g sucrose needed by the cell for growth. This value is based on the relative amount of sucrose to I (isoleucine) consumed. Isoleucine had the highest conversion of all the 20 amino acids assayed for cell growth in 0.5g/L yeast extract and 5.0 g/L sucrose (KE-25D). The sucrose to isoleucine ratio was then converted to a sucrose-per-gram-of-yeast extract-basis by using the average concentration of free isoleucine found when 1 gram of yeast extract in dissolved in deionized water.

3.3.3.1 Specific Growth Rate Model

The following assumptions were used in the development of a two parameter model:

1) the yeast extract, which contains an array of complex nutrients, is represented by the bulk concentration in the specific growth rate model, and

2) sucrose growth inhibition is neglected.

Also knowing that the yeast extract does not provide the same carbon constant per unit mass as sucrose, the multiple limiting nutrient concentration model can be reduced to:

$$\mu = \mu_{max} \left(\frac{C_{ye}}{K_{ye} + C_{ye}}\right) \left(\frac{\alpha C_{ye} + C_s}{K_s + \alpha C_{ye} + C_s}\right) \qquad 3.9)$$

where:

C_{ye} - yeast extract concentration (g/L),
C_s - sucrose concentration (g/L),

α - yeast extract conversion factor (g sucrose/g yeast extract),
K_{ye} & K_S - are the respective Monod constants for yeast extract and sucrose, respectively (g/L).

The kinetic parameters in Equation 3.9 were determined from the experimental results using the method of least-square error minimization. The parameter estimates are given in Table III.2. This model is valid for yeast extract and sucrose concentrations up to 10 g/L and 50 g/L, respectively.

Table III.2. List of parameter estimates for specific growth rate model.

Parameter	
μ_{max}	0.9 hr^{-1}
α	0.5 g sucrose/g yeast extract
K_{ye}	0.3 g yeast extract/L
K_S	2.5 g sucrose/L

3.3.4 Substrate Utilization Experimental Results

During growth in sucrose media it is not known whether or not dextransucrase is the sole enzyme responsible for the production of fructose, glucose, and dextran, as depicted by Figure 3.5. *Leuconostoc m.* bacteria may also produce other enzymes, such as invertase, that can catabolize sucrose to glucose and fructose for cell growth. The development of the kinetic model, however, can exclude the need to know the individual concentration of dextransucrase and invertase if one combines the effect of the enzyme(s) into a bulk enzyme activity measurement. Consequently, the effect of multiple enzymes is combined into a single bulk enzyme concentration that is responsible for dextran production and the liberation of glucose and fructose. Experimentally, the concentration of the enzyme

is not determined as a molar concentration but as an activity, *i.e.*, its ability to convert sucrose into glucose and/or fructose.

The results of the batch experiments for cell growth and free enzyme(s) activity are presented in Figure 3.9. As can be seen, the enzyme(s) activity matches the production of cells up to the time when the cells reach the stationary growth phase at which point the activity of the enzyme begins to decline. In general, the initial enzyme(s) activity is attributed to cellular enzyme generation when sucrose is abundant. The subsequent decrease in activity after the stationary phase occurs because enzyme synthesis ceases, due to the lack of sucrose in the feed, and existing enzyme(s) degrade from toxic and thermal effects.

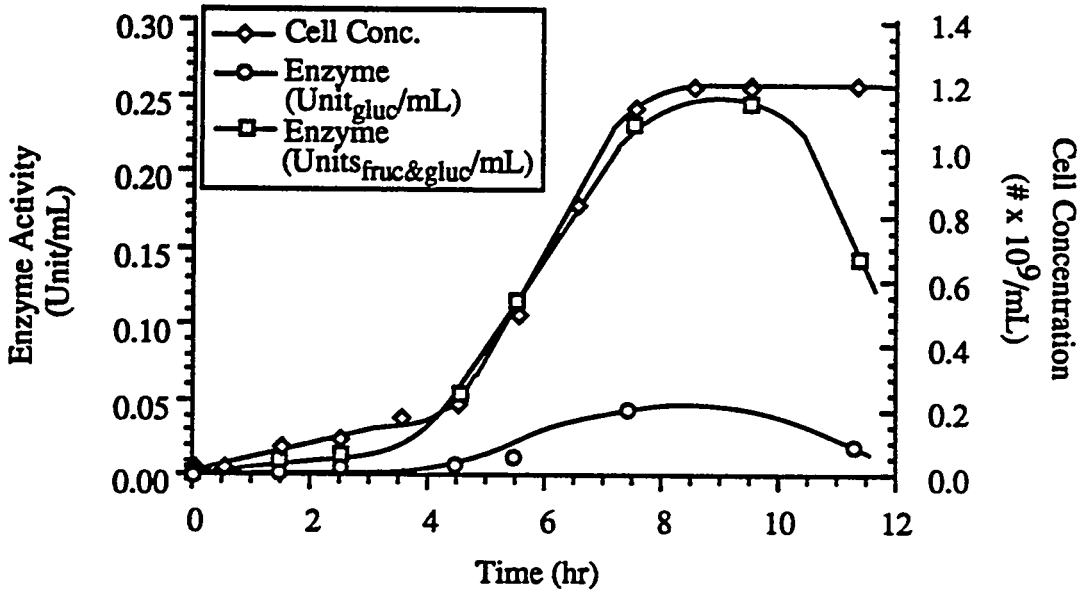

Figure 3.9. Enzyme and cell production during batch growth in 20 g/L sucrose and 10 g/L yeast extract

A series of batch growth experiments were carried out to determine the cell production yields on glucose and fructose. Figure 3.10 presents the cell concentration

from each batch reactor after 24 hours of growth as a function of initial monosaccharide concentration. The cell production yields would then be determined by calculating the ratio of the data (slope), assuming that all of the monosaccharide had been consumed during the 24 hour growth period, and that inoculum size was neglible with repects to final cell concentrations (which was verified experimentally). It can be seen from the data that the final cell yields were dependent upon the initial substrate concentrations up to concentrations of approximately 6.5 g/L. Cell growth under these conditions is believed to be substrate limited (substrate exhaustion). Above the 6.5 g/L limit, final cell concentrations did not vary with initial monosaccharide concentrations. This cell concentration plateau indicates that cell growth ceases in the batch reactor before complete substrate consumption. Most likely the production of metabolic toxins is responsible for this arrest in cell growth [Bailey and Ollis, 1977].

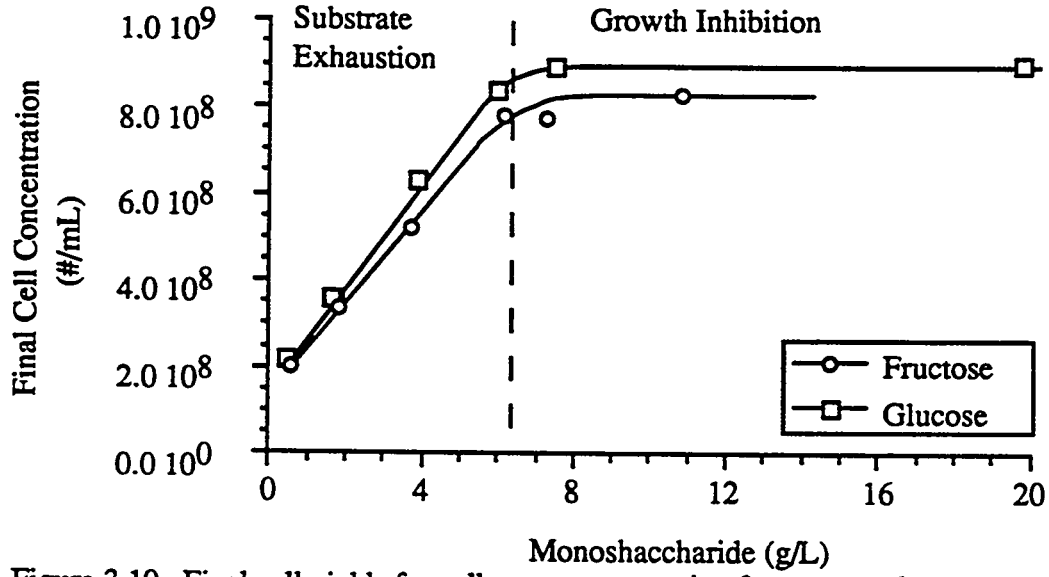

Figure 3.10. Final cell yields for cells grown on varying fructose or glucose media (media contains 10g yeast extract/L)

The cell production to substrate consumption yields for growth on the respective substrates were calculated from the slope of final cell concentration versus the initial substrate concentrations for only the substrate exhaustion region of Figure 3.10. Cell growth on glucose and fructose has a cell production to substrate consumption ratio of 1.1×10^{11} cells/g glucose and 9.9×10^{10} cells /g fructose, respectively.

3.3.4.1 Substrate Utilization Model

Sucrose, glucose, and fructose production and consumption balances for batch growth are:

$$\frac{dC_s}{dt} = -r_d - r_g \qquad 3.10)$$

$$\frac{dC_g}{dt} = \gamma r_g - Y_{g/x}\, r_x \qquad 3.11)$$

$$\frac{dC_f}{dt} = \gamma r_d + \gamma r_g - Y_{f/x}\, r_x \qquad 3.12)$$

where:

- r_i - is the rate of species i production (g/L·h or cells/L·h)
- Y_i - cell yield from species i consumption (cells/g),
- C_i - concentration of species i (g/L or cells/L),
- t - time (h),
- γ - 0.5263 (molecular weight ratio - monosaccharide to sucrose equivalent).

Subscript for kinetic parameters are:

x	- cell,	d	- dextran,
e	- enzyme,	g	- glucose,
f	- fructose,	s	- sucrose.

Using Lawford's model [1979] for dextran and glucose production (Equation 3.7), the above equations along with the cell balance can be rewritten:

$$\frac{dC_x}{dt} = \mu' C_x \qquad 3.13)$$

$$\frac{dC_s}{dt} = -(V_{max_d} + V_{max_g})\left(\frac{C_s}{K_d + C_s}\right) \quad 3.14)$$

$$\frac{dC_g}{dt} = \gamma V_{max_g}\left(\frac{C_s}{K_d + C_s}\right) - Y_{g/x}\frac{dC_x}{dt} \quad 3.15)$$

$$\frac{dC_f}{dt} = \gamma (V_{max_d} + V_{max_g})\left(\frac{C_s}{K_d + C_s}\right) - Y_{f/x}\frac{dC_x}{dt} \quad 3.16)$$

where:

K_d - Michaelis-Menten constant for sucrose utilization,

μ' - corrected specific growth rate for growth retardation (see Appendix 3.C).

The nutrient balance equations assumes that the maximal velocity for sucrose consumption is a function of the enzyme concentration [Fogler, 1992] as given by Equation 3.17:

$$V_{max_i} = \theta_i \frac{k_i}{k_f} C_e \quad 3.17)$$

where:

k_i - activity of the enzyme per volume per cell to produce product i @ 30 C and pH 5.2

θ_i - dimensionless reaction rate constant for sucrose consumption at reaction temperatures,

C_e - enzyme concentration responsible for fructose production.

The rate of enzyme production by the cells is modeled by the Leudeking and Piret equation [1959]. From the data presented in Figure 3.9, it is assumed that enzyme production rate, r_e, is strictly non-growth associated. Thus the following enzyme production model can be written as:

$$\frac{dC_e}{dt} = r_e = k_f C_x \quad 3.18)$$

By assuming that the specific growth constant, μ', is constant, the enzyme production equation can be integrated to produce the following relation between cell growth and enzyme production:

$$C_e = \frac{k_f}{\mu'} C_{xo} (e^{\mu'} - 1) \qquad 3.19)$$

From this equation the activity of the enzyme, k_f, was estimated and is presented in Table III.3. Similarly, k_d and k_g can be estimated from respective enzyme activity data for dextran and glucose production.

For the above model only the reaction rate constants (θ_i) in Equation 3.17 have not been defined. Using the data from a growth experiment that include cell, saccharide, and dextran concentrations as a function of time, in conjunction with the above model, allows for the determination of the reaction rate constants. These reaction rate constants are provided in Table III.3, while Figure 3.11 present the model prediction for one particular set of growth conditions and compares the prediction to experimentally determined data.

3.3.5 Polysaccharide Production Experimental Results

The batch experiments used to quantify the growth rate results were also used to obtain insoluble dextran production data. The dextran production curves for four batch reactor experiments in Figure 3.12 show an increase in dextran yields with increases in initial sucrose concentration. This result is expected because the rate of dextran production is dependent upon the concentration of sucrose provided in the media [Lawford *et al*, 1979].

Table III.3. Parameter estimates for substrate utilization model.

Parameter	
θ_d	0.07 g sucrose/Unit/hr
θ_g	1.23 g sucrose/Unit/hr
k_d	13.7 pUnits/cell/hr
k_g	84.1 pUnits/cell/hr
k_f	97.8 pUnits/cell/hr
K_p*	10.3 g sucrose/L

* - based on Ebert *et al* [1968] and Lawford *et al* [1979]

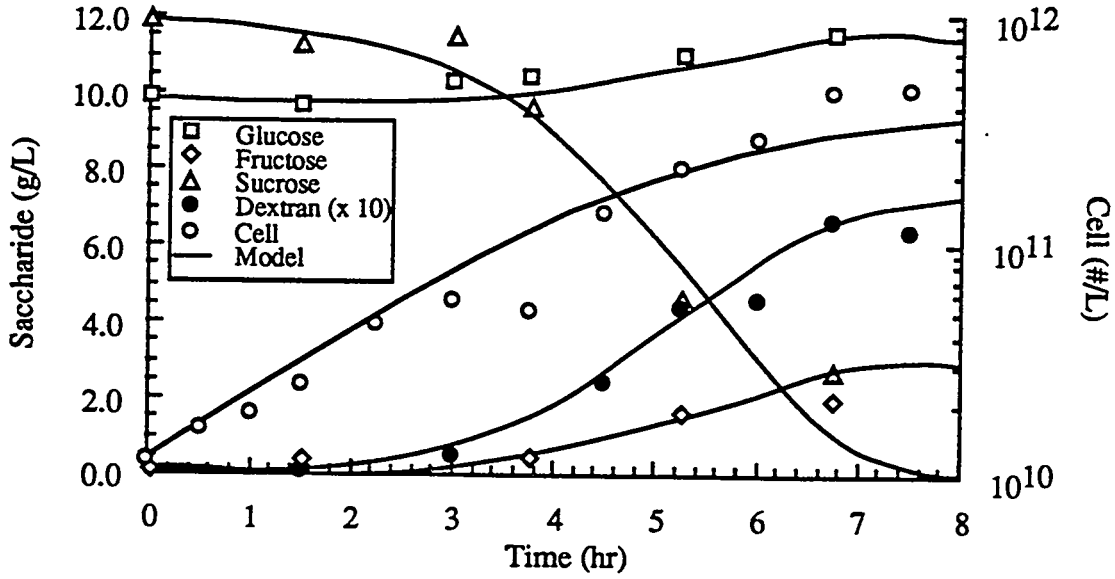

Figure 3.11. Predicted versus experimentally determined saccharide and cell concentration for batch growth.

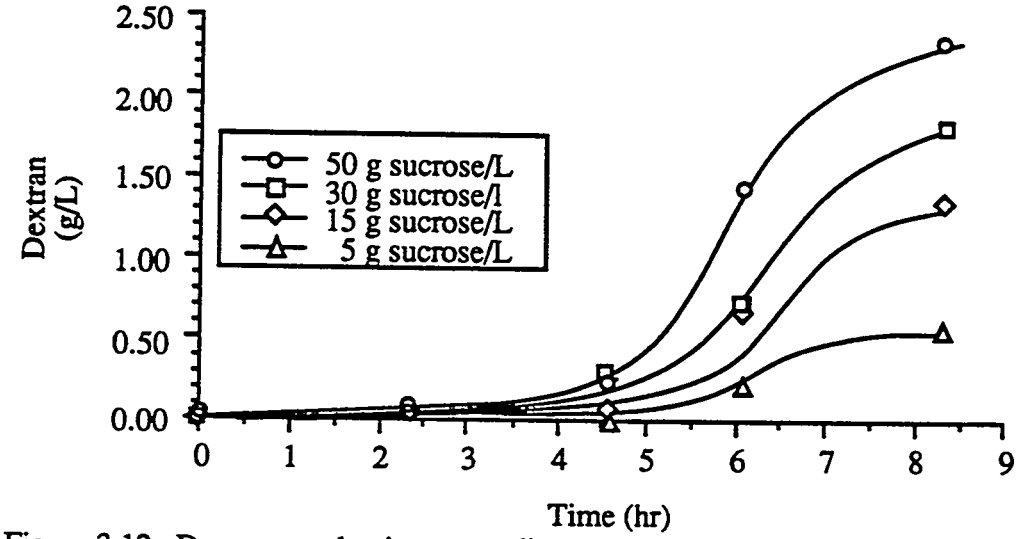

Figure 3.12. Dextran production on media containing 5, 15, 30 and 50 g sucrose/L and 0.5 g yeast extract/L

3.3.5.1 Polysaccharide Production Model

Recalling Equation 3.4, where dextran is synthesized at the expense of sucrose, the rate of dextran production can be equated with the rate of fructose liberated by the enzymes according to:

$$\frac{dC_d}{dt} = Y_{d/m} \frac{d(C_f - C_g)}{dt} \qquad 3.20)$$

where :

$Y_{d/m}$ - insoluble dextran to fructose production yield (g dextran/g monosaccharide),
C_d - product concentration (g/L),
C_f - concentration of fructose produced (g/L),
C_g - concentration of glucose produced (g/L).

Note that the above model excludes fructose liberated during glucose production, as given by Equation 3.5. The ratio $Y_{d/m}$ was estimated as 0.24 g dextran /g fructose from the polysaccharide production batch experiments. In addition to di- and mono saccharide consumption/production, Figure 3.11 present the model prediction for dextran production.

According to the stoichiometry of Reaction 4 the expected value of $Y_{d/m}$ is 1.0 g dextran /g fructose if all of the dextran produced is insoluble . However, dextran is a biopolymer that initially develops from a monomer into a polymer containing typically over one hundred thousand monomer units [Ebert *et al*, 1968]. This change in polymer length alters the chemical properties of the polymer molecule from soluble to insoluble. Thus a $Y_{d/m}$ value of 0.24 g dextran /g fructose implies a 76 % of all the dextran produced is soluble.

3.4 Manipulation of Nutrient Feed for Plug Control

As illustrated by the core plugging experiment, the plugging of porous media by *in situ* bacterial growth is dependent upon the cell's ability to produce polysaccharide. In addition, results from core staining[Lawford *et al*, 1979] have shown that the movement of cells within porous media is influenced by the cell's ability to produce polysaccharides. Hence, cell transport and retention in porous media can be facilitated by controlling the cell's ability to produce polysaccharide. Controlling bacterial production of polymers is accomplished by controlling the ratio of macro-nutrients such as nitrogen and phosphorous to carbon [Eavans *et al*, 1979]. Because yeast extract provides the *Leuconostoc m.* bacteria with the needed macro-nutrients, such as nitrogen and phosphorous to carbon, altering the ratio of yeast extract to sucrose would influence the amount of polymer produced per cell. Figure 3.13 shows the results from two growth model simulations at an initial sucrose concentration of initially 50 g/L with varying yeast extract concentrations. As seen from the predictions, dextran production per cell increases as the amount of yeast extract provided decreases. The model predicts a higher dextran to cell production yield on lower yeast extract concentration because yeast extract influcence the cell growth rate but does not influence enzyme production, since enzyme production is non-growth related product. Thus the result of varying yeast extract to sucrose concentration, when one considers two parallel growth systems with equal inoculum concentration, is the relatively equal initial enzyme production rates but a reduced cell production rate for low yeast extract concentrations and hence varying dextran per cell production rates. These results demonstrate that the plugging rate of porous media by *Leuconostoc m.* for BPM can be influenced by the concentration of the various nutrients provided to the cell for *in situ* growth.

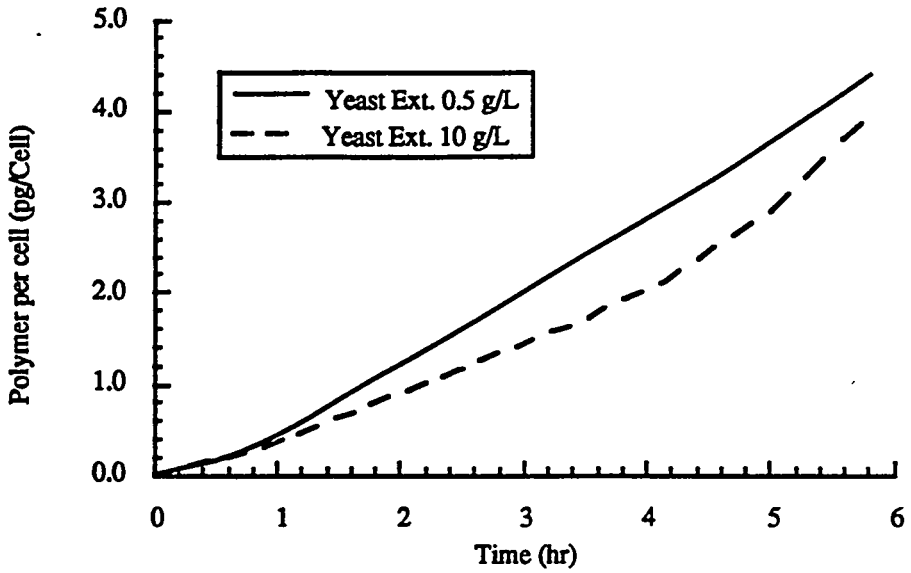

Figure 3.13. Dextran production per cell on media containing 50 g sucrose/L and 0.5 and 10 g yeast extract/L (Simulation results)

3.5 Conclusions

A model for the growth kinetics of cells grown on sucrose without product inhibition has been developed. The model reflects experimental results that show both the yeast extract and sucrose concentrations affect cell growth rate. Sucrose is used by cells as a carbon source while yeast extract primarily provides the cells with needed growth-factors for cell enzyme synthesis. Batch experiments have shown that sucrose is consumed at a faster rate than glucose or fructose, while cell growth on a glucose-fructose media has not shown any preference for either monosaccharides. This result supports the hypothesis that the cell is externally catabolizing the sucrose to produce dextran, glucose and fructose, and that the monosaccharides are then transported into the cell for growth. A substrate utilization model has been found to predict the growth rate of the cells. The insoluble dextran production experiments have demonstrated that final polymer production yields are dependent upon the availability of sucrose in the feed. These results can be modeled by equating dextran production with fructose production during dextran synthesis. Final model predictions show that the dextran (polysaccharide) to cell production ratio can be

altered by controlling the yeast extract to sucrose feed ratio. Controlling the amount of dextran produced per cell will be useful in the development of an injection strategy for *Leuconostoc m.* for Bacterial Profile Modification.

3.6 Nomenclature

C_i - concentration of component i (g/L or cells/L)
k_i - non-growth associated production constant (h^{-1})
K_i - Monod (or Michaelis) constant for component i (g/L)
Q_l/Q_h - flow rate of fluid through high permeability core relative to low permeability core
r_i - rate of product i formation (or nutrient consumption) per unit volume (g/L·h or cells/L·h)
t - time (h)
V_{max_i} - maximum velocity for species i (g/L·h)
$Y_{i/j}$ - growth attributed product i constant (g of i /g of j)
α - yeast extract conversion factor (g sucrose/g yeast extract)
γ - 0.5263 (molecular weight ratio - monosaccharide to sucrose)
μ - specific growth rate (h^{-1})
μ_{max} - maximum specific growth rate (h^{-1})
θ_i - dimensionless reaction rate constant for sucrose consumption-product i formation

Subscript

x	- cell	d	- dextran
e	- enzyme	g	- glucose
f	- fructose	s	- sucrose
m	-monosaccharide	ye	- yeast extract

3.7 References

Bailey, James E. and David F. Ollis, *Biochemical Engineering Fundamentals*, McGraw Hill Book Co., 1977

Chaplin, M.F. and J.F. Kennedy, Carbohydrate Analysis, IER Press, Oxford England, 1986

Ebert, K.H. and G. Schenk, "Advances in Enzymology and Related Areas of Molecular Biology", Editor F.F. Nord Vol. 30, 1968, International Publishers

Evans, C.G.T., Yeo, R.G., Ellwood, D.C., Continuous Culture Studies on the Production of Extracellular Polysaccharides by *Xanthomas Juglandis*, In: Microbial Polysacchrides and Polysaccharases, Berkeley, R.C.W., Gooday, G.W., Ellwood, D.C. (eds.), Acedemic Press, NewYork, 1979

Fogler, H.S., *Elements of Chemical Reaction Engineering*, Prentice Hall New Jersey, 1992

Geesey, G.G., M.W. Mittelman, and V.T.Lieu, Evaluation of Slime-Producing Bacteria in Oil Field Core Flood Experiments, *App. and Env. Micro.*, 278-283, Feb. 1987

Gottschalk, G. *Bacterial Metabolism*, Second Edition, Springer-Verlag, 1985

Hart, R.T., T. Fekete, and D.L. Flock, The Plugging Effect of Bacteria in Sansstone Systems, *The Canadian Mining and Metallurgical Bulletin*, 495-501, July, 1960

Jack, T.The Potential for use of Microbes in the Production of Heavy Crude, *Proceeding of International Conference on Microbial Enhancement of Oil Recovery*, May 16-21 1982, Shangri-La, Afton, Oklahoma

Lappan, R.E., Fogler,.H.S. 1990. The effects of bacterial polysaccharide production on formation damage. Soc. Petro. Eng. **SPE 19418**: 165-172

Lawford, G.R., A. Klingerman, T. Williams, "Dextran Biosynthesis and Dextransucrase Production by Continuous Culture of *Leuconostoc mesenteroides*", *Biotechnology and Bioengineering*, XXI, 1121-1131, 1979

Leudeking, R., Piret, E.L. A kinetic study of the lactic acid fermentation, *J. Biochem. Microbiol. Technol.* Eng., **1**: 393, 1959

Raleigh, J.T. and D.L. Flock, A Study of Formation Plugging with Bacteria, *J. of Petro. Tech.*,pg. 201, Feb. 1965

Stanier, Roger Y.,John L. Ingraham, Mark L. Wheelis, and Page R. Painter: The Microbial World, Fifth Edition, Prentice-Hall, New Jersey, 1986

Appendix 3.A
Surface Effects on Cell Growth

Two set of experiments were performed in agitated batch reactors with cells of *Leuconostoc. m.* using glucose or sucrose as substrates. All experimental conditions being identical, growth experiments were conducted in absence or in presence of clay particles (montmorillonite). Batch experiments were performed in 0.1 L sealed flasks, under a constant stirring, with an additional 0.1 g of montmorillonite clays in flasks used for the adsorption on clays. Whatever the sugar used, its concentration was 8.6 g/L for each experiment and other medium components were identical. Flasks were inoculated with 1 mL of a suspension of *Leuconostoc.m.* grown on sucrose. Samples of the culture were taken every 2 hours or after a significant increase in medium turbidity was observed. For samples taken from glucose medium and in absence of clays, cell concentration was determined spectrophotometrically. Samples taken from sucrose medium (no clays) and from experiments performed in presence of montmorillonite, were centrifuged (3000 g, 10 min.) prior to further measurements. Centrifugates were dried until constant dry weight and their mass was measured. For batch cultures realized with sucrose, the measured mass of cells included the mass of insoluble dextran produced around the cells (the mass of clays was deducted from the total sample mass for cells grown in the presence on montmorillonite).

Figure 3.A.1 reports the cell densities growth for the two batch experiments performed in the absence and presence of clays with glucose as the main carbon source, while Figures 3.A.2 illustrates the biomass increase obtained in absence and presence of clays with sucrose as the main nutrient component. A comparison of the specific growth rate constants for each growth curve, as given by Table 3.A.1, illustrates the influence the clay surface on the rate of cell growth. For both saccharides, the presence of the clays did not significantly enhanced the specific growth rate of the cells. Thus it is concluded that the

data obtained from the constant stirred batch reactor is the absence of any supporting surfaces will suffice for the development of an in situ bacterial growth model.

Table 3.A.1. Specific growth rates for of *Leuconostoc.m* bacteria growth in batch reactors in the presence or absence of montmorillonite

Saccharide	Specific Growth Rate Constant, μ (hr^{-1})	
	no clays	clays
Glucose	0.37	0.394
Sucrose	0.473	0.471

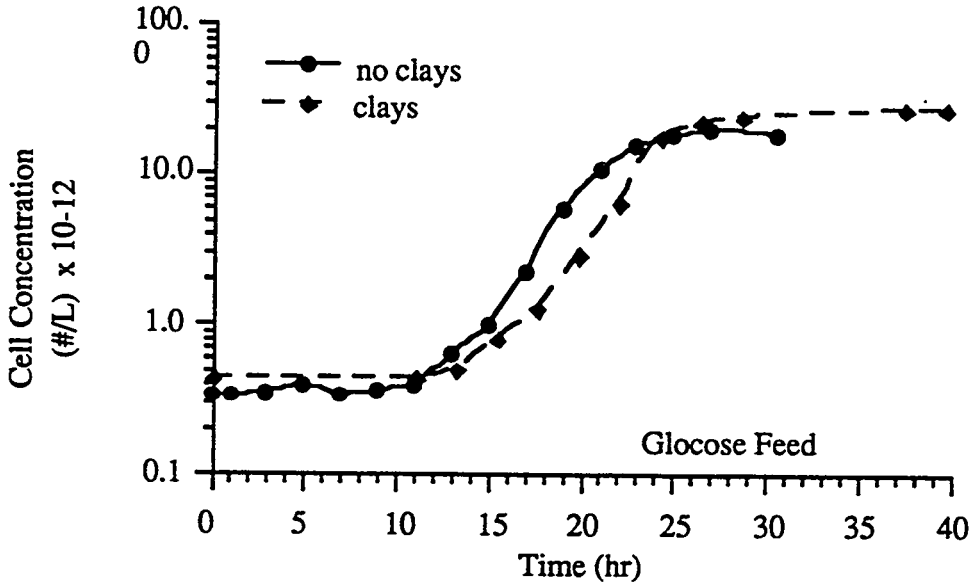

Figure 3.A.1. Batch growth curves for *Leuconostoc m.* on glucose in the presence and absence of montmorillonite

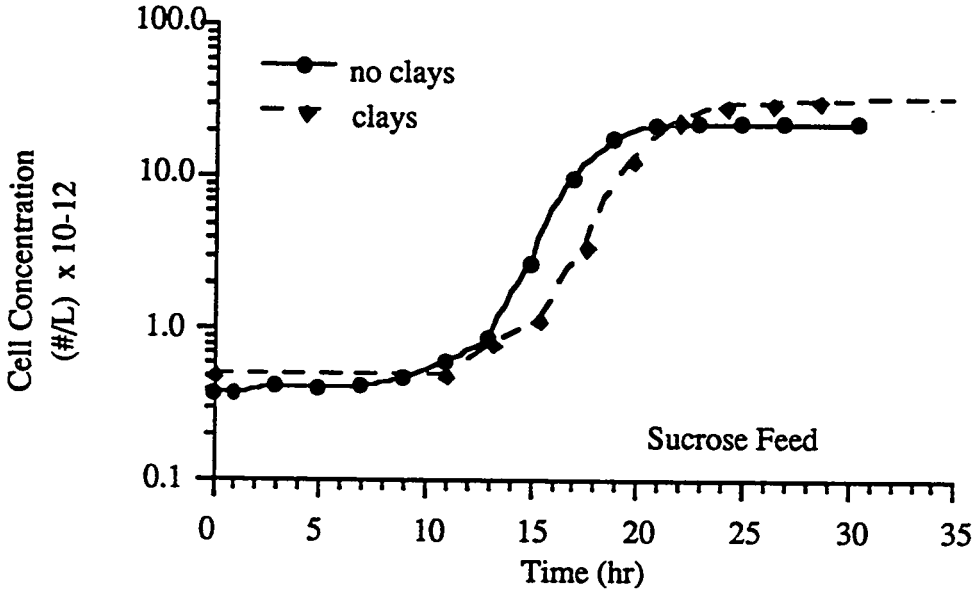

Figure 3.A.2. Batch growth curves for *Leuconostoc m.* on sucrose in the presence and absence of montmorillonite

APPENDIX 3.B

Nutrient Recipes

Table 3.B.1. Medium for carbohydrate experiments

Tap Water	1000 mL
Tryptone	20 g
Yeast Extract	5 g
NaCl	4 g
Sodium Acetate	1.5 g
Ascorbic Acid	0.5 g
Trace Elements (Ca,Mn,Fe,Mg)	
Carbohydrates	
Sucrose	15 g
or	
Fructose	7.9 g
Glucose	7.9 g

Yeast extract (and tryptone) are supplied to the cells as the sources of amino acids, purines, pyrimidines, and vitamins, which are needed by the cells for growth because *Leuconostoc* cells can not synthesize these compounds for themselves [Stanier*et al.*, 1986]

Table 3.B.2. Medium for kinetic experiments.

Tap Water	1000 mL
Yeast Extract	10 g
NaCl	4 g
Sodium Acetate	5 g
Ascorbic Acid	0.5 g
Potassium Phosphate dibasic	1 g
Trace Elements Ca,Mn,Fe,Mg	
Sucrose	

Table 3.B.3. List of recommended concentrations of amino acid content for cell growth compared to concentrations in yeast extract.

Amino Acid		Suggested Concentrations **		Yeast Extract Content †		
		mg/L	% (wt)	mg/L	% (wt)	ratio
alanine	A	200	6.36			
arginine	R	242	7.70	10	1.00	0.04
asparagine	N	400	12.72			
aspartic	D	100	3.18	50	5.00	0.50
cysteine	C	50	1.59			
glutamic	E	300	9.54	65	6.50	0.22
glycine	G	100	3.18	25	2.50	0.25
histidine	H	62	1.97	10	1.00	0.16
isoleucine	I	250	7.95	30	3.00	0.12
leucine	L	250	7.95	35	3.50	0.14
lysine	K	250	7.95	40	4.00	0.16
methionine	M	100	3.18	10	1.00	0.10
phenylalanine	F	100	3.18	20	2.00	0.20
proline	P	100	3.18			
serine	S	50	1.59			
theonine	T	200	6.36	35	3.50	0.18
trytophan	W	40	1.27			
tyrosine	Y	100	3.18	50	0.50	0.05
valine	V	250	7.95	35	3.50	0.14

** -based on recommendations by Stanier et al.[1986]; percentages relative to total amino acid added into growth media

† -based on 1 g yeast extract/L, percentages based on amino acid content relative to total mass

APPENDIX 3.C
Logistic Model

When comparing the kinetic model to the batch growth data for cell growth on sucrose and glucose (see Figure 3.3), it was noted that the predicted specific growth rate was overestimated by Equation 3.9. This discrepancy is due to the transfer of toxins with the inoculum in this batch experiments. The inoculum used for this experiment for which the results are also presented in Figure 3.11 were not separated from the initial growth media and thus toxins were transfered that impeded the cell growth.

A growth retardation model has been used to account for the effect toxins on the specific growth rate constant and is defined by Equation 3.C.1:

$$\mu' = \mu(C_s, C_{ye}) \left(1 - \frac{C_x}{C_{x_{max}}}\right) \qquad 3.C.1)$$

where:

$\mu(C_s, C_{ye})$ - the specific growth rate (given by Equation 3.9)

$C_{x_{max}}$ - maximum cell concentration.

$C_{x_{max}}$ was estimated from the batch data for cell growth as 4.2×10^{11} cells/L.

4.0 Task II - Cell Transport Experiments

Task Description:

a) Quantify the importance of polysaccharide production as the retention mechanism

b) Characterize and understanding this mechanism at the microscopic level through visualization experiments.

Quantifying the effect of polysaccharide (dextran) production on cell transport in porous media has been divided into three phases: cell transport experiments, *in situ* bacterial growth experiments in two micromodels and an *in situ* growth experiment in a consolidated core. The cell transport experiments were designed to demonstrate the importance of polysaccharides as a binding polymer that bridges cells to the internal surfaces of the porous media. In these experiments, transport of dextran coated bacteria was compared to transport of uncoated bacteria in a micromodel, under non-growth conditions. The *in situ* growth experiments in both micromodel and consolidated porous media were designed to study the effect of *in situ* dextran production during growth of cells. The effects of dextran production on cell retention and subsequently on the changes in permeability of the porous media were of particular interest. The micromodel experiments yielded visual results that provided an understanding of the retention mechanism; quantification of the effects of this mechanism on the overall permeability of the porous media and determination of a cell balance to quantify cell retention was accomplished in core flooding experiments. The consolidated core plugging experiments allowed for the correlation of permeability with *in situ* growth and dextran production. Understanding the over effect of the retention mechanism on the permeability of the porous media facilitated the development of a *in situ* growth model that describes porous media permeability reduction as presented in Task III (Chapter 5).

4.1 Materials and Methods

To investigate the influence of insoluble dextran on transport properties of *Leuconostoc mesenteroides*, two transport experiments were carried out under analogous conditions for cells grown on a glucose-fructose mixture (TE-1) and cells grown on sucrose (TE-2). In these experiments, cells were not growing as they were transported through the micromodel. During these two experiments, the flow of cells through a glass micromodel was monitored and recorded on video tape (see Appendix 4.A for a description of the apparatus). Micromodels allow visualization of physical phenomena in 2-dimensions. The micromodel pattern used for these transport experiments are illustrated in Figure 4.1 a) with further discussion of the pattern layout given below. In addition, the inlet pressure and effluent cell concentration were recorded. Effluent cell concentrations were monitored continuously by means of a flow-through spectrophotometer ($\lambda = 560$ nm, cell volume 100 μL.) The complete procedure involved three steps that allowed for the examination of polysaccharides on cell transport:

1. Injection of a 0.1M NaCl solution in the clean network.
2. Injection of bacteria suspended in a 0.1M NaCl solution, until reaching stationary conditions at the outlet of the network (saturation with cells). The cell concentration was approximately 10^8 cells/mL for TE-1 and 2.0 10^9 cells/mL, for TE-2.
3. Injection of deionized water.

All steps were performed at a flow rate of 0.02 cm^3/min. which corresponds approximately to 5 ft/day. Prior to cell injection, the residence time distribution of the fluid in the network was determined from a tracer experiment.

The *in situ* growth experiments, both micromodel and consolidated core plugging experiments, were conducted using similar procedures. These experiments consisted of two phases: the initial injection of bacteria into the porous medium followed by the injection

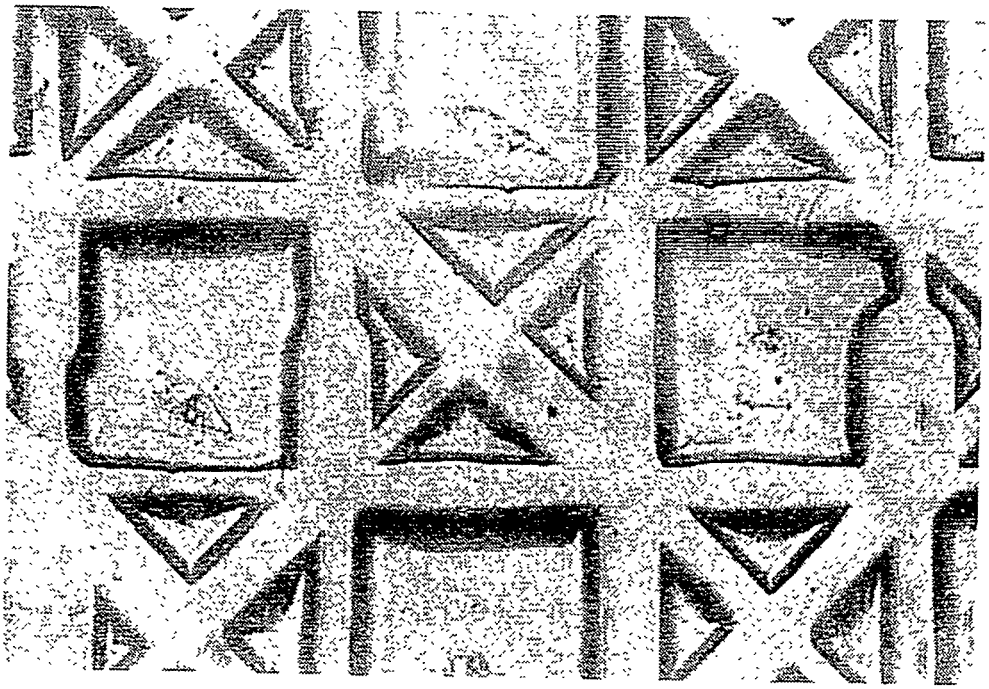

a) transport experiments

b) *in situ* growth experiments

Figure 4.1. Magnification of the 2-dimensional micromodel for transport experiments and *in situ* growth experiments

of a nutrient feed into the porous medium to promote cell growth and polymer production. The inoculum cells were grown in a feed solution, that promoted cell growth and excluded any dextran production, as a batch culture for a 24-hour period. In both types of experiments, the inoculum was removed by centrifuging (@4480 g for 5 min.) and the cells were suspended in new growth media. Cell separation and suspension in new growth media eliminates the time required to displace the original feed from the porous media once the cells are injected and feeding has commenced. The porous media was saturated before inoculation. In the micromodel experiments, a back pressure of 50 psi (nominal) was applied during this saturation and maintained throughout the experiment. The purpose of the back pressure was to keep CO_2 generated during cell metabolism in solution so that the gas bubbles did not displace cells from the network. For both types of experiments, the inoculum was injected as a pulse at a constant volumetric flow rate into the porous media. Nutrient feed was subsequently injected into the porous media at a constant volumetric flow rate (see Table 4.1 for feed composition). The pressure drop across the porous media was monitored. The consolidated core apparatus also has pressure taps located along the length of the core, as lists in Table 4.1. The composition of the inoculum growth media, the feed composition, and the location of the pressure taps for the experiments are presented in Table 4.1. Effluent cell concentrations were determined by Coulter Counter. Sucrose concentrations (consolidated core) were assayed using the invertase-dinitrosalicylic acid technique, as detailed in Chapter 3. The apparatus and procedures used for the *in situ* growth experiments are detail in Appendix 2.A for consolidated cores and Appendix 4.A for the micromodel experiment. The micromodel pattern used for the *in situ* growth experiments is presented in Figure 4.1 b). This patterns illustrates the channel, which represents the throat, and the node which emulate the pore bodies. Note that in this pattern each node has 6 connecting bonds, giving the network a connectivity of 6 which is representative of typical porous media [Rege and Fogler, 1987].

Table 4.1. Experimental material characteristic and procedures for *in situ* growth experiments

	Micromodel (ME-1)	Micromodel (ME-2)	Consolidated Cores
Inoculum			
-initial growth media	10 g YE/L 7.9 g glucose/L 7.9 g fructose/L	10 g YE/L 7.9 g glucose /L 7.9 g fructose /L	10 g YE/L 7.9 g glucose /L 7.9 g fructose /L
- inoculum preparation centrifuged at 4400 g and suspended †	yes	yes	no
- injection rate (mL/min)	0.008	0.008	5.0
- injection duration (min)	18 hr	20 hr	57
- cell concentration (cells/L)	-	-	1.14×10^{11}
Core			
- diameter (cm)	-	-	2.58
- length(s) (cm)	-	-	10.1
- pore volume (cm^3)	0.08	0.08	
- permeability(ies) (mD)	-	-	3 000
- core presaturation composition	same as nutrient media	same as nutrient media	same as inoculum media
Feed			
- composition	10 g YE/L and 15.8 g each of glucose & fructose for 48 hours, followed by 10 g YE/L and 30 g sucrose/L	10g YE/L 30 g sucrose/L	10 g YE/L 20 g sucrose/L
- injection rate (mL/min)	0.008	0.008	5.0 (t<30 min.) 1.0 (t≥30 min.)
- pressure tap locations from injection face (mm)	inlet outlet	inlet outlet	inlet 5 30 81

† - suspended in a ~500 mL of feed solution
YE - yeast extract (Diffco)

For the consolidated core plugging experiment the core sample was prepared by taking a ceramic rod and fracturing its ends to the desired length of 10 cm (4 in.). The fracturing procedure was used to eliminate cutting fines that may interfere with the injection of bacteria into the core. This procedure is a modification of the core preparation techniques used for the earlier experiments, as presented in the Background section.

4.2 Results and Discussion

The experimentation was divided into three parts: the transport experiments and the *in situ* growth experiments in both the micromodels and consolidated cores. Results demonstrate the effect of increased cell retention in porous media when cellular polysaccharide is present, resulting in a reduction of porous media permeability.

4.2.1 Transport Experimental Results

The injection pressure (P/P_0) and the effluent cell concentration (C/C_0) are reported in Figures 4.2 (TE-1: non-coated cells) and 4.3 (TE-2: dextran-coated cells). During TE-1, no channel plugging was observed and cell capture was in the form of aggregates rather than single cells. The building of these aggregates (clusters of cells) was a slow process that only became visible after 1 hour of injection. Aggregates were located mainly on the edges of the network as depicted on Figure 4.4 (a). No meaningful variation in pressure was recorded during the run, and the shape of the cell breakthrough curve showed a temporary increase when the injection solution was shifted to deionized water (see Figure 4.2). This increase in cell concentration is possibly the result of switching the injection solutions from concentrated cell suspension to deionized water causing readjustments of pressure. The effluent cell concentration results can not be used for quantification of the retention of cell in the porous media because the results do not provide an accurate cell balance. It was speculated that bacteria adhered to the wall of the quartz flow through cuvet that interfered with effluent cell concentration measurements and provided inaccurate cell

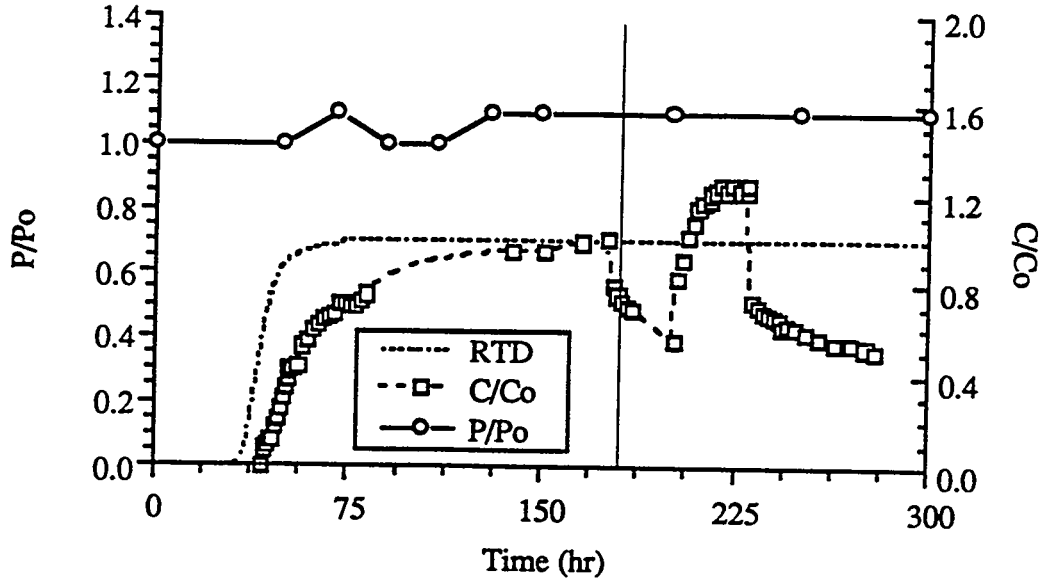

Figure 4.2. Normalized pressure, uncoated cell breakthrough curves, and RTD for micromodel

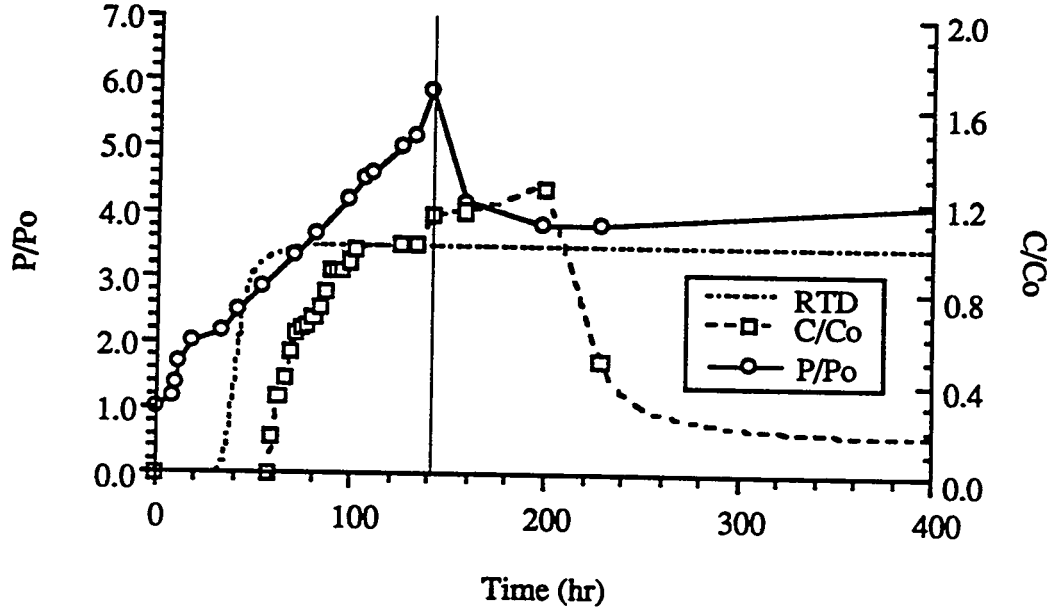

Figure 4.3. Normalized pressure, dextran coated cell breakthrough curve, and RTD for micromodel

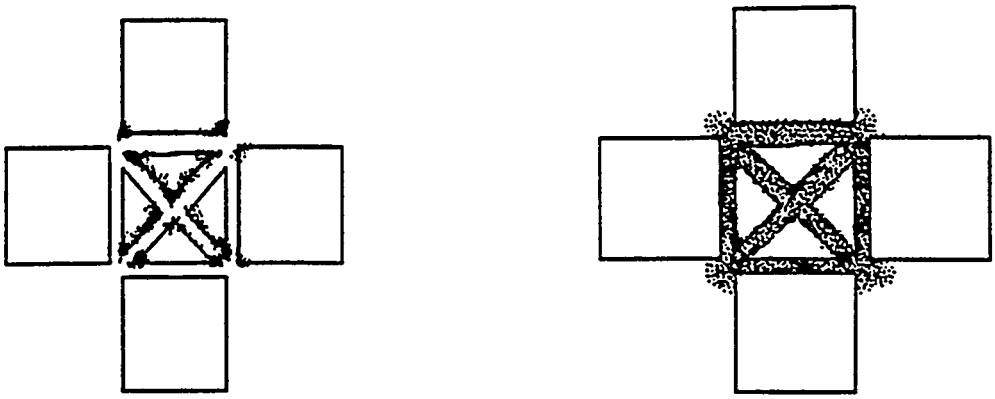

(a) (b)

Figure 4.4. Final state of a representative network's element for TE-1 and TE-2

concentration readings. For this reason effluent cell concentration in the subsequent *in situ* growth experiments were determined by periodic sample collection and Coulter Counter analysis.

During TE-2 (see Figure 4.3) channel plugging was observed after 2 hours of injection. Cells were in the form of aggregates rather than single cells as in TE-1. Examination of the video recording showed that the build up of aggregates on the walls was faster and more significant, however, as compared with TE-1. In addition, aggregates invaded the void space as well as all the surfaces. A rapid and dramatic increase in pressure was recorded during the cell injection step. Pressure began to decrease immediately as deionized water was injected. At the end the water injection step, however, the pressure was still about 4 times the initial pressure.

Main comparisons between TE-1 and -2 are reported in Table 4.2. Comparison between TE-1 and -2 suggest that the presence of dextran around the cells is dramatically affecting cell transport efficiency. It was initially assumed that the dextran caused cells to adhere to surfaces thus reducing transport through the porous media. However, further cell growth experiments in capillary tubes have shown (as detailed in Appendix 4.B) that

the dextran does not bind cell to surfaces. It was then speculated that aggregate formation occurs from cell replication in which new cells remained as aggregates due to the presence of dextran. Mechanical capture of these aggregates would then be one of the key mechanism controlling the retention of bacteria. The *in situ* growth experiments in the micromodel confirmed this speculation as discussed in the next section.

Table 4.2. Summary of the two cell transport experiments using polymerically coated and uncoated cells.

Characteristics	TE-1 (non coated cells)	TE-2 (Dextran-coated cells)
Pressure Drop	Almost negligible	$P/P_O = 5.6$
Localization of Adsorbed Cells	Network's Edges	All the Available Surfaces
Desorption and Permeability Restoration (by the injection of distilled water)	Partial Desorption	Partial Desorption No Restoration

4.2.2 Micromodel Plugging Experiment

Unlike the transport experiments reported in Section 4.2.1, *in situ* cell growth and polymer production occurred in the micromodel plugging experiment. Under these conditions, corresponding changes in cell morphology, location of biomass within the porous media, and pressure responses could be observed directly. These observations provided insight into cell capture, retention, and release mechanisms occurring on the microscopic level.

The change in pressure with time is presented in Figure 4.5 for the first micromodel experiment (ME-1). For the first 48 hours, the nutrient contained of glucose and fructose

as carbon source. Under these conditions, polymer was not produced. As can be seen in Figure 4.5, there was no measurable increase in pressure during this period. After 48 hours, the nutrient was changed and sucrose at the stoichiometric equivalent of the glucose-fructose was used as summarized in Table 4.1. Approximately five hours after sucrose injection was initiated (at 53 hours of total time), small pressure oscillations began (< 10 psi). Nineteen hours after initiation of sucrose injection (at 67 hours of total time), the pressure had increase dramatically. For all later times, large oscillations in pressure occurred. The maximum and minimum pressures during these oscillations did not change greatly in magnitude between 67 and 80 hours.

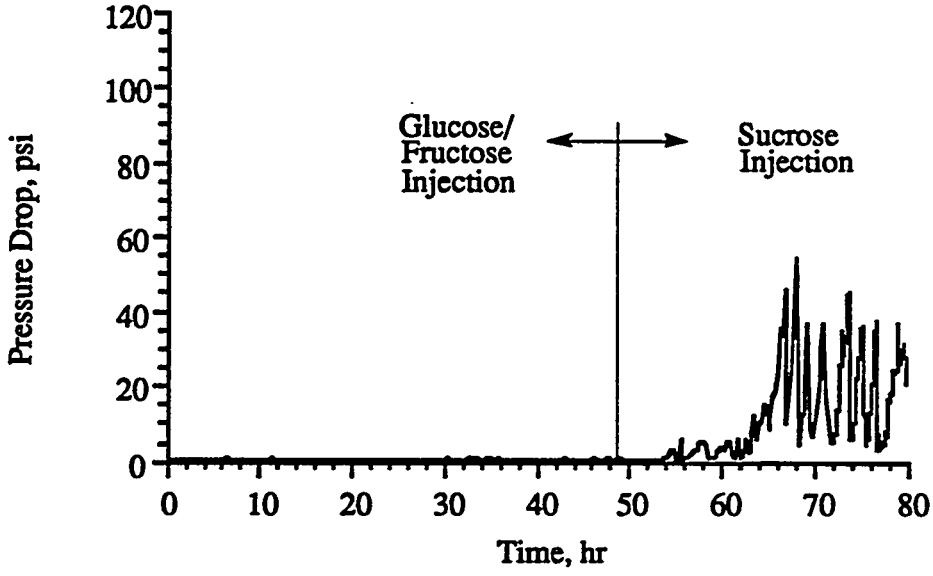

Figure 4.5. Pressure drop across micromodel for experiment ME-1

Visual observations of biofilm development within the micromodel revealed a change in cell morphology and location that corresponded to these changes in pressure. During inoculation, individual cells could be seen flowing through the micromodel network. After initiation of glucose-fructose injection, the planktonic cells were washed out of the network and the remaining cells that were immobilized on the surfaces of the micromodels were not visible at the available magnification. After 9 hours of nutrient injection and cell growth, however, the first visual evidence of a developing biofilm was observed. As shown in Plate 1 a), cells collected first in the pore throats as noncontiguous cell units. The cross section of these pore throats have a tear-drop shape as shown in Figure 4.6. At the corners of these tear-drop shaped channels, crevices exist which appear to have encouraged mechanical capture of cells in the pore throats and may have protected the developing biofilm from hydrodynamic shearing forces.

a) un-coated cells b) coated cells

Figure 4.6. Cross sectional view of pore throats in micromodel

Biofilm development due to cell growth in the pore throats continued until channels for flow were formed as shown in Plate 1 b) and c). In addition to cell growth, cell aggregates are sheared from upstream cell units and are recaptured downstream, contributing to the build up of biomass in the pores; an example of a recaptured cell aggregate is shown in Plate 1 b). After 48 hours of glucose-fructose nutrient injection, approximately 80% of the area in the inlet region of the micromodel was covered with biofilm. The coverage decreased to approximately 30% in the outlet region. This

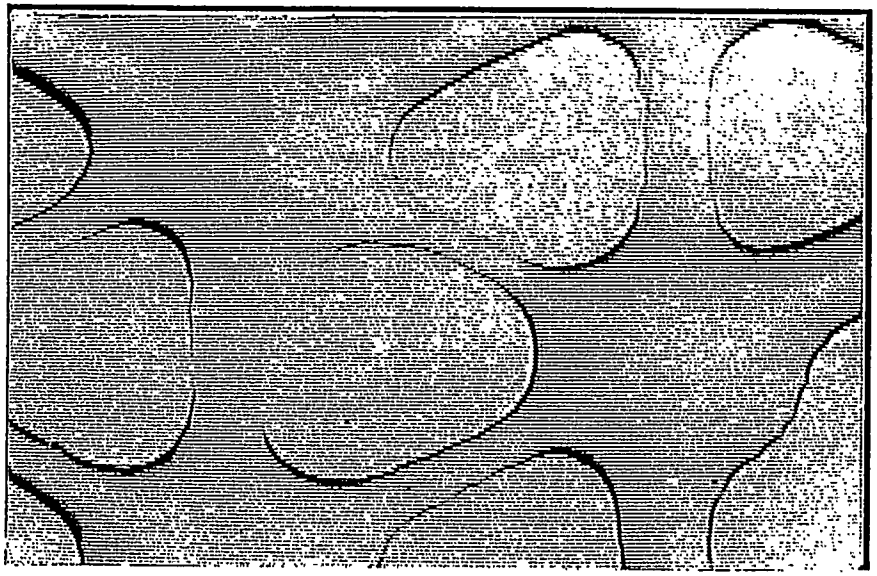

a) initial cell capture

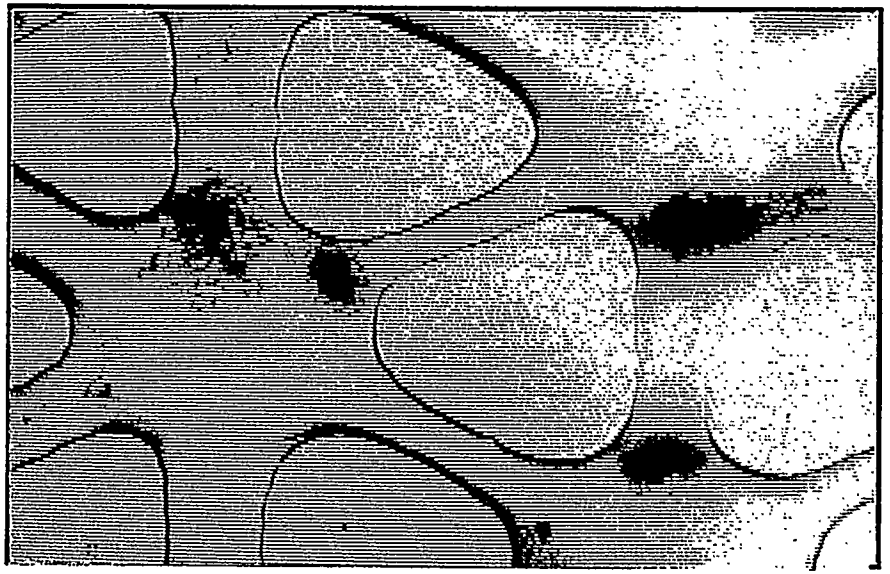

b) surface film and cell aggregate

c) Flow channels after 48 hrs glucose-fructose injection

Plate 1. Biofilm development of nonpolymer-producing cells

difference in biofilm coverage corresponds to availability of higher concentrations of nutrients at the inlet. Due to nutrient consumption within the inlet region, concentration of nutrients at the outlet is reduced and biofilm development is slower.

Based on these visual observations, there appeared to be a large amount of biomass in the micromodel after 48 hours of glucose-fructose feed injection. Nonetheless, a measurable increase in pressure was not observed. This result may be due to two factors. First, although there was a large aerial extent of surface coverage by the biomass, the corresponding volume may not be great enough to significantly decrease the porosity, i.e., the biofilm thickness appears to have been small. Alternatively, the flow channels that were formed through the biomass provided essentially the same hydraulic conductivity as the clean network based on the pressure measurements achievable with this system.

Changes in biofilm morphology and in biomass location within the network occurred as sucrose nutrient was injected. After five hours of sucrose injection, the flow channels observed in Plate 1 c) had become coated with a translucent, gelatinous substance as shown in Plate 2 a). The appearance of this substance corresponds with the beginning of small pressure oscillations across the micromodel which continued from hour 54 to 64 (see Figure 4.5). After 10 hours of sucrose injection, the biofilm along the flow channel shown in Plate 2 a) was dislodged from the pore throat and pushed into the pore body as shown in Plate 2 b).

There are several plausible reasons for this movement of biofilm from the pore throat to the pore body. First, local velocity changes may have occurred, due to blocking of some of the local pore throats, that sheared the biofilm from the wall. Second, the presence of the polymer may have altered the surface characteristics of the biofilm such that cell-to-cell interactions were dominant over cell-to-wall interactions. This change could include increased hydrophobicity of the cell surface with polymers present which would

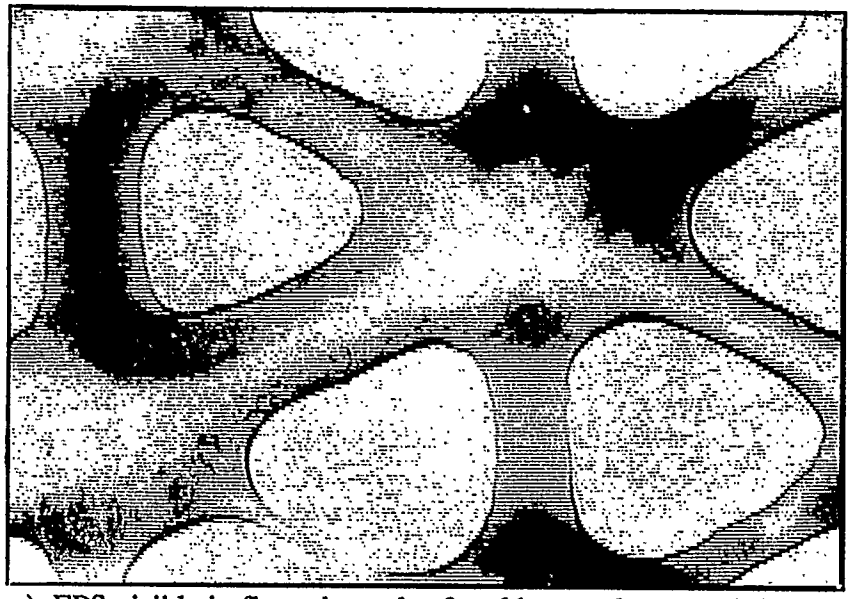

a) EPS visible in flow channels after 6 hours of sucrose injection

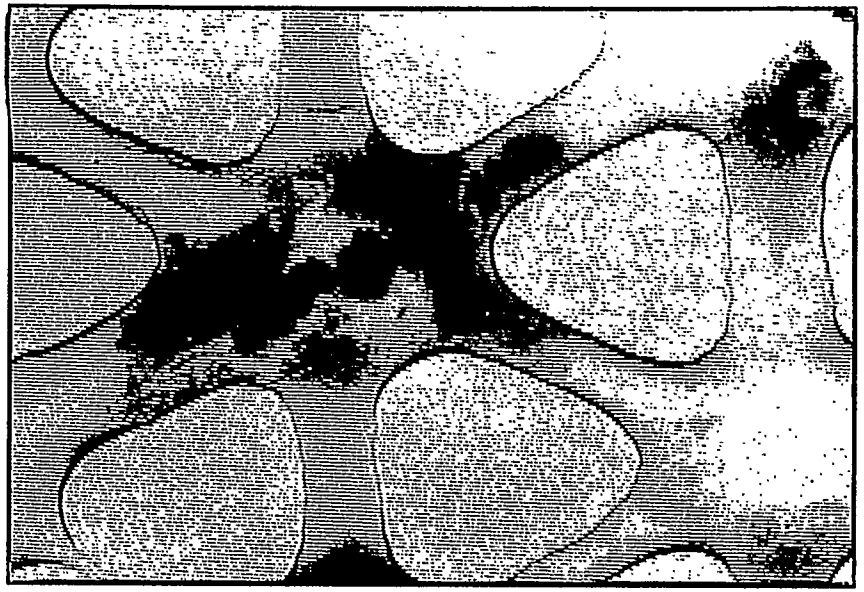

b) collapse of biomass into pore body after pressure oscillation of 3 psi

c) transformation of biomass to gelatinous units

d) all pore volume is filled with EPS-producing biomass and pressure is near maximum before the onset of oscillations

Plate 2. Change in biomass morphology after initiation of sucrose injection

tend to decrease the interaction of the cell with the hydrophilic wall. These reasons for the release of biofilm from the surface of the porous media are not mutually exclusive and the release is likely to be a combination of these phenomena. One could also speculate that the cells in contact with the surface of the porous media were no longer viable due to limitations of nutrient transport and hence, were more readily sheared. However, this explanation seems less likely due to the high concentrations of nutrient available in this system.

After release of the biofilm into the pore bodies, new surfaces of the biofilm were exposed to the sucrose. The formation of polymer proceeded until the opaque cell units created during the glucose-fructose injection were fully transformed to the translucent, gelatinous structures associated with the polymer-producing cells as can be seen in Plate 2 c). These gelatinous structures filled the pore bodies and appeared to have greater thickness than the nonpolymer-producing cell units. As these gelatinous cell units formed the pressure rose rapidly as can be seen in Figure 4.5 between hours 64 and 67.

In the micromodel, pressure oscillations were first observed when the large cell units forming in the pore bodies were sheared into globules with sizes now on the order of pore throats. This shearing occurred when a critical pressure was reached and the deformable biomass yielded, causing the large mass to be sheared into smaller units as it was forced from one pore body to the next through a pore throat. This observation is captured in Plate 2 d).

After the globules were formed, redistribution of the biomass occurred during oscillations. As the pressure increased during an oscillation, the redistribution was local. Namely, the globules would be carried by transporting fluid (i.e., nutrient) into adjacent pore bodies along dominant flow channels of least resistance. At some location(s) along these flow channels, the globules would create a logjam and block downstream pore throats

preventing further movement of the cell units. At a critical pressure, however, the log jam would yield and globules would once again flow some distance (i.e., distance greater than one pore body) through the network with the transporting fluid until another log jam occurred or the cell units were washed out of the network. The movement of cells via this cycle of fill and release of globules from pore bodies resulted in pressure oscillations as observed in Figure 4.5 from hours 67 and 80.

The micromodel plugging experiment was repeated in a second system in which sucrose was the only nutrient used (ME-2). Under these conditions, the biofilm developed with polymer being produced concurrently. This approach differs from the first experiment in which the biofilm was first developed with nonpolymer-producing cells and then sucrose was injected and polymer production occurred within a well developed biofilm. The purpose of this second experiment was to determine whether the pressure, morphological, and positional changes of biomass were the same as in ME-1.

The pressure changes with time are shown in Figure 4.7. When comparing these results with those for the first experiment (see Figure 4.5) between 48 and 80 hours, similar trends in pressure are observed. Namely, there is a period in which no changes in pressure are measured; visually this period corresponded to the collection of biofilm in the pore throats as before. Then there is a pressure increase; visually this pressure increase corresponded to the shearing of biomass from the pore throats, collection of this biomass in the pore bodies, and subsequent growth of biofilm units within these pore bodies. This biofilm appeared translucent and gelatinous as that formed in ME-1 after sucrose injection and subsequent polymer production. Finally, there is a period of pressure oscillations which corresponded to the shearing of large cell units within the pore bodies into smaller globules which flow through pore throats. As before, it was observed that these globules logjam and release through dominant flow channels within the network.

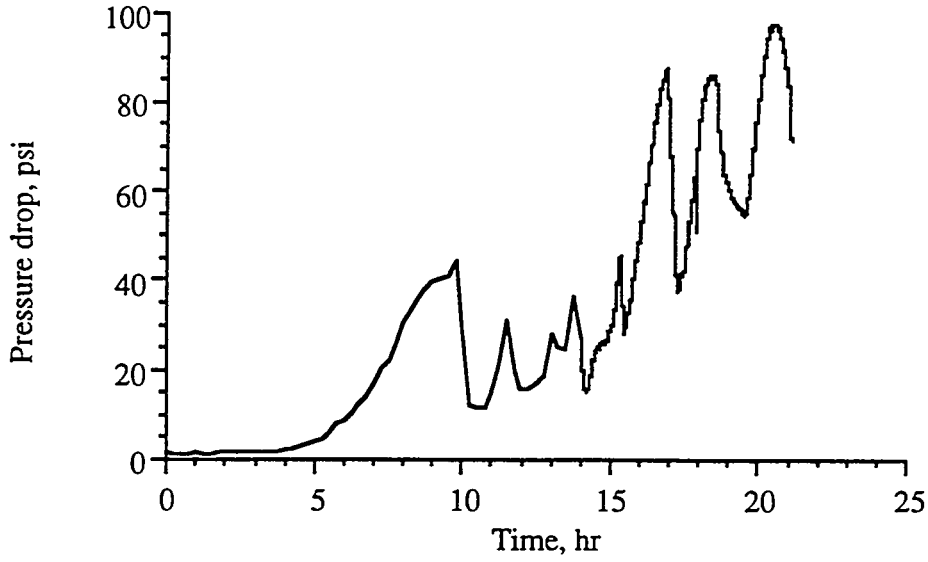

Figure 4.7. Pressure changes in ME-2 in which only polymer-producing bacteria were grown in the micromodel

The results from the two micromodel plugging experiments indicate that three characteristic pressure regimes can be used to describe cell capture, retention, and release. These pressure regimes correspond to location of biomass as shown in Figure 4.8. In addition, it was observed that changes in pressure and consequently permeability were not due to adhesion of polymer-producing biofilm to the walls of the porous media. Instead, gelatinous aggregates formed and mechanically blocked pore throats.

4.2.3 Consolidated Core Plugging Experiment

The influent and effluent cell concentration, the inlet pressure, and the effluent sucrose and monosaccharide concentrations data for one of the consolidated core experiments are presented in Figures 4.9, 4.10, and 4.11, respectively. Again, as found in the above experiments, the cell injection phase did not produce any measurable changes in the inlet and the 6.4 mm pressure taps. This result indicates that the injection of cells did not produce any measurable damage to the porous media. In addition, the appearance of bacteria in the effluent indicates that the cells were transported through the core. From

these events, it can be assumed that skin plugging was minimal during the injection phase of the experiment.

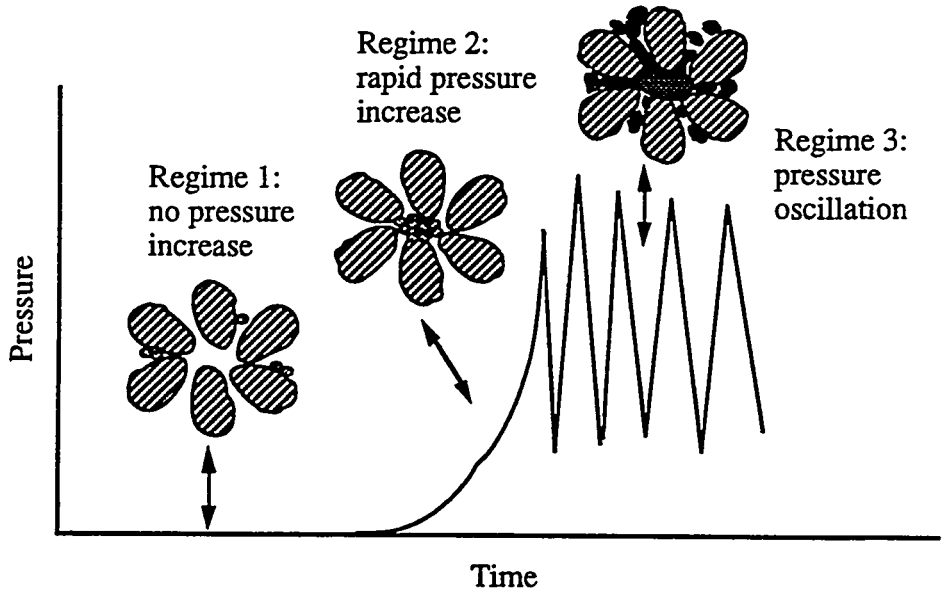

Figure 4.8. Characteristics of pressure regimes

After cell injection, sucrose feed was injected at the same volumetric flow rate as the cells had been. In Figure 4.11 the resulting effluent sucrose concentration data as a function of time are presented. This effluent sucrose concentration exhibits a period of no appreciable change, followed by a sharp decline of total sucrose consumption to an essentially zero effluent concentration. Sucrose is an indicator of the total amount of biomass that develops in the porous media based on stoichiometry (i.e. maximum cell yields). The initial lack of sucrose consumption by the cell retained within the core can be attributed to growth limitation, which includes mass transfer limitation and/or cell growth lag time. Mass transfer can occur under two possible scenarios. The first is the result of

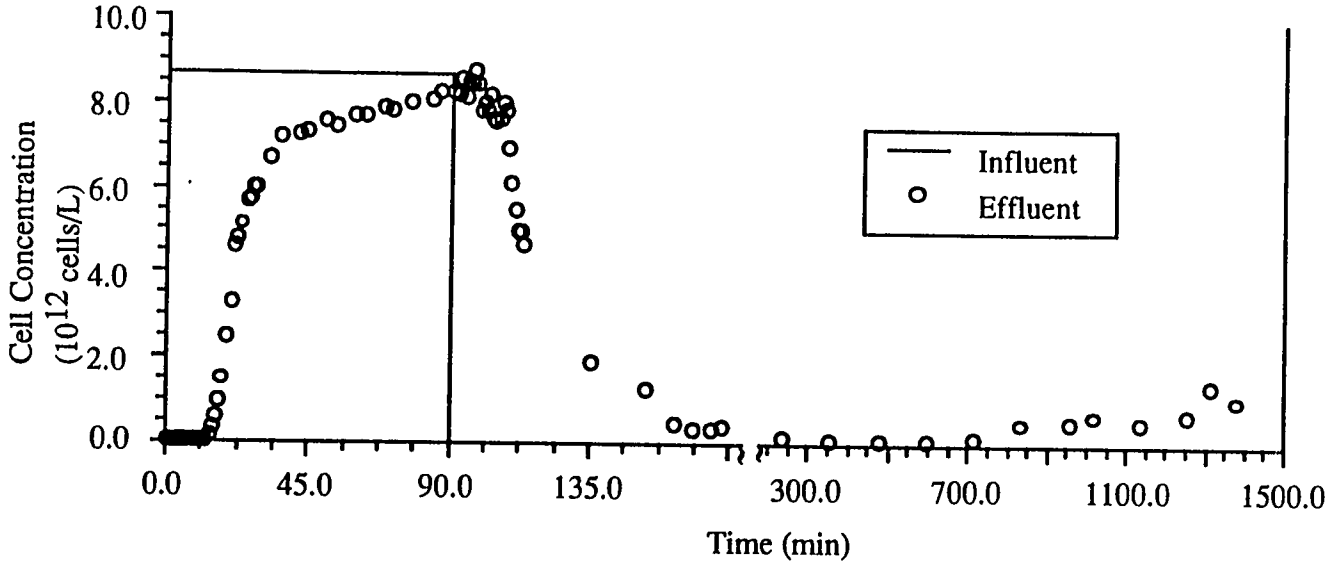

Figure 4.9. Influent and effluent cell concentrations from core plugging experiment

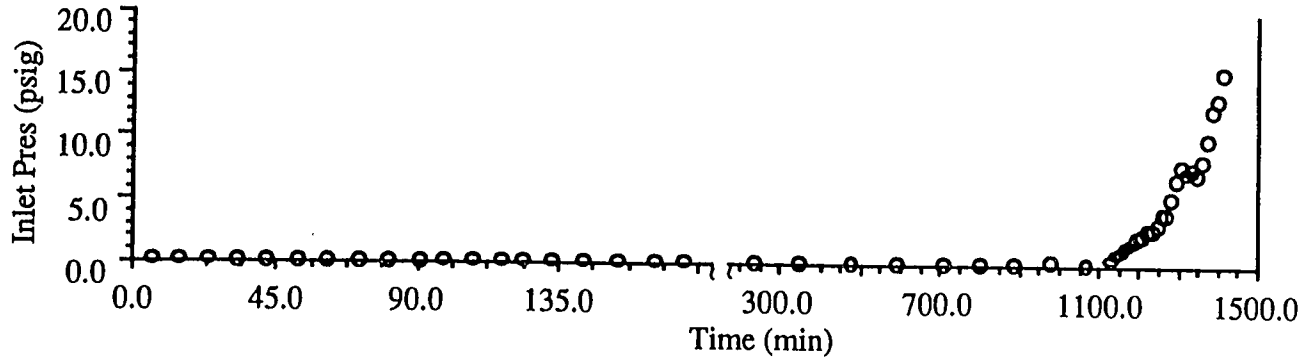

Figure 4.10. Resulting pressure drop through 11.8 Darcy ceramic core for core plugging experiment

biofilm mass transfer restriction. Biofilm mass transfer limitation occurs when cells deep within the biofilm (multilayer) are nutrient restricted due to the diffusion rate of the nutrients from the bulk solution through the upper layers of cells and polysaccharides (see Figure 4.12). Mass transfer limitation can also occur if a cell is deposited within a dead pore (non-conducting pore) and hence nutrients are prevented from being convectively transported to the cell. Dead pores can occur naturally, i.e. they can be a part of the porous media before any bacteria are injected or they can be created by the cell when it deposits in pore and prevents fluid (nutrient) convection.

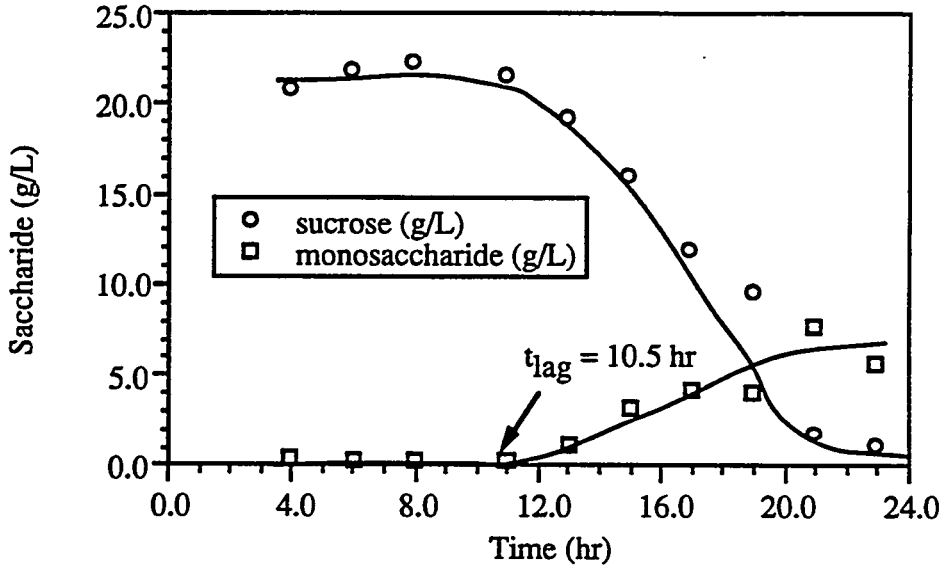

Figure 4.11. Effluent sucrose and monosaccharide concentration for core plugging experiment

A growth-related lag time is the second possible cause for no initial sucrose consumption. Such a phenomenon can be explained by applying Dean and Hinshelwood [1966] model for lag time prediction that correlates the length of lag time to the concentration of a critical intracellular constituent (i.e. no growth until the constituent reaches a crucial concentration). This constituent may be a diffusional species, such as a vitamin or activator that is lost from the cell into the bulk nutrient solution. In a batch

system the loss of the constituent is limited due to its accumulation in the bulk solution. However, a continuous flow system does not allow for any bulk accumulation due to the constant flushing of the system with fresh nutrient solution. The results of flushing would be a lag time that is longer than the time realized during batch cultivation, which was reported to be less than one hour for batch growth (see Chapter 3). From the data presented in Figure 4.11, a lag time of 10.5 hours can be calculated by defining the length of the lag time as the time when a growth product appears in the effluent. For this work, the appearance of monosaccharides in the effluent has been selected as the product best suited for product measurement. Appendix E discusses this criteria for lag time selection.

Finally, the effluent cell concentration results (Figure 4.10) exhibit an almost steady release of cells from the porous media up to the time when effluent sucrose concentrations have dropped to zero. Afterward, the effluent cell concentration increases, accompanied by an increase in inlet pressure, during constant volumetric feed injection. These data imply that as cell growth occurs, more cells are available for release and thus account for the increase in the cell effluent concentration.

4.3 Conclusions

Each of the three experiments shown higher cell retention with the presence of polysaccharides. The transport experiments have shown that *Leuconostoc m.* cells that are grown in the presence of sucrose, i.e. dextran coated, are likely to remain as agglomerates.

The *in situ* growth experiments have demonstrated the effects of polysaccharide on cell capture and retention mechanisms. For cell growth in the absence of polymer inducing nutrients it was found that cell retention in the micromodel is realized by the developments of a thin biofilm coating on the pore walls. This thin coating appears to reach a constant thickness, meaning a balance exist between the rates of cell growth and shearing. Pressures drops through the micromodel, under these condition, have been found to remain

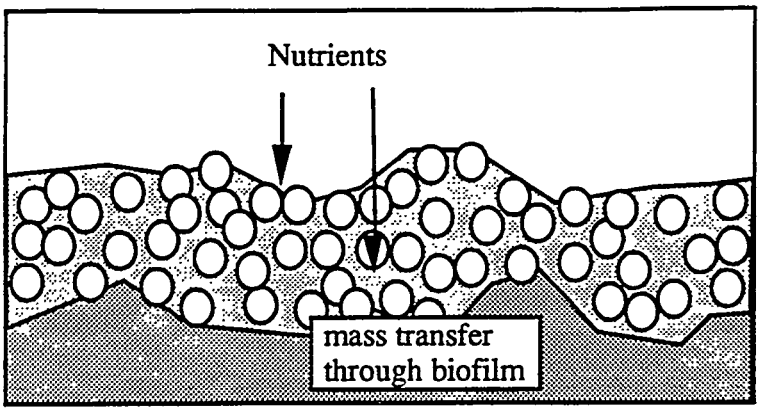

a) biofilm mass transfer

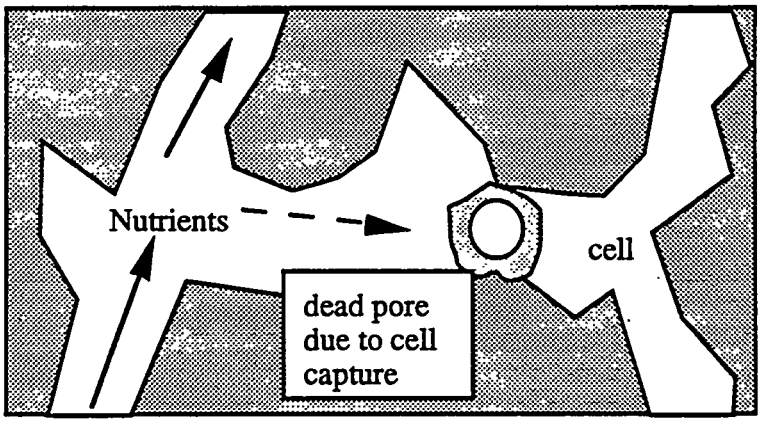

b) dead pore body mass transfer

Figure 4.12. Two possible mass transfer scenarios that can control *in situ* growth

unchanged. Once sucrose is supplied to the cell it was observed that the biofilm had changed morphologically; the biofilm became gelatinous and thickness increased. This coincided with a pressure increasing from initially un-measurable change in pressure drop to a dramatic increase and finally to a oscillatory pressure drop. These three pressure phases: no pressure increase, swift pressure increase, and finally oscillatory pressure drop reading are caused by the development (growth) and sloughing of the biofilm. Biofilm sloughing is the result of increased shear forces due to flow path blockage (under constant volumetric injection) and/or changes of cell and pore wall charge.

Finally the consolidated core plugging experiments have further suggested that this *in situ* biofilm development is governed by mass transfer and also appears to show a characteristic lag time before growth commences. These lag times are more profound in a continuous feed systems because of the loss of critical component(s) produced by the cell to the bulk solution. Mass transfer limitation will occur as the result of biofilm nutrient transport retardation and/or mass transfer in dead pores due to nutrient diversion as a result of biofilm growth in the pore channels.

4.4 References

Cunningham, A.B., W.G. Characklis, F Abedeen, D. Crawford, Inffluence of Biofilm Accumulation on Prous Media Hydrodynamics, *Environ. Sci. Technol.* 1991, **25**, 1305-1311

Dean, A. C. R., S.C. Hinshelwood, Growth, *Function and Regulation in Bacterial Cells*, Oxford University Press, Ely House London, 1966

DiGiano, F. A., G.E. Speitel, Biofilm Shearing Under Dynamic Conditions, *J. of Env. Eng.*, **113**, 464-475, 1987

Fowler, H.W. and A.J. McKay, Chapter 7, *Microbial Adhesion to Surfaces*, edited by R.C.W. Berkeley, J.M. Lynch, J. Melling, P.R. Rutter, and B.Vincent, Ellis Horwood Limited, West Sussex, England, 1980

Rege, S.D., H.S Fogler, Network Model for Straining Dominated Entrapment in Porous Media", *Chemical Engineering Science*, **42**, 1553

Rittmann, B.E., The Efeect of Shear on Biofilm Loss Rate., *Biotechnol. Bioeng.* **24**, 501 1982

Yen, T.F. *Bacterial Transport Through Porous Media*, Annual Report, Dec. 1985, DOE/BC/10508-36, Bartlesville Project Office U.S. Department of Energy, Bartlesville, Oklahoma

Appendix 4.A
Micromodel Apparatus

Figure 4.A.1 illustrates the micromodel apparatus used to demonstrate the importance of the polysaccharide in retention mechanisms. The major components of this apparatus are: the glass micromodel, the syringe pump, the CCT camera and the super-VHS recorder. The glass micromodel is the key component; it contains the etch network pattern that simulates the channel network that exist in the porous medium. Figure 4.1 illustrates elements of this network for both the transport and the *in situ* growth experiments. Homogeneous versus heterogeneous and high and low connectivity networks can be studied individually to determine how the previously described phenomena influence the flow profile as a function of time. The pattern used during the transport experiments used a micromodel pattern originally developed by Marathon Oil company. Figures 4.1 a) and b) are a magnification of this micromodel network. Typical pore sizes are between 10 and 50 μm. The pattern used for the *in situ* growth experiments has a triangular network with a co-ordination number of 6 which has been chosen for network modeling. This particular pattern has been shown to closely simulate natural system as detailed by Rege and Fogler [1987].

Fluid injection into the micromodel is accomplished by using a syringe pump. From the syringe, the solution is pumped through stainless steel tubing and into the manifold distribution plates, which are attach to the micromodel, forcing the injection solution into the network. At the inlet of the network, a pressure gauge is connected, allowing for inlet pressure measurements. From the outlet of the network, a conductimeter and/or spectrophotometer (λ = 560 nm) is connected allowing for tracer test experiments and cell concentration determination, respectively. The CCT camera, Stereo-Zoom microscope, and super-VHS recorder allows for the collection of real time images. The Stereo-Zoom microscope can magnify the image by a factor of 10x to 70x. The super-VHS recorder

allow for the storage of the images so that they can be further analyzed by digitizing and processing them on an Apollo computer.

The system was modified for the *in situ* growth experiments. The Stereo-Zoom microscope magnification was increased to the range of 18x to 110x. Teflon tubing was used for both inlet and outlet lines. Check valves were used on inlet lines to avoid back contamination. Plug valves were used on the outlet lines to control direction of flow. All effluent was captured in a stainless steel sample bottle which had a nitrogen blanket at ~50 psi pressure to create a back pressure on the system.

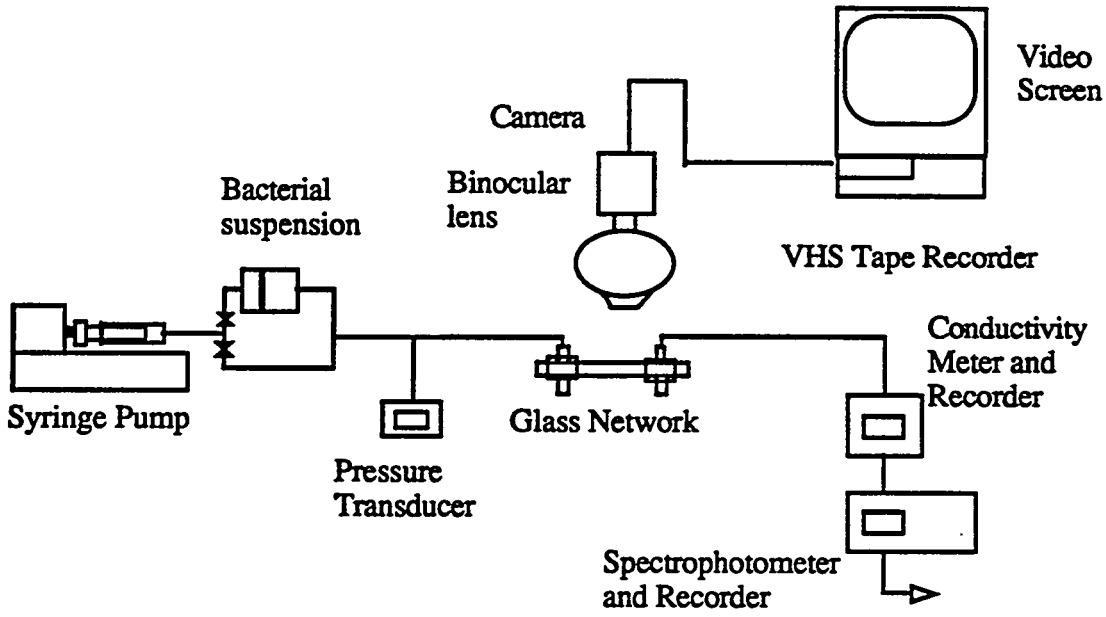

Figure 4.A.1. Schematic of the micromodel apparatus

Appendix 4.B

Capillary Experiments

Experiments conducted by:

Katherine Hoffman

Capillary experiments were conducted to demonstrate the adsorption (or bridging when dextran is present) of *Leuconostoc m.* bacteria to glass surfaces and to measure their binding strength by subjecting the retained cells to varying shear forces. Changes in shear occurs when the feed solution injected to promote cell growth is undergoing flow constriction due to biofilm generation. Feed volumetric flow rates are held constant for each experiment. The amount of cells and dextran, i.e. biofilm resulting is a measure of the binding strength of the cells to the surface. Rittmann [1982], DiGaiano et al. [1987], and Fowler et al. [1980] have shown that the cell sloughing rate to be dependent on the shear rate, while Cunningham [1991] has found that an equilibrium is reached between cell growth and shear sloughing for cell grown in glass bead packs.

The experimental procedure started with the injection of cells into the capillary apparatus followed by the injection of sucrose feed that supports cell and dextran production. These cells had been separated from the glucose-fructose feed for which they were grown for a 24 hour period. These cells were injected at a rate of 0.002 mL/min for a 12 hour period by means of a syringe pump into the 152 μm capillary tube (10 cm length) as illustrated by Figure 4.B.1. After cell injection, the 15 g sucrose/L feed solution was injected continuously at the rate of 0.002 mL/min. This experiment was repeated several times.

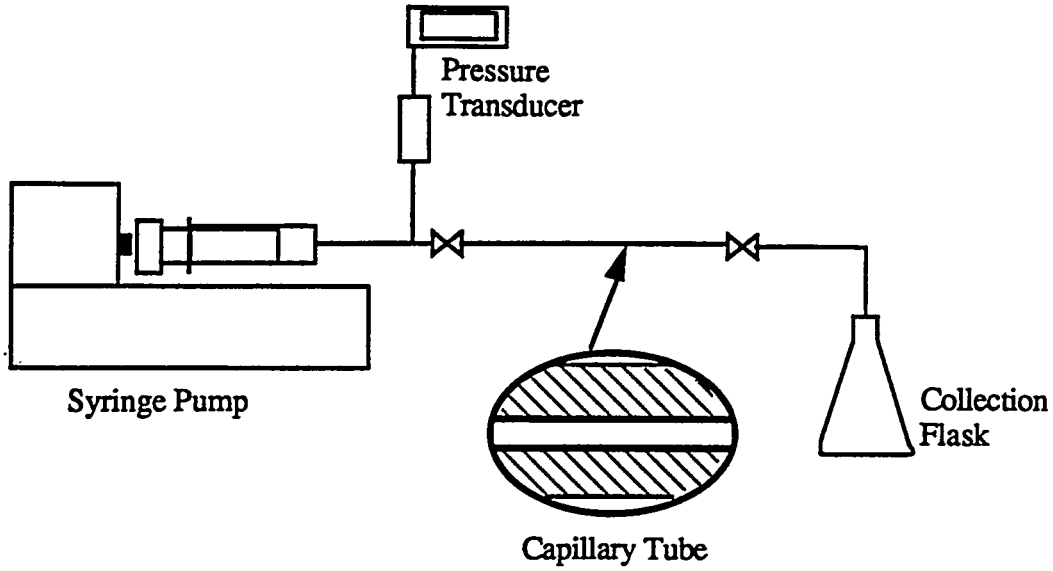

Figure 4.B.1 Capillary tube apparatus

No visible accumulation of cell on the internal surface of the capillary tube was observed for any of these experimental runs. This lack of cell adhesion is explainable by considering either surface roughness and/or electrostatic repulsion effects. The capillary tube is relatively smooth surface that does not shield any deposited cell from fluid shear forces. Hence cell adhesion may be occurring but the weakness of the bond accompanied by the shear forces prevent the retention of cell to the surface.

In addition, electrostatic forces of this system do not favor the bridging of the cells to the surface. Typically bacteria and quartz (pure SiO_2 - glass being amorphous SiO_2) [Yen et al. 1985] are negatively charged, which in themselves does not favor bacterial -glass attraction. And because dextran is a neutral polymer, it is not expected that these repulsive forces can be overcome by attractive van der Waals forces to favor bridging.

5.0 Task III - Damkohler Experiments

Task Description:

To elucidate the rate of polysaccharide production and the combination of polysaccharide production and cell growth (biomass) on plugging. The rate of consumption by reaction to the rate of convective transport on this phenomena will be studied to determine a) the plugging rate and b) plugging structure.

The two previous tasks have demonstrated the technical feasibility of using *Leuconostoc mesenteroides* bacteria for the plugging of high permeability zones. The parallel core plugging experiment has further demonstrated that this phenomena can be beneficially for profile modification and thus has been given the name Bacterial Profile Modification or BPM. However the application of a BPM technique requires a thorough understanding of reservoir conditions, bacteria growth kinetics, and bacterial and nutrient transport within porous media.

The successful application of a BPM technique is highly dependent upon the reservoir conditions, such as pH, salinity, temperature, pressure, and permeability [Clark *et al.* 1981]. If a reservoir is suitable, the only control in BPM implementation is through controlled bacterial placement and *in situ* growth (i.e. injection strategy). The objective of this task is to determine the effect of nutrient injection rates and nutrient concentration on *in situ* growth of *Leuconostoc m.* in porous media and the resulting permeability decline from the *in situ* growth of these cells. This study was accomplished through both Damkohler experiments and model development.

5.1 Material and Method

Damkohler experiments have been conducted to determine how *in situ* cell growth and accompanying polysaccharide production can influence the permeability of porous media. These experiments consisted of two phases: 1) the initial injection of bacteria into

the porous medium, 2) the subsequent injection of a nutrient feed into the porous medium to promote cell and polymer production. These procedures are similar to the *in situ* growth experimental procedures detailed in Task II. The specifics of the inoculum growth media, its preparation, the sucrose feed composition, and the location of the pressure taps for the three experimental series are presented in Table 5.1. The apparatus and procedures used for the Damkohler experiments are similar to the procedures used for the *in situ* growth experiment, are detailed in Chapter 4.

5.2 Theory

The overall metabolic reaction for sucrose consumption and polysaccharide (dextran) production by *Leuconostoc m. follows* [Stanier, *et al.* 1986]:

$$\text{Sucrose} \xrightarrow{E} \text{Dextran} + \text{Fructose} \qquad 4.1)$$

$$\text{Sucrose} \xrightarrow{E} \text{Glucose} + \text{Fructose} \qquad 4.2)$$

$$\text{Glucose} + \text{Cells} \rightarrow \text{Ethanol} + \text{Acetate} + \text{Lactate} + CO_2 + \text{Cells} \qquad 4.3)$$

$$\text{Fructose} + \text{Cells} \rightarrow \text{Mannitol} + \text{Cells} \qquad 4.4)$$

The cell and dextran production and sucrose consumption rates have been defined by the following set of equations:

$$r_x = \mu C_x \qquad 4.5)$$

$$r_e = k_f C_x \qquad 4.6)$$

$$r_1 = V_{max_{td}} \left(\frac{C_s}{K_d + C_s}\right) \qquad 4.7)$$

$$r_2 = V_{max_g} \left(\frac{C_s}{K_d + C_s}\right) \qquad 4.8)$$

$$r_g = \gamma r_2 - Y_{g/x} r_x \qquad 4.9)$$

$$r_f = \gamma r_1 + \gamma r_2 - Y_{f/x} r_x \qquad 4.10)$$

Table 5.1. Experimental material characteristic and procedures

Inoculum	
-initial growth media	10 g yeast extract/L 7.9 g glucose /L 7.9 g fructose /L
- inoculum preparation centrifuged at 4400 g and suspended †	yes
- injection rate (mL/min)	5.0
- injection duration (min)	60
- cell concentration (cells/L)	~ 1×10^{11}
Core	
- diameter (cm)	2.54
- length (cm)	5.1
- permeability (mD)	11 000
- core saturation composition	same as feed
Feed	
- composition	all 10 g yeast extract /L DE-I- 15 g sucrose/L DE-II - 15 g sucrose/L DE-III - 1.5 g sucrose/L
- injection rate (mL/min)	DE-I - 0.1 DE-II - 1.0 DE-III - 1.0
- pressure tap locations from injection face (mm)	inlet 12 38

† - suspended in a ~500 mL of feed solution

yeast extract - (Diffco)

$$r_S = -(r_1 + r_2) \quad 4.11)$$

$$r_{id} = Y_{d/f}\,\gamma\, r_1 \quad 4.12)$$

with:

$$\mu = \mu_{max}\left(\frac{C_{ye}}{K_{ye} + C_{ye}}\right)\left(\frac{\alpha_{s/ye}\,C_{ye} + C_s}{K_s + \alpha_{s/ye}\,C_{ye} + C_s}\right) \quad 4.13)$$

$$V_{max_i} = \theta_i \frac{k_i}{k_f} C_e \quad 4.14)$$

where:

C_i - concentration of species i (g/L or cells/L),
k_i - activity of the enzyme per volume per cell to produce product i @ 30 C and pH 5.2
K_i - Monod constant for component i (g/L).
r_i - rate of product i formation per unit volume or rate of reaction i (g/L·h or cells/L·h)
t - time (hr)
V_{max_i} - maximum velocity for species i (g/L·h)
Y_i - cell yield from species i consumption (cells/g),
$\alpha_{s/ye}$ - yeast extract conversion factor (g sucrose/g yeast extract),
γ - molecular ratio - monosaccharide to sucrose
θ_i - dimensionless reaction rate constant for sucrose consumption at reaction temperatures,
μ - specific growth rate (h^{-1}),
μ_{max} - maximum specific growth rate (h^{-1}),

Subscript for kinetic parameters are:

x	- cell	ye	- yeast extract
id	- insoluble dextran	td	- total dextran
e	- enzyme	g	- glucose
f	- fructose	s	- sucrose

Equations 4.5 and 4.13 predict the cell production rates with Equation 4.6 predicting the enzyme synthesis rate. Equations 4.7 and 4.8 are rate models used to predict reactions 4.1 and 4.2, respectively. Equations 4.9 through 4.12 predict sucrose, glucose, fructose and dextran consumption or production rates. Parameter values for these equations are presented in Chapter 4.

5.2.1 Bacterial Transport and *In situ* Growth Modeling in Porous Media

The simplified one-dimensional form of the transport equations for species i in porous media are written as:

$$\varepsilon \frac{\partial \sigma_i}{\partial t} = \varepsilon r_{i\ generation} - \varepsilon \Sigma r_{i\ transport} \qquad 4.15)$$

$$\varepsilon \frac{\partial C_i}{\partial t} + U_s \frac{\partial C_i}{\partial z} = D_i \frac{\partial^2 C_i}{\partial z^2} + \varepsilon r_{i\ generation} + \varepsilon \Sigma r_{i\ transport} \qquad 4.16)$$

where:

ε	- porosity,
U_s	- darcy or superficial velocity (cm/hr),
z	- length dimension (cm),
t	- time (hr),
D_i	- dispersion (cm^2/hr) [equal to αU_s],
σ_i	- concentration of species i on surface (fluid volume basis) (g/L).
$r_{i\ generation}$	- rate of generation of species i (g/L/hr),
$\Sigma r_{i\ transport}$	- sum of the rate expressions for i partitioning between surface retained and suspension states (g/L/hr).

These equations assume that porosity does not change throughout the time period for which species i is being modeled. These transport equations can also be used for the case of porosity change by assuming a pseudo-steady state condition for porosity, over which porosity is constant (it is assumed that the change in porosity is small and slow as compared to the change in the concentration of species i). After each time integration, the porosity is updated according to the following equation:

$$\varepsilon = \varepsilon^{\bullet} \left(1 - \sum \sigma_i / \rho_i \right) \qquad 4.17)$$

where:

$\varepsilon^{\bullet}$ - initial porosity,

ρ_i - density of material i (cells/L or g/L).

Equation 4.17 was derived from a differential volume balance.

5.2.2 Permeability Reduction

The change in local permeability for a differential volume of porous media is assumed to be functionally dependent on the change in local porosity of the finite element according to the following equation [McCune *et al.*, 1973]:

$$\frac{k_{loc}}{k_o} = e\,(\beta\,\Delta\varepsilon) \qquad 4.18)$$

where:
$\Delta\varepsilon$ - change in local porosity.

Equation 4.18 is used to determine the overall permeability of the porous media by integrating the local permeability over the entire length of the core according to the following equation:

$$\frac{K}{K_o} = \frac{L}{\int_0^L \frac{k_o}{k_{loc}}\,dx} \qquad 4.19)$$

5.3 Results & Discussion

Table 5.2 list the Damkohler experimental feed conditions and the time before apparent damage, with Figures 5.1 a), b) and c) illustrating the respective pressure versus time data. Time was plotted as the abscissa because the cell's growth rate (*in situ*) is believed to be influenced by both time and flow rate, but not uniquely by the dimensionless combination of both. A number of interesting effects have been demonstrated by these experiments, the first being the time required by the cells to damage (i.e. reduce permeability) the porous media. For DE-I where the high-sucrose-content feed (15 g

sucrose/L) was injected at a rate of 0.1 mL/min, the elapsed time until core damage to this core was long, taking over 69 hours before any apparent damage occurred. Apparent elapsed time for damage being defined as the time until the pressure drop across the core is statistically different from the pressure drop immediately after cell injection. DE-II shows contrary results; damage to the porous media occurred immediately. The feed for DE-II contained the same sucrose concentration as DE-I, however, the feed injection rate was ten times greater, at 1.0 mL/min. Thus, it can be concluded that the transport of nutrient to the bacteria within the core significantly affect the rate of damage to the core.

Table 5.2. List of Damkohler experiments and respective lag periods before measurable permeability damage

Run	Sucrose Concentration (g/L)	Feed Injection (mL/min)	Lag Time before Damage † (hr)	Lag Time/ Space Time
DE-I	15	0.1	69	29
DE-II	15	1.0	Immediately	0
DE-III	1.5	1.0	>96‡	> 400

‡ - after 96 hours of feed injection, no core damage was apparent
† - measurable damage translates to a minimal permeability decline of 0.0013 for DE-I and 0.014 for DE-II and DE-III

The effects of the nutrient concentration, or the rate of polymer production, on the damage to the core is demonstrated by the results in Figure 5.1 c) (DE-III). The sucrose concentration of the feed used for DE-III was one tenth of the concentration of DE-II (i.e. 1.5 g/L), while the feed injection rate was the same as for DE-II. The run was terminated after 91.75 hours, during which no measurable damaged occurred. To demonstrate that cells were still present within the core, a second feed solution containing 15 g/L of sucrose was injected at a rate of 0.5 mL/min. Within 1 hour after commencement of the injection of this modified feed, the core began to show signs of damage, hence, indicating that the cells

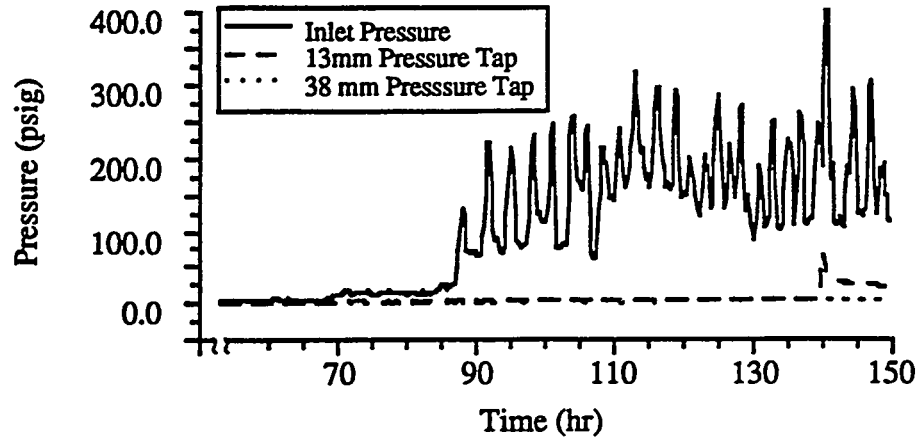

a) DE-I - 15 g sucrose/L @ 0.1 mL/min

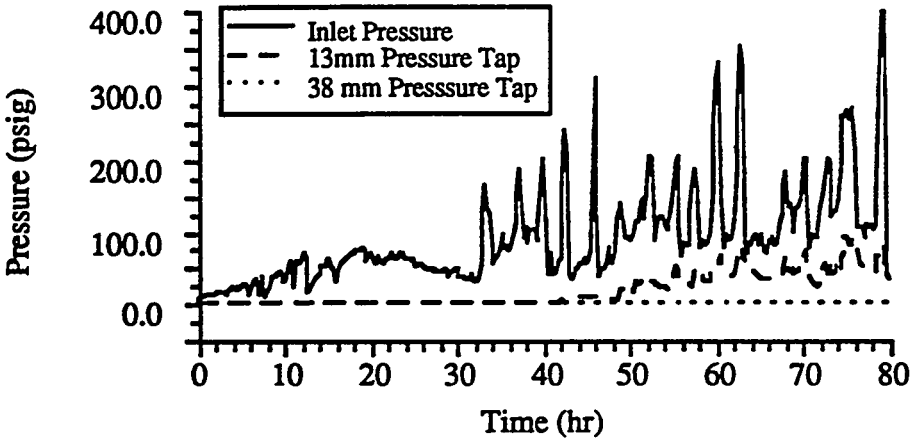

b) DE-II - 15 g sucrose/L @ 1.0 mL/min

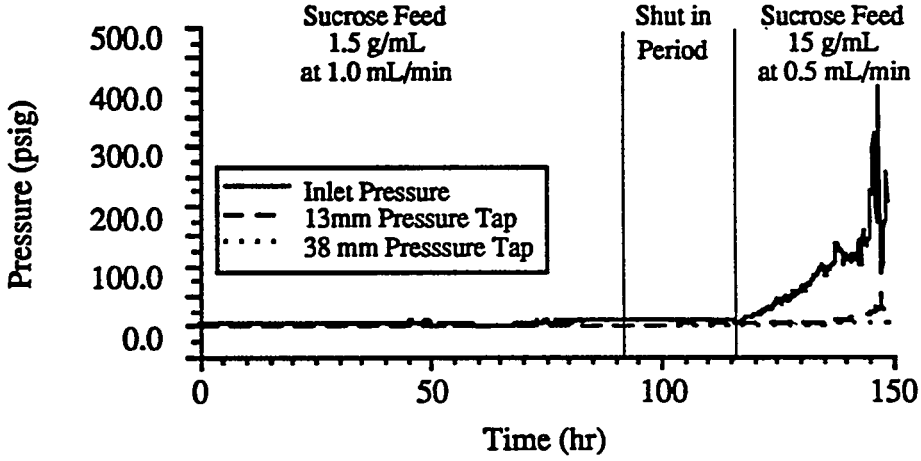

c) DE-III - 1.5 g sucrose/L @ 1.0 mL/min

Figure 5.1. Pressure drop across consolidated cores under varying injection conditions

were present within the core but didn't damage the core. This lack of damage is the result of insufficient nutrients to induce significant porosity reduction and, therefore, permeability changes.

Both these effects, the reduction of damage when the feed injection rate is reduced and the lack of damage at low sucrose feed concentrations, indicate that the damage to the porous media is dependent upon the Damkohler number. The Damkohler number being defined as the ratio of reaction rate of species i to the convective transport of species i. (Calculating this number for each of the three experiments however is reserved for the modeling section because the mathematical definition depends on the type of model used to describe the system. The mathematical definition of the Damkohler numbers for these three experiments is present in Appendix E.) However, other effects such as the lag in cell growth may also account for the variation in elapsed time before the plugging of the media (i.e. the time after the commencement of the nutrient feed into the core to the moment when the core demonstrates a statistical increase in inlet pressure).

A third phenomena, more prominently displayed during all three experiments and other experimental results, are the occurrences of pressure fluctuations recorded for the inlet pressure and axial pressure taps after the cores demonstrated statistically measurable plugging. These pressure oscillations are postulated as being the result of a sequence of biomass development and biofilm sloughing. Initially, it is believed that the inoculating cells are retained mechanically in the porous media. With the constant introduction of nutrients, the cells begin to grow and subsequently fill the void within the core with biomass. Since the feed is injected at a constant flow rate, the inlet pressure begins to increase due to flow constriction. When the local permeability and porosity are reduced to the point where the injected fluid induces a local shear stress that is approximately equal to the biomass's critical shear stress, the biofilm commences to slough off as fragments and is transported further into the core. This concept of sloughing has been observed by Fowler *et al.* [1980] for biofilm growth in a radial-flow parallel-plate geometry. These competing

phenomena, plug formation and plug removal, would then produce the overall pressure fluctuations observed for these plugging experiments.

5.4 Model Development

The development of an overall model was divided into two sections: the inoculation model and the *in situ* growth model. These models coincide with the inoculation and *in situ* growth phases of the experiment. Transition for the inoculation model to the in situ model occurs at the end of lag time. The development of this model is based on the nutrient balance experimental data.

5.4.1 Inoculation Model

The simplified one-dimensional form of the transport equations can be written as:

$$\varepsilon \frac{\partial \sigma_x}{\partial t} = - \varepsilon \Sigma r_{\text{cell transport}} \qquad 4.20)$$

$$\varepsilon \frac{\partial C_x}{\partial t} + U_s \frac{\partial C_x}{\partial z} = \alpha U_s \frac{\partial^2 C_x}{\partial z^2} + \varepsilon \Sigma r_{\text{cell transport}} \qquad 4.21)$$

To model the inoculation phase results one must determine the functionality of the cell transport rate between the sessile phase (cell deposited on interstitial surfaces) and the planktonic phase (cell's freely suspended). The rate expressions for deposition and entrainment can be expressed by many mathematical or functional forms [Tien *et al.* 1979, Herzig *et al.* 1970]. However, for the development of this model the simplest mathematical form was utilized; that is, the rate of deposition and entrainment were assumed to be first order as expressed by the following equations:

$$r_{\text{entrainment}} = k_1 (\sigma_x - \sigma_{x_o}), \quad \sigma_x > \sigma_{x_o} \qquad 4.21)$$
$$= 0, \quad \sigma_x < \sigma_{x_o}$$

$$r_{\text{deposition}} = k_2 C_x, \qquad 4.22)$$

with: $\Sigma r_{\text{cell transport}} = r_{\text{entrainment}} - r_{\text{deposition}}$ 4.23)

The rate of entrainment includes the term σ_{x_0} (minimal sessile cell concentration) which accounts for cells that are irreversibly captured within the porous media [Tien *et al.* 1979].

Table 5.3 presents the initial and boundary conditions used to compute the parameter values for Equation 4.20 and 4.21. The parameter values presented in Table 5.4 were determined by solving the PDE equations for various sets of parameter estimates, then determining which set resulted in the minimization of the absolute error as calculated by the Least Square Parameter Technique. Optimization of the error function was accomplished with the Simplex Method. The Method of Lines technique used to solve Equations 4.20 and 4.21 is a spatial discretization method that reduces the PDE's to a set ODEs (ordinary differential equations) which are then solved by any numerical integration technique [Schiesser, 1991]. The resulting set of ODE's for these equations were solved using LSODA (Livermore Solver for Ordinary Differential Equations) software package.

Solving for the set of parameter constants numerical was accomplished, for a given step size, in a two-step process of : 1) determining the dispersion coefficient and deposition constant (neglecting the entrainment term) for approximately 2 pore volume of cell injection, and 2) determining the entrainment parameters for the whole data set up to the end of the lag. The final parameter values for each of the above time ranges were then determined by using the model parameter estimates for a given step size and plotting the various parameter predictions versus their corresponding spatial discretization values and extrapolating the data to a zero step size. Figure 5.2 shows the predicted results relative to the experimental data, while Figure 5.3 is a plot of the cell profiles at 10.5 hours, i.e. $t=t_{lag}$. Figure 5.3 predicts that most cells within the core are sessile. Hence the planktonic cells concentration profile of the core can be neglected as an initial condition for the *in situ* growth model.

Table 5.3. Inoculum model boundary and initial conditions

(discretization)	30, 40 ,50, 70, 120, 150 equal segments
Δt (time step size)	controlled by LSODA (error control)
Boundary Conditions	C_X (inlet) $= 8.61 \times 10^{11}$ cell/L $\quad t < 60$ min C_X (inlet) $= 0.0 \quad t > 60$ min $\frac{\partial C_X(z=0,t)}{\partial z} = (C_X(z=0,t) - C_X(\text{inlet})) / \alpha$ $\frac{\partial C_X(z=L,t)}{\partial z} = 0$
Initial Conditions	$C_X (z,t=0) = 0.0$ $\sigma_X (z,t=0) = 0.0$

Table 5.4. Parameter value estimates.

Superficial Velocity (cm/min)	dispersivity α (cm)	k1 (min^{-1})	k2 (min^{-1})	σ_{X_O} (cell/L)
0.9564	0.23	1.3×10^{-2}	8.9×10^{-3}	5.9×10^{9}

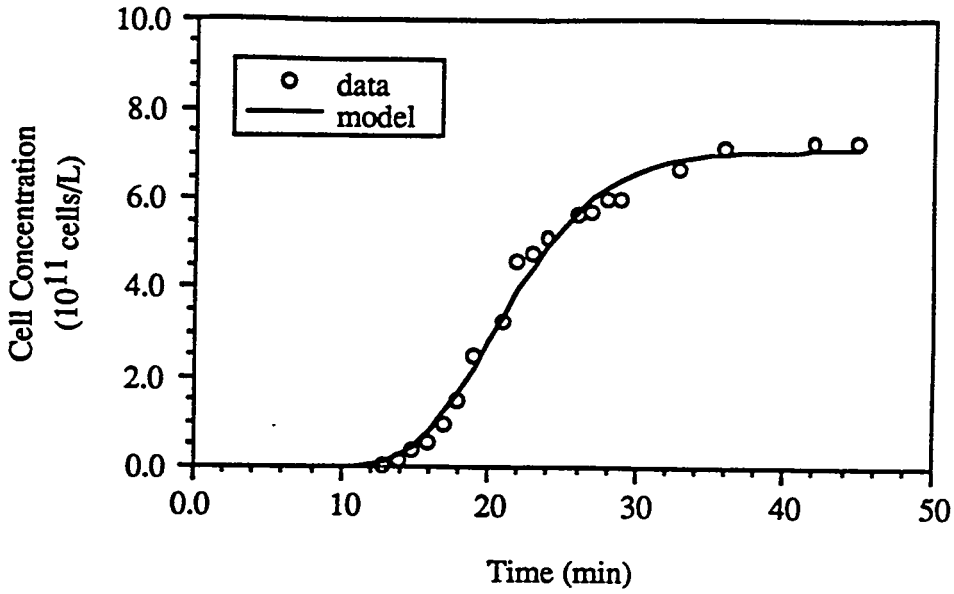

a) effluent cell concentrations

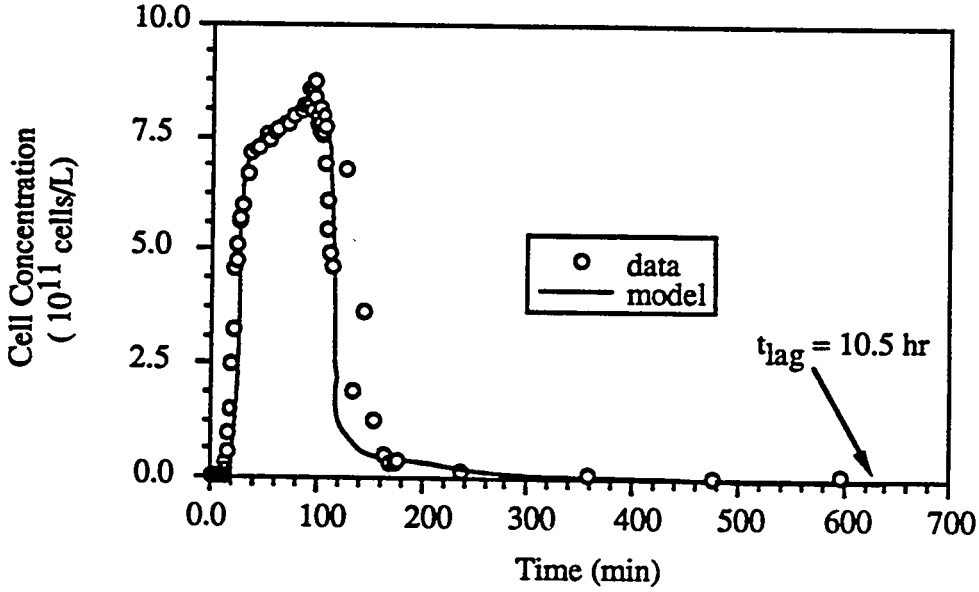

b) sessile cell profile at 630 minutes

Figure 5.2. Model results compared to experimental data

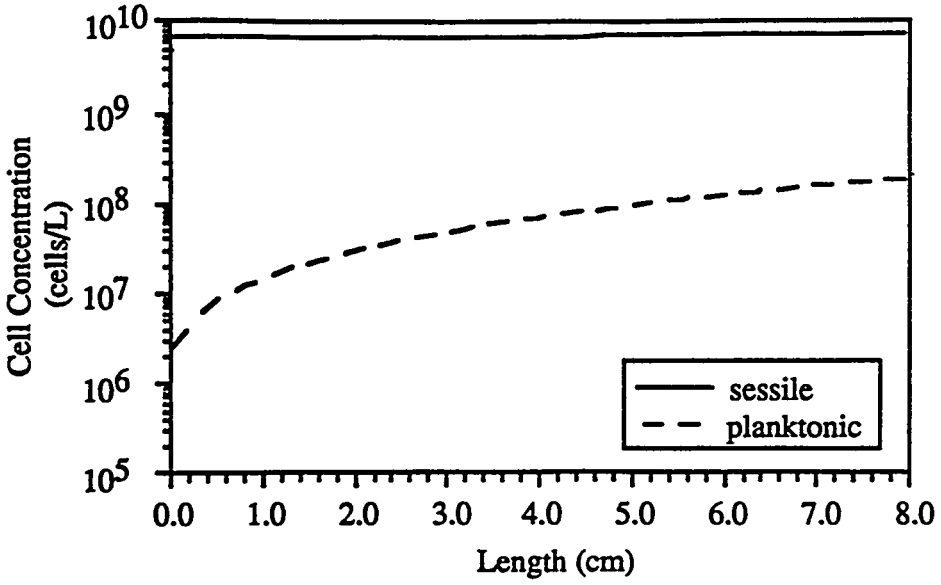

Figure 5.3. Inoculum model sessile and planktonic cell concentration profiles

5.4.2 *In situ* Growth Model

Including mass transfer and the *in situ*-growth lag time (growth when $t > t_{lag}$) allows for the expression of the *in situ* -growth model as:

$$\varepsilon \frac{\partial \sigma_x}{\partial t} = \varepsilon r_{\text{cell production}} \qquad 4.24)$$

$$\varepsilon \frac{\partial \sigma_e}{\partial t} = \varepsilon r_{\text{enzyme production}} \qquad 4.25)$$

$$\varepsilon \frac{\partial \sigma_{id}}{\partial t} = \varepsilon r_{\text{polymer production}} \qquad 4.26)$$

$$\varepsilon \frac{\partial C_{si}}{\partial t} = \varepsilon \Sigma r_{\text{sucrose consumption}} + \Sigma r_{\text{sucrose transport}} \qquad 4.27)$$

$$\varepsilon \frac{\partial C_s}{\partial t} + U_s \frac{\partial C_s}{\partial z} = - \Sigma r_{\text{sucrose transport}} \qquad 4.28)$$

where:

C_S - concentration of sucrose in the bulk feed (g/L)
C_{Si} - concentration of sucrose at the sessile interface (g/L)

The above model assumes that sessile cells within the core remain sessile once growth starts due to polysaccharide production. This implies that cell removal rate (rate of cells becoming planktonic) is negligible relative to the cell's growth rate throughout growth. Also, the insoluble dextran and the enzyme produced by the cells are assumed to remain with the cell once growth starts. This assumption is validated by considering the results presented by Brooker [1979]. In his micrographs of various lactic acid bacteria, Brooker has clearly shown that the dextran produced by the cells remain on the surface of the cells. Since the enzyme dextransucrase, which is the enzyme responsible for the production of dextran, is typically attached to the polymer [Ebert *et al.*, 1968], it is justifiable to assume that the enzyme will also remain with the cell.

This model also neglects any yeast extract balance. This assumption is based on the fact that yeast extract is provided to the cells in excess. In addition, the porosity in the above model was determined by assuming a pseudo-steady-state condition where changes in porosity are negligible. The porosity can then be calculated from Equation 4.17 using cell and dextran density values that were determined experimentally and are presented in Appendix F.

The mass transfer rate law is assumed to be linearly proportional to the concentration differences between the bulk solution and that surrounding the immediate vicinity of the biofilm, and is written as:

$$r_{\text{sucrose transport}} = k'a\,(C_S - C_{Si}) \qquad 4.29)$$

The mass transfer coefficient, k'a, used in the rate law is actually a grouping of the mass transfer coefficient and the mass transfer flux area. The results of using the mass-

transfer limitation and the lag-time assumption in the model can be see in Figure 5.4. The criteria used for model determination, i.e. mass transfer and cell-growth lag time, was the result of matching the experimental effluent sucrose concentration as a function of time with the model prediction. Effluent cell release was neglected. The reason for the selection of effluent sucrose matching was the need to determine the amount of biomass produced *in situ*. Appendix E details the progression of the model to its final version, as presented above. The result of matching the effluent sucrose concentration yields the mass transfer coefficient values as 12.5 hr^{-1} (3.47 x 10^{-3} s^{-1}) which is comparable to mass transfer values found by others [Vaidya, 1991]. Again, as with the transport coefficients, the mass transfer coefficient was determined by solving the above equations at varying spatial discretizations and extrapolated optimum coefficients (for each discretization size) to a zero step size. Table 5.5 presents the boundary and initial conditions used to solve the above equations.

Table 5.5. *In situ* model boundary and initial conditions

(discretization)	30, 40 ,50 equal segments
Δt (time step size)	controlled by LSODA (error control)
Boundary Conditions	C_S (z= 0, t) = 21.5 g sucrose/L t > t_{lag}
Initial Conditions	σ_X (z, t = t_{lag}) = given by inoculation model σ_e (z, t = t_{lag}) = 0.0 σ_{id} (z, t = t_{lag}) = 0.0 Csi (z, t = t_{lag}) = 21.5 g sucrose/L

Figures 5.5 a), b), c) and d) presents the resulting internal bulk sucrose, cell, and dextran concentration, and porosity profiles, respectively. As can be seen from the prediction, the injection face of the core eventually experiences the high increases in cell and dextran production. This high cell concentration at the injection face is the result of the high growth rate of the cell which itself is based on the availability of nutrients for growth. Core staining results verify this prediction.

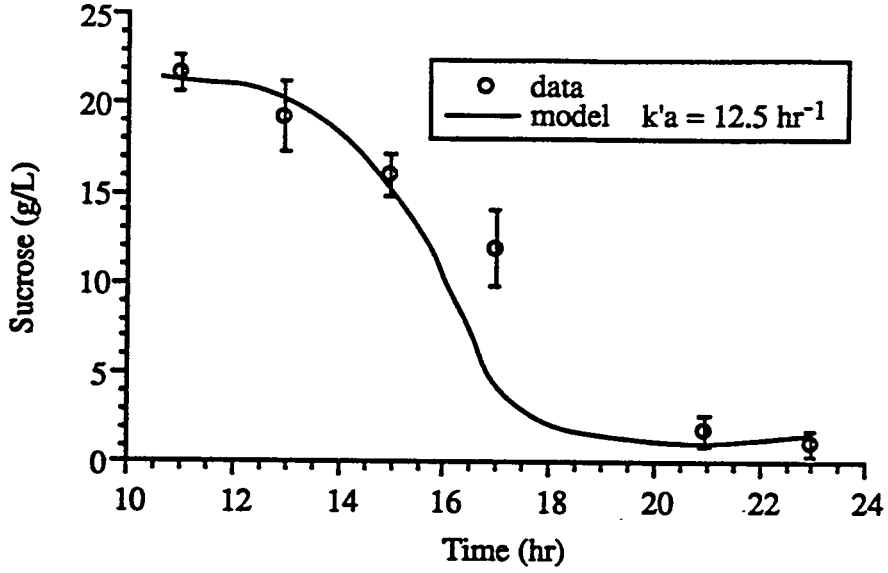

Figure 5.4. Model and experimental effluent sucrose concentration

5.4.3 Permeability Model

From the resulting porosity prediction the porosity-permeability correlation constant, β, of Equation 4.19 was determined to be 33.8 using the Least -Square technique. Figure 5.6 illustrates the resulting model's permeability prediction and experimental data.

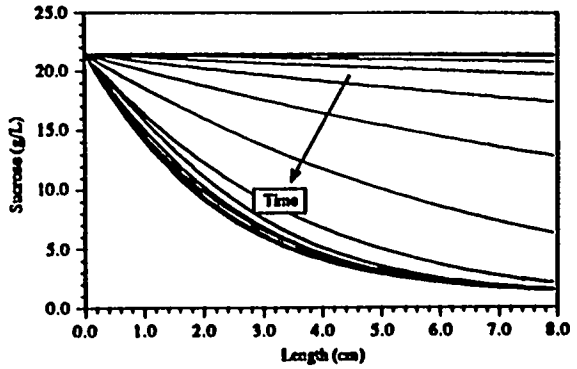

a) bulk sucrose concentraion

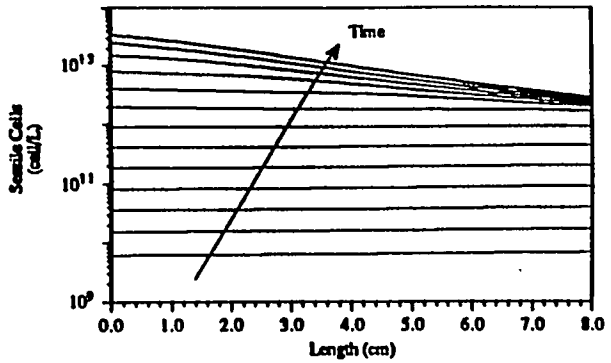

b) sessile cell concentration

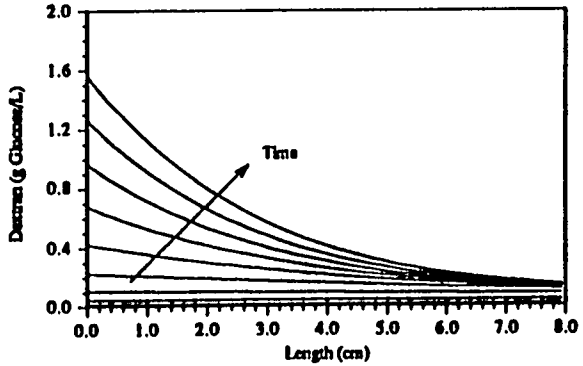

c) dextran concentration

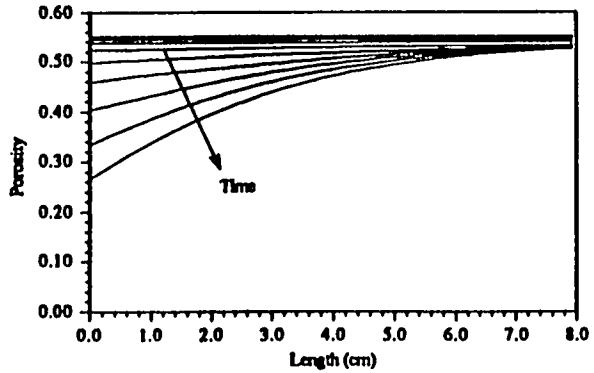

d) local porosity

Figure 5.5. Internal a) sucrose, b) cell, c) dextran, and d) porosity profiles at varying time (time steps are every hour, start time is t= 10.5 hr)

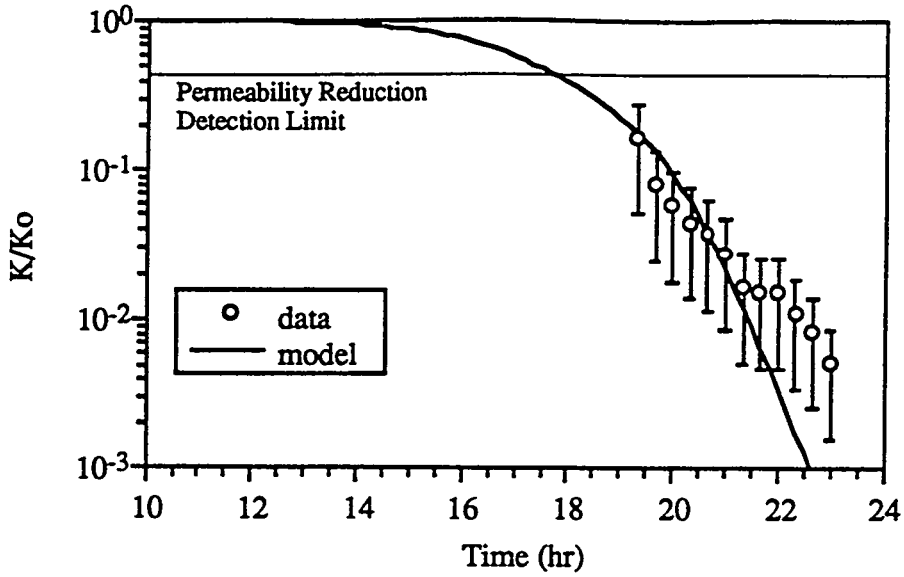

Figure 5.6. Predicted versus experimental permeability reduction for 3 Darcy ceramic core (*in situ* growth experiment - see Chapter 4)

5.5 Model Prediction

The *in situ*-growth model that describes cell and dextran production and sucrose consumption in the porous media requires both the cell profile in the core and the injection condition, such as nutrient concentration and injection rate. Thus, manipulating the initial cell profile and the injection conditions can be used as the strategy to control the BPM technique.

5.5.1 Effect of Cell Profile on Core Permeability

The cell profile used in the development of the *in situ* model had been dictated by the assumption of deep-bed filtration during porous media inoculation and had been matched to the effluent data. However, such a profile could be manipulated by means of the cell injection strategy by altering the surface chemistry of the cells and/or the porous

media [Sharma *et al.* 1985, Vaidya 1991] or controlling the cell injection rate, the cell concentration, and the injection duration [Hart *et al.*, 1960].

Assuming that various final profiles could be placed in the porous media as illustrated in Figure 5.7 a) , the question of how this profile influences the development of the plug profile and resulting permeability reduction can be determined by the *in situ* model. To make a comparison between the three profiles, the *in situ*-growth along with the permeability models were used to predict the resulting permeability decline for the three cell profile over a 15-hour duration, assuming no lag time. The resulting permeability decline for each of the three runs is illustrated by Figure 5.7 b). For each of the runs it must be noted that the total number of cells in the cores are initially the same and that the same nutrient injection rate and concentrations were used.

As can be seen, from Figure 5.7 b), the most dramatic permeability reduction occurs to the core that initially had most of the cells near the injection face. The core that contained a constant profile was followed in order of damage, and minimal plugging occurring to the core that contained most of the cells at the exit. These results are expected because the highest cell growth and dextran production rates should occur at the injection face where the nutrient concentrations are at their maximum. Thus, these results illustrate that the plugging rate of the porous media is dependent on the initial cell profile.

5.5.2 Effect of Injection Rate and Nutrient Concentration on Core Permeability

The Damkohler experiments demonstrated that the time required for apparent damage depends on the rate of nutrient injection and nutrient concentration. This experimental observation is reflected in the model prediction which is illustrated by Figure 5.8. For these predictions a constant cell concentration profile was used, and the cell-growth lag time was neglected. The three runs used the same nutrient injection rates and nutrient concentrations as those realized in the experiments. The point where measurable damage occurs is illustrated by the plot as the time where the permeability curve

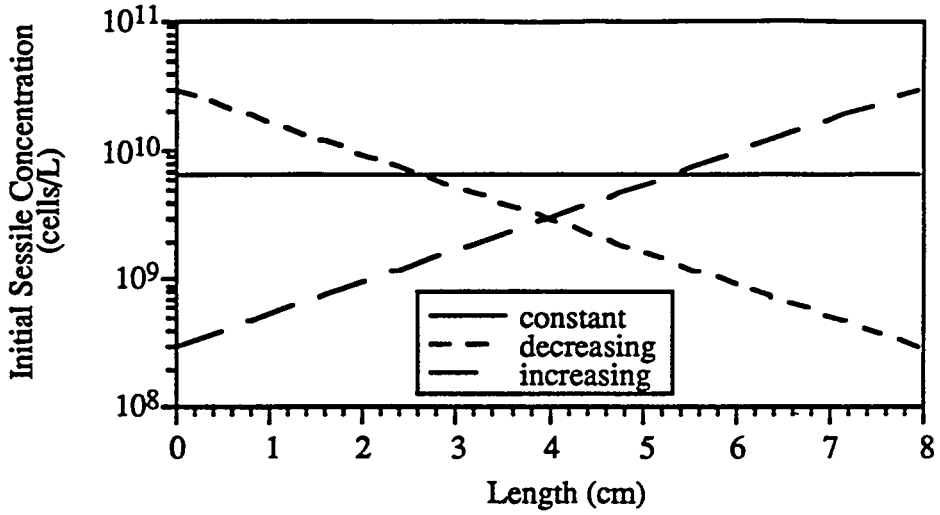

a) initial cell profile

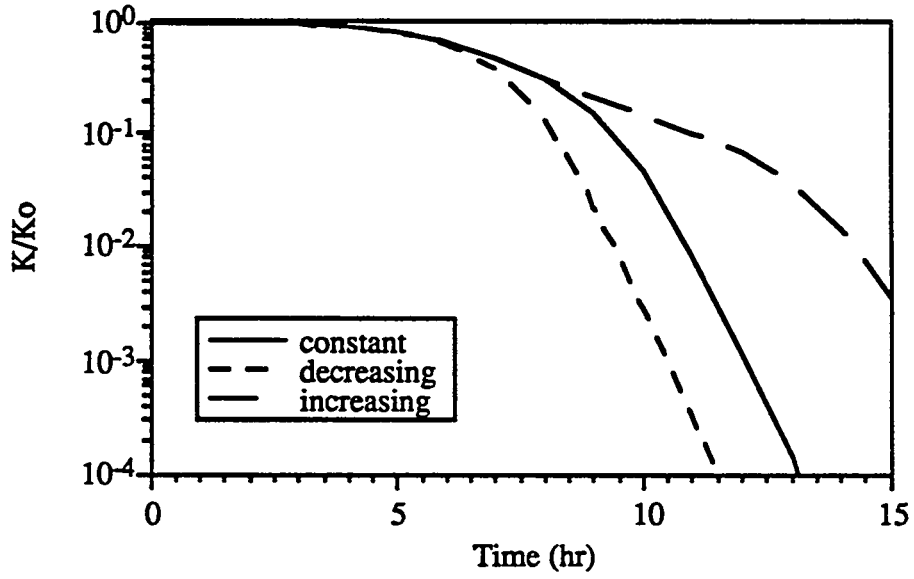

b) resulting permeability reduction

Figure 5.7. Effect of cell profile on core permeability

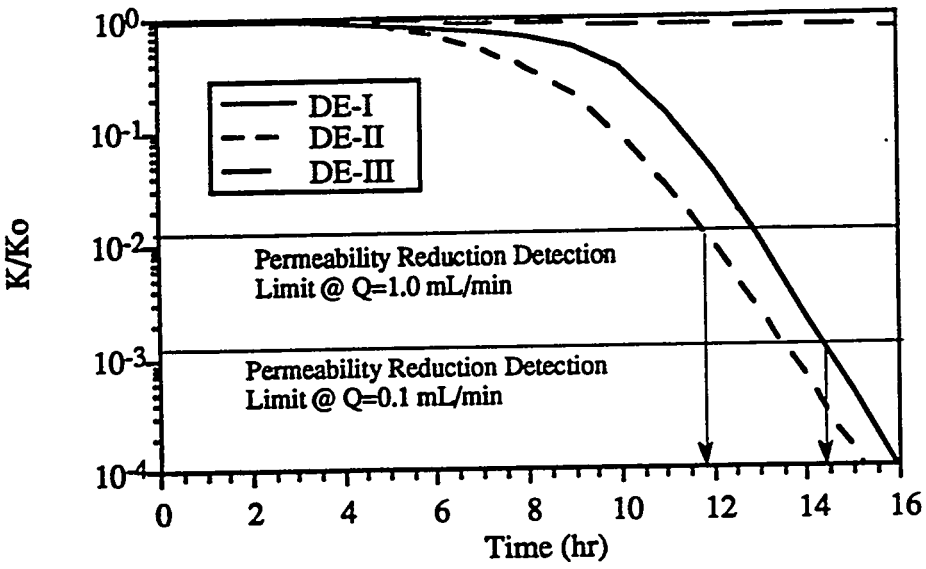

Figure 5.8. Effect nutrient injection rate and nutrient concentration on core permeability
DE-I - 15 g sucrose/L @ q=0.1 mL/min $Da_d = 142$
DE-II - 15 g sucrose/L @ q=1.0 mL/min $Da_d = 1.42$
DE-III - 1.5 g sucrose/L @ q=1.0 mL/min $Da_d = 14.2$
See Appendix E for Da_d (Damkohler) definition.

intersects the permeability reduction detection limit line (which is flow-rate dependent). This line is calculated by dividing the theoretical pressure as calculated by Darcy's law with the statistically measurable pressure (i.e. average pressure drop for given flow plus 3 standard deviations). As seen in the figure, DE-III demonstrated no measurable plugging (damage), while DE-I and DE-II both demonstrated measurable plugging at approximately 15 and 12 hours, respectively. DE-III didn't demonstrate damage because insufficient nutrients were injected to produce sufficient biomass within the 15 hours. DE-I and DE-II were cases where sufficient biomass were generated and the generation as found experimentally did cause damage. The time when DE-I and DE-II did not coincide with the results found experimentally may be explained by the fact that: 1) the initial cell profiles may have not be linear, 2) total number of cells captured at the end of inoculation may not

have been the same, and 3) the lag time was not used in the model due to lack of an estimated value. These three factors would all have to have been determined experimentally at the same time that the core plugging experiment was conducted. However, these results do demonstrate the trend which dictates that the rate of permeability decline is dependent upon the nutrient concentration and the injection rate.

5.6 Conclusions

The parallel-core plugging experiments have demonstrated the feasibility of using *L. mesenteroides* for profile modification and have shown that diversion susceptible to a degeneration if nutrient injection is not controlled. In addition, the ability to divert fluid has been found to be dependent upon the biomass profile that develops in the porous media. The Damkohler experiments have shown the dependency of the plugging rate on the injection conditions such as nutrient concentration and injection rate. These experiments with the nutrient balance experimental results have aided in the development of a continuum model that describes *in situ* cell growth and dextran production with resulting permeability decline. This model incorporates a cell-growth lag time and nutrient mass transfer coefficient that control the growth of the biomass. From the model it has been shown that the initial cell profile (when cell growth commences) influences the rate of plugging. In addition, parallel to the Damkohler experimental results, the model predicts that the plugging rate of the porous media is dependent upon the concentration of the nutrients and their injection rate. Thus controlling the cell placement, the nutrient injection rate and nutrient concentration are all variables which will help in the development of an injection strategy for BPM.

Nomencalture

C_i - bulk concentration of species i (g/L or cells/L)

C_{si} - concentration of sucrose at the sessile interface (g/L)

D_i - dispersion (cm^2/h)

k_i - activity of the enzyme per volume per cell to produce product i @ 30 C and pH 5.2

k'a - mass transfer coefficient flux area product (h)

k_{loc}/k_o - local permeability (Darcies)

K_i - Monod constant for component i (g/L)

K/Ko - permeability ratio

r_i - rate of product i formation per unit volume (g/L·h or cells/L·h)

$\Sigma r_{i\ transport}$ - sum of the rate expressions for i partitioning between surface retained and suspension states (g/L/h)

t - time (h)

t_{lag} - *in situ*-growth lag time (h)

Us - darcy or superficial velocity (cm/hr)

V_{max_i} - maximum velocity for species i (g/L·h)

Y_i - cell yield from species i consumption (cells/g)

z - length dimension (cm)

$\alpha_{s/ye}$ - yeast extract conversion factor (g sucrose/g yeast extract)

α - dispersivity coefficient (cm)

ε - porosity

ε^* - initial porosity

$\Delta\varepsilon$ - change in local porosity

γ - molecular ratio - monosaccharide to sucrose

σ_i - concentration of species i on surface (fluid volume basis) (g/L)

ρ_i - density of material i (cells/L or g/L)

θ_i - dimensionless reaction rate constant for sucrose consumption at reaction temperatures

μ - specific growth rate (h^{-1})

μ_{max} - maximum specific growth rate (h^{-1})

Subscript for kinetic parameters are:

x	- cell	ye	- yeast extract
e	- enzyme	g	- glucose
f	- fructose	s	- sucrose
id	- insoluble dextran	td	- total dextran

5.7 References

Clark, J.B., Munnecke, D.M., and Jenneman, G.E., 'In-Situ Microbial Enhancement of Oil Production', Developments in Industrial Microbiology, 1981, **22**, 695-701

Fowler, H.W. and A.J. McKay, Chapter 7, *Microbial Adhesion to Surfaces*, edited by R.C.W. Berkeley, J.M. Lynch, J. Melling, P.R. Rutter, and B.Vincent, Ellis Horwood Limited, West Sussex, England, 1980

Herzig, J.P., D.M. Leclerc, and P. Le Goff, Flow of Suspensions Through Porous Media-Application to Deep Filtration, *Ind. and Eng. Chem.*, **62**, 8-35, 1970

McCune, C.C. and Fogler, H.S. *74th National Meeting of AIChE*, New Orleans, March 11-15 1973

Schiesser, W.E., *The Numerical Method of Lines*, Academic Press, New York, 1991

Sharma, M.M., Y.I. Chang, T.F. Yen, Reversible and Irreversible Surface Charge Modification of Bacteria for Facilitating Transport Through Porous Media, *Colloids and Surfaces*, **16**, 1985, 193-206

Stanier, Roger Y.,John L. Ingraham, Mark L. Wheelis, and Page R. Painter: The Microbial World, Fifth Edition, Prentice-Hall, New Jersey, 1986

Tien, C.R.M. Turian, and H. Pandse, Simulation of the dynamics of deep bed filtration, AiChE J., 25,1979

Vaidya, R.N. Ph.D. Thesis, *Fines Migration and Formation Damage*, The University of Michigan, Ann Arbor, Michigan, 1991

Appendix 5.A

Cell and Dextran Densities

The density of *L. mesenteroides* cells was determined by measuring the volume occupied by a known number of cells. The cells had initially been grown in a glucose-fructose media for a 24-hour period. After incubation, a known volume of suspended cells was centrifuged at 4400g for 10 minutes. The volume of the pellet was then measured. Simultaneously, the concentration of cells in the suspension was determined by Coulter Counter. The ratio of the suspended-cell concentration to cell-per-unit volume in the pellet yields a cell density of $1.2 \times 10^{14} \pm 2.3 \times 10^{13}$ cells/L.

The density of dextran was determined by measuring the amount of dextran produced resulting from cell growth and the volume the dextran occupied. Initially, the cells were grown in a sucrose feed solution for 24 hours. The cell concentration of this solution was then determined by Coulter Counter. Dextran concentration was assayed by the dextranase - phenol sulfuric acid assay detailed in Chapter 3. In addition, the suspension volume (cells and dextran) was determined by centrifuging a known volume of sucrose-grown cells at 4400 g for 10 minutes and then measuring the volume of the pellet. The ratio of the dextran concentration to the pellet volume (excluding cell volume) allowed for the determination of the dextran densities as $6.9 \times 10^{-2} \pm 5.9 \times 10^{-3}$ g/mL. All measurements were conducted in triplicate.

Appendix 5.B

In situ Growth Model Development

The development of the *in situ* growth model was an iterative process between model development and experimental data comparison for model verification. Initially, a zero-parameter model (no lag time and no mass-transfer limitation) was developed to describe the *in situ* growth and plugging of the porous media. This model assumed that all cells which were sessile at the termination of the cell injection phase (90-minute mark on Figure 4.4) remained sessile due to polysaccharide production. With this assumption it was also assumed that enzyme and polysaccharide were retained at their production location.

In addition, the model neglected dispersion, diffusion, and a yeast-extract balance but included porosity changes. By neglecting a yeast-extract balance in the model the additional problem of continuous growth even after total sucrose consumption (sucrose being within the limit of detection) became a problem. The kinetic experiments have shown that growth can occur on yeast extract alone, but the cell yield is typically very low when compared to growth on yeast extract and sucrose. To correct for this over-prediction in growth, it was assumed that local cell replication stopped when the local sucrose concentration had dropped below the detectable limit of 1.0 g sucrose/L. This detection limit is the average of the limit of detection, i.e. 3 standard deviations in data (99.5 % confidence), for all the effluent measurements as determined from the results presented in Chapter IV - the nutrient balance growth experiments in consolidated cores.

Solving this zero-parameter model, numerically, predicted an immediate and near complete drop of effluent sucrose within one hour, as seen in Figure 5.B.1. Hence, this model was rejected because the effluent sucrose concentration, which is the indicator of *in situ* biomass production, predicts higher than experimentally realized *in situ* cell production.

A further improvement to the *in situ* growth model included a cell-growth lag time, which accounts for the time required by the cell to create the various metabolic pathways needed for nutrient consumption and growth. During this lag time there is no growth and no dextran production. Because of this assumption, the time period for which the inoculation model applies is extended to include the lag time since cell transport can occur when there is no dextran production. For the data presented in Chapter IV (see Figure 4.5), a lag time of 10.5 hours was estimated by fitting the monosaccharide data (for data between 11 hr < t < 17 hr) with an exponential function and then determining the lag time from equation coefficients. The result of including this lag time in the model did allow for the matching of the initial drop in sucrose, but the model over predicted sucrose consumption, as seen in Figure 5.B.1. These results led to the present model that includes both a lag time and mass transfer.

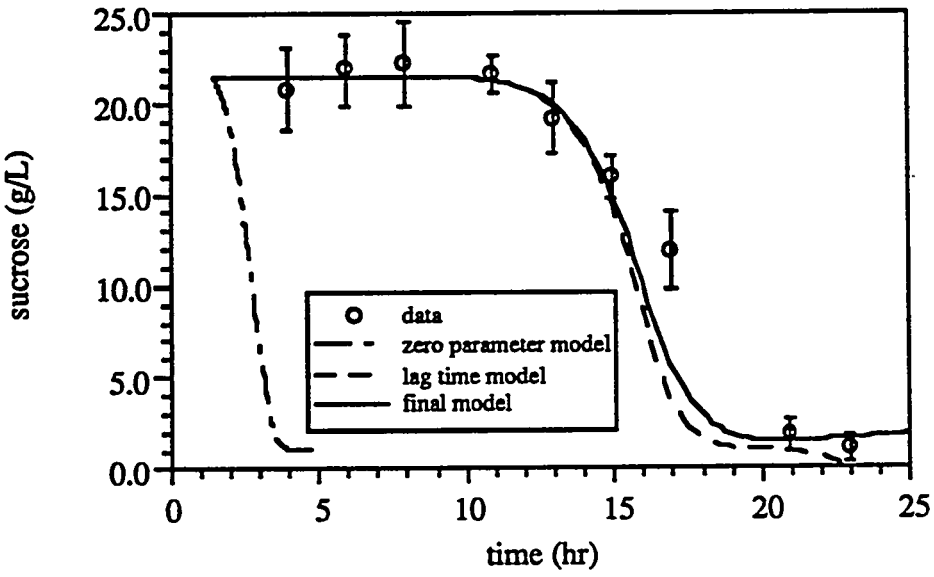

Figure 5.B.1. *In situ* growth model prediction including lag time only

Dimensionless *In situ* Growth Model

By defining the following parameters:

$$\Psi_S = \frac{Cs}{Cs^o}, \qquad \Psi_{Si} = \frac{Csi}{Cs^o},$$

$$\Phi = \frac{\sigma_d}{\gamma\, Cs^o}, \qquad X = \frac{\sigma_x}{\rho_x}, \qquad \chi = \frac{\sigma_e\, U_S}{k_f\, \rho_x\, L},$$

$$\zeta = \frac{z}{L}, \qquad \tau = \frac{t\, U_S}{L},$$

the one-dimensional *in situ* growth model (including kinetic rate laws) can be written in dimensionless form as:

$$\varepsilon \frac{\partial X}{\partial \tau} = \varepsilon\, Da_X\, F(\Psi_{Si})\, X \qquad \text{E.1)}$$

$$\varepsilon \frac{\partial \chi}{\partial \tau} = \varepsilon\, X \qquad \text{E.2)}$$

$$\varepsilon \frac{\partial \Phi}{\partial \tau} = \varepsilon\, Y_{id/td}\, Da_d\, G(\Psi_{Si})\, \chi \qquad \text{E.3)}$$

$$\varepsilon \frac{\partial \Psi_{Si}}{\partial \tau} = -\varepsilon\, (Da_d + Da_g)\, G(\Psi_{Si})\, \chi + Bi\, (\Psi_S - \Psi_{Si}) \qquad \text{E.4)}$$

$$\varepsilon \frac{\partial \Psi_S}{\partial \tau} + \frac{\partial \Psi_S}{\partial \zeta} = -Bi\, (\Psi_S - \Psi_{Si}). \qquad \text{E.5)}$$

The various dimensionless groups are defined as:

$$Da_d = \left(\frac{L}{U_S}\right)^2 \frac{\theta_d\, k_d\, \rho_x}{Cs^o} \qquad \text{E.6)}$$

$$Da_g = \left(\frac{L}{U_S}\right)^2 \frac{\theta_g\, k_g\, \rho_x}{Cs^o} \qquad \text{E.7)}$$

$$Bi = \frac{L\, k'a}{U_S} \qquad \text{E.8)}$$

$$Da_X = \frac{L\,\mu_{max}}{U_S} \qquad \text{E.9)}$$

and functional groups defined as:

$$G(\Psi_{Si}) = \frac{\Psi_{Si}}{\kappa_d + \Psi_{Si}} \qquad \text{E.10)}$$

$$F(\Psi_{Si}) = \frac{\kappa_{S1} + \Psi_{Si}}{\kappa_{S2} + \Psi_{Si}} \qquad \text{E.11)}$$

where:

$$\kappa_d = Kd/Cs^o \qquad \kappa_{S1} = \alpha_{S/ye}\,Cye/Cs^o \qquad \kappa_{S2} = (\alpha_{S/ye}\,Cye + Ks)/Cs^o$$

Note that yeast extract was provided in excess and thus the term $Cye/(Cye + Kye) \approx 1$.

There are three Damkohler numbers associated with the above model; two associated with the products from enzymatic consumption of sucrose (dextran and glucose), and the third representing cell production. Since the system is defined for the reactor initial conditions, defining any one of the three will fix the other two (when yeast extra is provided in excess.) The dextran production Damkohler number has thus been selected as the Damkohler number needed to represent the system because dextran is the product responsible for plugging.

Nomenclature

The notation in this appendix is the same as Chapter IV with the addition of the following:

Cs^o - inlet sucrose concentration (g sucrose/L)

6.0 Conclusions

The core plugging experiments have demonstrated the importance of polysaccharide production on cell transport in porous media. In high permeability cores (Darcy range), the polymer appeared to be the sole cause of core plugging, while low permeability cores (100 mD) demonstrated damage due to both cell growth and polymer production with cells producing polysaccharides creating more damage. In addition, the core stainings have shown that the ability of cells to produce polysaccharide greatly control their distribution within the core.

The results of the parallel core plugging experiment demonstrated the potential for using a bacterial system for profile modification. As observed in this experiment, the parallel system when inoculated and fed sucrose will divert flow, but the system will revert back into its initial condition of flow supported by the high permeability zone if cell growth is not controlled. Thus, to further develop this technique for field application, a thorough understanding of the bacterial growth under varying nutrient conditions was determined.

The growth kinetics for cells grown on sucrose has been modeled. The model reflects experimental findings that indicate both the yeast extract concentration and sucrose concentration affect cell growth rate. Sucrose is used by cells as a carbon source while yeast extract primarily provides the cells with needed growth-factors for cell enzyme synthesis. Batch experiments have shown that sucrose is consumed at a faster rate than glucose or fructose, while cell growth on a glucose-fructose media has not shown any preference for either monosaccharides. This finding supports the postulate that the cell is externally catabolizing the sucrose to produce dextran, glucose, and fructose; subsequently the monosaccharides are transported into the cell for growth. The substrate utilization model, which is based on experimental findings, has been found to predict the growth rate of the cells.

The dextran production experiments have demonstrated that final polymer production yields are dependent upon the availability of sucrose in the feed. These findings are modeled by correlating dextran production with fructose production during dextran synthesis and assuming that only a fraction of the produced dextran is insoluble. Finally, the model has been shown to predict the ability to control the dextran to cell production ratio by fixing the yeast extract to sucrose ratio. This approach will aid in the development of a Bacterial Profile Modification technique.

The transport experiments in micromodels have shown that polysaccharides influence the retention of cells in porous media. Cells grown in the presence of sucrose will produce agglomerates of cells held together by dextran. These agglomerates aid in capture and retention of cell.

The *in situ* growth experiments in micromodels show that the biofilm thickness increases as cells produce dextran. The micromodel experiments show that initially only a thin biofilm coating develops on the pore walls when cells are provided with monosaccharides. This thickness appears to reach a steady state, meaning a dynamic equilibrium is developed between cell growth and sloughing rates. However, if the feed is switched to a sucrose-rich media, the biofilm begins to increase in thickness and the injection pressure (under constant volumetric injection) begins to show a measurable change from the initial value. With additional time the inlet pressure increases rapidly which implies that the polysaccharides are increasing the shear strength of the biofilm which enhances the retention of cells in the porous media. This development of the biofilm continues to the point where shear takes place which results in pressure oscillations as sheared biofilm is recaptured and released throughout the downstream network of porous media.

Finally, the results from the *in situ* growth experiment in consolidated porous media has aided in the development of an *in situ* growth model. From the experiment, effluent

sucrose data were used to develop a model which incorporates mass transfer and cell growth lag time. Mass transfer is hypothesized as limiting growth because the retained cells in the porous media which are consuming the nutrients plug the flow channels and divert nutrients away. Cell growth lag times result from losses of critical cellular constituents into the constantly flowing (flushing) feed solution. Using these phenomena in the model has produced a model that predicts the cell and dextran concentration profiles, and local permeability changes. Using the *in situ* growth model under varying sucrose injection rates and feed concentrations has reproduced the experimental trends. In addition, the model has demonstrated the importance of the inoculum cell profiles on the resulting permeability reduction rates of the porous media.

☆U.S. GOVERNMENT PRINTING OFFICE: 1995 - 660-029/00066